Department of Spatial Sciences

Spatio-Temporal Analysis of GRACE Gravity Field Variations Using the Principal Component Analysis

Ira Mutiara Anjasmara

This thesis is presented for the
Degree of Master of Science (Surveying and Mapping)
of Curtin University of Technology

March 2008

Declaration

To the best of my knowledge and belief this thesis contains no material previously published by any other person except where due acknowledgement has been made.

This thesis contains no material which has been accepted for the award of any other degree or diploma in any university.

Signature: .....

Date: .....

ABSTRACT

Gravity Recovery and Climate Experiment (GRACE) mission has amplified the knowledge of both static and time-variable part of the Earth's gravity field. Currently, GRACE maps the Earth's gravity field with a near-global coverage and over a five year period, which makes it possible to apply statistical analysis techniques to the data. The objective of this study is to analyse the most dominant spatial and temporal variability of the Earth's gravity field observed by GRACE using a combination of analytical and statistical methods such as Harmonic Analysis (HA) and Principal Component Analysis (PCA). The HA is used to gain general information of the variability whereas the PCA is used to find the most dominant spatial and temporal variability components without having to introduce any presetting. The latter is an important property that allows for the detection of anomalous or a-periodic behaviour that will be useful for the study of various geophysical processes such as the effect from earthquakes.

The analyses are performed for the whole globe as well as for the regional areas of: Sumatra-Andaman, Australia, Africa, Antarctica, South America, Arctic, Greenland, South Asia, North America and Central Europe. On a global scale the most dominant temporal variation is an annual signal followed by a linear trend. Similar results mostly associated to changing land hydrology and/or snow cover are obtained for most regional areas except over the Arctic and Antarctic where the secular trend is the prevailing temporal variability. Apart from these well-known signals, this contribution also demonstrates that the PCA is able to reveal longer periodic and a-periodic signal. A prominent example for the latter is the gravity signal of the Sumatra-Andaman earthquake in late 2004. In an attempt to isolate these signals, linear trend and annual signal are removed from the original data and the PCA is once again applied to the reduced data. For a complete overview of these results the most dominant PCA modes for the global and regional gravity field solutions are presented and discussed.

Keywords *: GRACE, PCA, Earth's gravity field, spatial and temporal variability*

ACKNOWLEDGEMENTS

First of all I would like to express the best gratitude to my supervisor, Dr-Ing Michael Kuhn, for his guidance, support and supervision whilst undertaking this project. I am indebted to him not only for scientific supervision, but also for his understanding, help, and friendship.

I also gratefully acknowledge Dr-Ing Oliver Baur for providing the routine for mass estimate calculation and Dr-Ing Michael Kuhn for the PCA routine used in this study.

In addition, my thanks go to those who provide and manage my scholarship, the Australia Partnership Scholarship (APS), in Indonesia and Australia. Many thanks also go to the people in Geodesy group and Department of Spatial Sciences, Curtin University of Technology for providing me not only a conducive research environment but also friendly and kind supports.

Finally, I would like to thank my family, especially my parents, in Indonesia for their continuing supports, encouragements and prays.

TABLE OF CONTENTS

ABSTRACT ii
ACKNOWLEDGEMENTS iii
TABLE OF CONTENTS vi
LIST OF FIGURES ix
LIST OF TABLES xi
LIST OF ACRONYMS xii
LIST OF SYMBOLS xiv
1. INTRODUCTION 1
1.1 Background 1
1.1.1 Static and Time-variable Gravity 2
1.1.2 Dedicated Satellite Missions for the Earth's gravity field 3
1.1.3 PCA 6
1.2 Research Objectives 7
1.3 Thesis Outline 7
2. THE GRACE SATELLITE MISSION 9
2.1 GRACE Satellites and Technology 9
2.2 GRACE Gravity Field Measurement Concept 16
2.3 GRACE Science Data System 17
2.3.1 GRACE Level-0 Data 18
2.3.2 GRACE Level-1 Data 19
2.3.3 GRACE Level-2 Data 19
2.4 GRACE Data Limitations, Errors and Filtering Methods 21
2.5 GRACE Gravity Models 24
2.6 GRACE Data Applications in Earth Sciences 28
2.6.1 Time-variable Gravity 29
2.6.2 Geodynamics 29
2.6.3 Hydrology 30

2.6.4 Geodesy 31
2.7 Other Gravity Dedicated Satellite Missions 31
2.7.1 ARISTOTELES 31
2.7.2 CHAMP 32
2.7.3 GOCE 32
2.8 Summary 32
3. SPATIAL AND TEMPORAL VARIATIONS OF THE EARTH'S GRAVITY FIELD 34
3.1 Theoretical Foundation of the Earth's Gravity field 34
3.2 Spatial and Temporal Variations of the Earth's Gravity field 37
3.3 Inferring Changes in the Earth's Mass Distribution from Time-variable Gravity 40
3.4 The Earth's Gravity field Data Sources 43
3.5 Summary 44
4. TECHNIQUES FOR SPATIAL AND TEMPORAL SIGNAL ANALYSIS 45
4.1 Spatial and Temporal Systems 45
4.2 Techniques for Analysing Spatio-temporal Signal 45
4.2.1 Harmonic Analysis 46
4.2.2 Wavelets 47
4.2.3 Empirical Orthogonal Function or Principal Component Analysis 47
4.3 Summary 48
5. PRINCIPAL COMPONENT ANALYSIS 49
5.1 History of Principal Component Analysis 49
5.2 Theoretical Background of the PCA 50
5.2.1 Data Preparation 50
5.2.2 Formulation and Computation of EOFs and PCs 51
5.3 PCA in Earth Sciences 53
5.4 Summary 54
6. SPATIO-TEMPORAL VARIABILITY OF GRACE GRAVITY FIELD 55
6.1 GRACE Data Used 55
6.2 Method and Processing 56
6.2.1 Data Preparation 58
6.2.2 Harmonic Analysis 59
6.2.3 PCA 60

6.3 Results and Analysis 61
6.3.1 Global Analysis 61
6.3.2 Localized Analysis 68
6.4 Summary 88
7. SUMMARY, CONCLUSION AND OUTLOOK 89
7.1 Summary 89
7.2 Conclusion 91
7.3 Outlook 92
REFERENCES 92
APPENDIX A: ANNUAL VARIABILITY OF GRACE GRAVITY FIELD 105
APPENDIX B: SEASONAL VARIABILITY OF GRACE GRAVITY FIELD 107
APPENDIX C: PCA RESULTS 112

LIST OF FIGURES

Figure 1.1 Concept of satellite-to-satellite tracking : (a) in the high-low mode (SST-*hl*) (b) in the low-low mode (SST-*ll*) (c) satellite gradiometry combined with SST-*hl* (Rummel et al., 2002) 5

Figure 2.1 GRACE's altitude decay scenario (GFZ Postdam, 2008)..... 10

Figure 2.2 GRACE: Flight configuration 11

Figure 2.3 The GRACE satellite (a) front view, (b) bottom view, (c) internal view 13

Figure 2.4 GRACE gravity field measurement [adapted from UTCSR (2008)] 17

Figure 2.5 GRACE science data flow (UTCSR, 2008) 18

Figure 2.6 Gravity model resolutions (GFZ Postdam, 2008) 26

Figure 2.7 GRIM5-S1 model(top left), EIGEN-CHAMP02S model (top right) and EIGEN-GRACE01S model (bottom) 28

Figure 3.1 Equipotential surface and plumb lines near the Earth's surface [adapted from Torge (1989)] 35

Figure 3.2 Mass redistribution beneath and on the Earth's surface (from Cazevane and Nerem, 2002) 38

Figure 3.3 The space-time spectrum of principal geodynamic processes that are expected to cause temporal variations in the Earth's gravity field. [adapted from Lambert et al. (1995)] 38

Figure 4.1 Harmonic oscillation illustrated as wave 46

Figure 6.1 Flowchart on GRACE gravity field analysis using HA and PCA 57

Figure 6.2 Global distribution of (EWT) RMS value. Robinson projection 62

Figure 6.3 Global distribution of (EWT) amplitude of the annual signal. Robinson projection 62

Figure 6.4 Global trend distribution of EWT between April 2002 and May 2007. Robinson projection 63
Figure 6.5 The unreduced data show that more than 50% signal variability is captured in mode 1 and mode 4 of the PCA result is an annual signal.. 64
Figure 6.6 Trends are shown in mode 2 and mode 3 of the PCA results of the unreduced data 65
Figure 6.7 Power spectral density of the PCA shows that most energy in mode 1 of the reduced PCA for the global coverage is captured by a semi-annual signal. 66
Figure 6.8 A long term changes found in mode 5 of the unreduced PCA (left) and mode 2 of the reduced PCA (right)..... 67
Figure 6.9 Annual signals with disturbances around December 2004-January 2005 are shown in mode 1 and mode 2 of on the unreduced PCA. 71
Figure 6.10 The anomalous signals are clearly shown in mode 1 and mode 4 of reduced PCA in Sumatra-Andaman region. 71
Figure 6.11 Power spectral density of the PC of mode 4 (left) and mode 5 (right) of the unreduced PCA in the Sumatra-Andaman region. 72
Figure 6.12 Annual signals are shown in mode 1 and mode 2 of the unreduced PCA over Australia. Disturbance is visible in mode 1 coinciding with the Sumatra-Andaman earthquake event. 73
Figure 6.13 Power spectral density of the PCs of mode 3 (left) and mode 4 (right) of the unreduced PCA in Australia region..... 74
Figure 6.14 The results of the unreduced PCA over Africa. The PC of mode 1 shows clearly an annual signal (left) and the PC of mode 2 shows a small trend with a superimposed inter-annual signal (right). 75
Figure 6.15 Mode 1 of the reduced PCA over Africa shows first a negative and then a positive trend..... 76
Figure 6.16 The results of the unreduced PCA over the Antarctic region. Mode 1 (left) and Mode 2 (right) show trends related to ice mass loss and gain. 77
Figure 6.17 Mode 1 (left) and mode 2 (right) of the unreduced PCA show the largest variability in this area is captured by the annual signal. 79

Figure 6.18 The results of unreduced PCA over Arctic region. Mode 1 (left) clearly shows trend and mode 2 (right) shows annual signal. 80
Figure 6.19 Mode 2 of the reduced PCA indicates accelerated mass loss has occurred in large part of the Arctic region over the last two years. 81
Figure 6.20 The results of the unreduced PCA over Greenland. Mode 1 (left) clearly shows a trend and mode 2 (right) shows an annual signal with trend over the first two years. 83
Figure 6.21 Mode 2 of the reduced PCA shows a possible long-periodic mass variations over Greenland. 83
Figure 6.22 The results of the unreduced PCA over South Asia. Mode 1 (left) clearly shows an annual signal and mode 2 (right) shows a trend that presumably is related to the Sumatra-Andaman earthquake. 85
Figure 6.23 The results of the unreduced PCA over North America. Mode 1 (left) clearly shows a significant trend and mode 5 (right) shows low-frequency signal. 86
Figure 6.24 Mode 2 and mode 3 of unreduced PCA over Central Europe show the trends that distributed in different part of the region. 88

LIST OF TABLES

Table 1.1 Static field: Improved geoid and gravity commission errors after GRACE and GOCE [adapted from Rummel (2005)] 6

Table 2.1 GRACE science payload status (Tapley et al., 2004b) 12

Table 2.2 The anticipated geoid height errors derived from monthly GRACE data (GFZ Postdam, 2008) 15

Table 2.3 Available Level-2 data at GRACE data centres (JPL NASA, 2008) 20

Table 2.4 Global geopotential models derived from GRACE data 27

Table 3.1 Time variable gravity field, scientific requirements [Beutler et al. (2003)] 39

Table 3.2 Elastic love numbers taken from Wahr et al. (1998) 42

Table 6.1 CSR RL04 GRACE Level-2 data, gray (no): no observation; red (nd) : no data; green (du) : data are used ; yellow (dnu) : data available but not be used 56

Table 6.2 Variability of the five most dominant signals for global coverage of the unreduced PCA and the reduced PCA. 67

Table 6.3 Overall variability taken up by trend and annual signal in each region. . 68

Table 6.4 More than 5M earthquakes in Sumatra-Andaman region between April 2002 and May 2007 compiled from USGS. 70

Table 6.5 Variability of the five most dominant signals in the Sumatra-Andaman region of the unreduced PCA and the reduced PCA. 70

Table 6.6 Variability of the five most dominant signals for the Australia region of the unreduced PCA and the reduced PCA. 74

Table 6.7 Variability of the five most dominant signals for the Africa region of the unreduced PCA and the reduced PCA. 76

Table 6.8 Variability of the five most dominant signals for the Antarctic region of the unreduced PCA and the reduced PCA. 78

Table 6.9 Variability of the five most dominant signals for the South America region of the unreduced PCA and the reduced PCA. 79
Table 6.10 Variability of the five most dominant signals for the Arctic region of the unreduced PCA and the reduced PCA. 82
Table 6.11 Variability of the five most dominant signals for the Greenland of the unreduced PCA and the reduced PCA. 84
Table 6.12 Variability of the five most dominant signals for the South Asia region of the unreduced PCA and the reduced PCA. 85
Table 6.13 Variability of five most dominant signals for the North America region of the unreduced PCA and the reduced PCA. 87
Table 6.14 Variability of the five most dominant signals for the Central Europe region of the unreduced PCA and the reduced PCA. 88

LIST OF ACRONYMS

ARISTOTELES	Application and Research Involving Space Techniques to Observe the Earth's fields from Low Earth Orbiting Satellites	31
AOD1B	Atmosphere and Ocean De-aliasing Level-1B	22
CHAMP	Challenging Mini-satellite Payload	4
CSR	Centre for Space Research (University of Texas)	17
DLR	Deutsches Zentrum Für Luft und Raumfahrt	9
ECMWF	European Centre for Medium-Range Weather Forecasts	22
EIGEN	European Improve Gravity Model of the Earth by New Technique	26
EOF	Empirical Orthogonal Function	46
ESA	European Space Agency	31
EWT	Equivalent Water Thickness	55
GBVP	Geodetic Boundary Value Problem	37
GFZ	Geo Forschungs Zentrum (Postdam)	17
GGM	Global Geopotential Model	26
GOCE	Gravity Field and Steady-State Ocean Circulation Explorer	4
GPS	Global Positioning System	3
GRACE	Gravity Recovery and Climate Experiment	1
GSM	GRACE Satellite only Monthly Model	55
HA	Harmonic Analysis	6
JPL	Jet Propulsion Laboratory (NASA)	17
KBR	K-band ranging (system)	11
NASA	(US) National Aeronautics and Space Administration	9
PAGEOS	Passive Geodetic Satellite	3
PC	Principal Component	48
PCA	Principal Component Analysis	1

PGR	Post Glacial Rebound	65
POD	Precise Orbit Determination	13
POP	Principal Oscillation Pattern	92
RDC	Raw Data Centre	18
RMS	Root Mean Square	7
SDS	Science Data System	17
SHC	Spherical Harmonic Coefficients	36
SST	Satellit-to-Satellite Tracking	4

LIST OF SYMBOLS

A	Amplitude	47
b	gravitational acceleration	35
C_{lm}, S_{lm}	gravity field SHC / Stokes coefficients	20
$\bar{C}_{lm}, \bar{S}_{lm}$	fully normalized gravity field SHC	36
D	spatial-scale (half wavelength given in km)	36
δN_l	error on the average geoid height due to degree amplitude	25
$\delta C_{lm}, \delta S_{lm}$	errors in the GRACE geoid coefficients	25
$\Delta C_{lm}, \Delta S_{lm}$	time-varying gravity field	40
$\Delta\sigma(\phi, \lambda)$	surface mass density	40
$\Delta g(\phi, \lambda)$	gravity anomaly	36
F	force of gravitation	34
G	Newton's gravitational constant	34
γ	mean gravity (on reference elliposid)	36
k_l	load Love number	41
λ	longitude	36
M	the Earth's mass	36
m	order	20
$N(\phi, \lambda)$	geoid height	36
l	degree	20
L	maximum resolvable degree	36
p	maximum number of modes	50
Φ	phase	47
ϕ	latitude	36
$\bar{P}_{lm}$	fully normalized associated Legendre polynomial	36
R	the Earth's mean radius	36
r	geocentric radius	36
ρ_{ave}	average density of the Earth	40
ρ_w	density of fresh water	41

t	time	50
s	spatial position	50
T	periode	47
V	gravitational potential	35
$V(\phi, \lambda, r)$	Earth's gravity field potential	36
ω	frequency	47
$X(t, s)$	space-time field	50
$u_k(s)$	function of space	50
$c_k(t)$	function of time	50
λ_k^2	eigenvalue	52
a_{tk}	PC	52
u_{kj}	EOF	52

1. INTRODUCTION

The Gravity Recovery and Climate Experiment (GRACE) satellite mission has provided significant information on the static as well as time variable part of the Earth's gravity field. With monthly temporal resolution and spatial resolution of $\sim$ 200-500 km (e.g., Wahr et al., 1998; Nerem et al., 2003; Ramillien et al., 2004; Han et al., 2004; Tapley et al., 2004b), GRACE is capable of mapping the spatio-temporal variations of the Earth's gravity field with unprecedented accuracy (e.g., 2-3 mm for geoid height) and almost global coverage. The GRACE mission has been operational for over five years and has collected 64 monthly gravity field solutions (as of January 2008), which makes it possible to apply statistical analysis techniques such as the principal component analysis (PCA) to the data.

This thesis investigates the spatial and temporal variations of the Earth's gravity field derived from the GRACE data by the application of PCA. This will be one of the first studies that apply the PCA to the time-variable Earth's gravity field since this technique is rarely used in the field of gravity signal analysis. In this chapter, a brief overview of the GRACE satellite mission, time-variable gravity signal and the PCA will be given. The main objectives of the research and the thesis outline will be presented in Sections 1.2 and 1.3, respectively.

1.1 Background

One of the objectives of geodetic science is to determine the Earth's gravity field and its temporal variations (e.g., Vaníček and Krakiwsky, 1986). In geodesy, this information is needed to transform geodetic observations made in the real (physical) space (which is affected by gravity) to a geometrical space (e.g., an ellipsoid of revolution). Spatial variations in the Earth's gravitational field, which reflect the non-uniform density distribution of the Earth (e.g., Garland, 1977), also have been studied in other Earth sciences such as geophysics, geology, oceanography and climatology (e.g., Hofmann-Wellenhof and Moritz, 2005). Re-

cently, temporal changes of the Earth's gravity field have gained a lot of interest as they are taken as indicators of global environmental changes such as sea level and climate change (e.g., Chao and O'Connor, 1988; Cazevane et al., 1999; Leuliette et al., 2002); the GRACE mission has been brought to the attention of all geosciences and the wider community.

The knowledge of time-variable gravity has been significantly improved by the introduction of space-based observation techniques, which started with the launch of the first artificial satellite Sputnik in 1957 (e.g., Seeber, 1993; Nerem et al., 1995; Dickey et al., 1997; Torge, 2001). In principle, each satellite can be regarded as a sensor for spatial and temporal gravity changes since its orbit is affected by Earth's gravity field. However, due to type, characteristic and altitude of each satellite, not all can be used specifically for Earth's gravity field monitoring. In the early 1980s, the idea to develop a gravity dedicated satellite mission emerged. Currently, GRACE is one of the gravity dedicated satellite missions that has collected the nearly global information of the Earth's gravity field continuously for over five years. This has sparked many new applications and methods being applied to the GRACE data to get a better understanding of the dynamics of the Earth.

1.1.1 Static and Time-variable Gravity

There are two aspects of the Earth's gravity field: static gravity and time-variable gravity. Static gravity treats the Earth's gravity field as steady-state or invariable with time, even though it has small temporal variations (e.g., Biro, 1983; Dickey et al., 1997; Dickey, 2001). Static gravity field is also known as mean gravity field, as it is determined by the long-term average distribution of the mass within the Earth. The assumption of static gravity (in terms of long-term average) is mostly violated by irregularities of the solid Earth that are caused by long-term processes that occur on time scales of thousands to millions of years and over a wide range of spatial scales, from global (10,000 km) for mantle convection to regional (30 km) for tectonic, magmatic and sedimentary processes (e.g., Dickey et al., 1997).

The time-variable gravity aspect considers the Earth's gravity field as changing over time. This point of view is based on the fact that the Earth's mass distribution is constantly chang-

ing over time and, applying Newton's law of gravitation (cf. Equation 3.1), gravity should also change over time. The time-variable gravity refers mainly to short-term gravity variations, which are the result of mass re-distribution in the atmosphere, oceans, hydrosphere, cryosphere and within the Earth, or of mass exchange between these component (e.g., Dickey et al., 1997; Wahr et al., 1998; Rummel, 2005). Practically, the magnitudes of short-term variations of the Earth's gravity field are very small (in comparison to the magnitude of the Earth's gravity field); they range in terms of time from short periodic (sudden events, sub-daily, daily, seasonal and annual) to long periodic and secular events (e.g., Biro, 1983; Rummel, 2005). Therefore, to observe the broad range of time-variable gravity, dense temporal and spatial coverage and highly accurate measurements are necessary. This can be acquired by space techniques (e.g., Dickey et al., 1997), such as the GRACE satellite mission.

1.1.2 Dedicated Satellite Missions for the Earth's gravity field

Starting first with Sputnik in 1957, artificial satellites have been used for geodetic purposes such as positioning and Earth's gravity field determination (e.g., Nerem et al., 1995; Torge, 2001; Hofmann-Wellenhof and Moritz, 2005). The analysis of satellite orbit perturbations, which reflect the varying forces acting on the satellite, can be used to determine global gravity field models by inversion techniques (e.g., Balmino, 2001). Various methods have been developed to collect the information of satellite orbit perturbations, primarily through tracking the satellite's orbit.

Tracking satellite orbits between 1958 and 1970 was done by optical-photographic observation, such as BC4 cameras of Passive Geodetic Satellite (PAGEOS). Laser ranging and altimetry (doppler positioning) methods were developing in the 1970s; for example, the TRANSIT system. These methods not only refined satellite orbits observation techniques, but also increased the accuracy of the data , which made it possible to measure geodynamical phenomena such as crustal deformation. The development of NAVSTAR Global Positioning System (GPS) around 1980 also improved satellite-to-satellite tracking (SST) methods through precise orbit monitoring. However, by using those conventional techniques, the accuracy needed specifically for geodetic purposes that is mGal gravity anomaly and mm geoid

height yet have not been achieved. Therefore, a satellite mission that is specifically dedicated to gravity mapping was required.

Space technique gravity mapping missions can amplify insight to both static and time-variable aspects of the Earth's gravity field. With such mission a global extent and homogeneous quality of the gravity field would be obtained, without geographic or geopolitical limitations as surface gravity anomaly surveys might do (e.g., Dickey et al., 1997). To map the gravity field with space techniques, two broad categories of dedicated gravity satellite missions can be considered: gravity gradiometry, which measures the differences in acceleration of two masses within the same spacecraft; and satellite-to-satellite tracking (SST), which utilizes differential tracking of two satellites (e.g Dickey et al., 1997; Rummel et al., 2002). Figure 1.1 illustrates some different SST concepts, which are described in more detail below.

The new era of gravity dedicated satellite missions began with the launch of the Challenging Mini-satellite Payload (CHAMP) satellite mission in July 2000. This mission adopted high-low SST using GPS and on-board accelerometer combined with a low-altitude and near polar orbit (e.g., Reigber et al., 2003). GRACE is the second satellite mission that is designed to map the Earth's gravity field with an expected lifetime of five years (e.g., Tapley et al., 2004a; Wahr et al., 2004; Kusche and Schrama, 2005; Fengler et al., 2006; Hinderer et al., 2006), although recently the mission has been extended until early 2010 (e.g., Chen et al., 2006a). GRACE measures the Earth's gravity field using the low-low SST mode and its satellite constellation, which comprises of two satellites, is tracked by GPS. The time-variable gravity is obtained through the measurement of the changing distance between the two satellites using a very precise K-band microwave ranging system. The GRACE mission looks at both the static and the time-variable part of the Earth's gravity field whereas CHAMP mostly looks only at the static field.

Gravity gradiometry combined with SST will be realized by a future Gravity field and Ocean Circulation and Explorer (GOCE) satellite mission that is anticipated to be launched in 2008 (e.g., European Space Agency, 2007). This mission is designed to observe the static gravity field of the Earth with an unprecedented geoid accuracy of several centimeters and a mini-

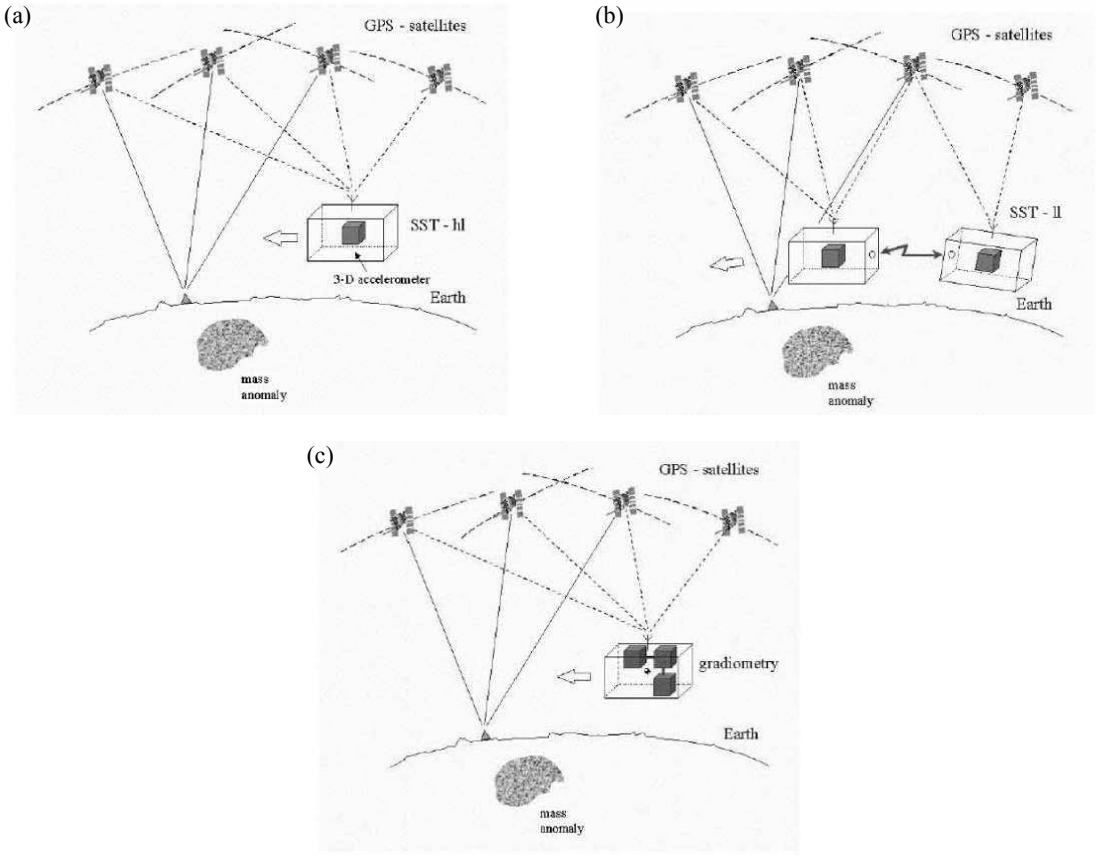

Figure 1.1: Concept of satellite-to-satellite tracking : (a) in the high-low mode (SST-*hl*) (b) in the low-low mode (SST-*ll*) (c) satellite gradiometry combined with SST-*hl* (Rummel et al., 2002)

mum resolution of 65 km (e.g., Rummel, 2005; Han et al., 2006b). GOCE satellite will be equipped with onboard gradiometer to measure the Earth gravity gradient tensor and GPS receivers to determine its precise orbit.

With the completion of the dedicated gravity satellite mission, particularly GRACE and GOCE, the knowledge of the global gravity field and its temporal variation will improve considerably. The remaining commission errors in gravity and geoid height with respect to certain spatial scales as presented by Rummel (2005) are summarised in Table 1.1.

Table 1.1: Static field: Improved geoid and gravity commission errors after GRACE and GOCE [adapted from Rummel (2005)]

Geoid (mm)	Gravity (mgal)	Spatial scale (km)	
45	2.0	200	variable gravity
10	0.2	100	
1	0.03	65	static gravity

1.1.3 PCA

PCA is a classical statistical method that reduces the dimensionality of data sets consisting of large numbers of interrelated variables, while retaining as much as possible the variation present in the data set (e.g., Jolliffe, 2002). In meteorology and oceanography, PCA is a common tool for the analysis of the spatial and temporal variability of physical fields (e.g., Preisendorfer, 1988). This technique decomposes a given time varying field in modes of variabilities, in such a way that the most dominant parts of the variance can be retrieved from only a few modes. For a spatio-temporal signal each mode will consist of a time series (principal component) and its associate spatial mode (empirical orthogonal function). Importantly, PCA does not require any pre-setting as are required by other analytical techniques such as harmonic analysis (HA). Moreover, the PCA is also capable to viewing the whole field of the data set (ie. spatial field and time field).

For the GRACE data, the application of PCA have been done by Rangelova et al. (2007); Rangelova and Sideris (2007) and Viron et al. (2006). Rangelova et al. (2007); Rangelova and Sideris (2007) applied PCA to reveal the hydrology signal in Canada, whereas Viron et al. (2006) have been doing a global analysis by applying PCA to find the dominant climate signal from the GRACE data. However, different from those studies, this research will apply PCA not only to the original GRACE data but also to the data that has been reduced by the physical meaningful signal such as annual signal and trend. The reduction parameters will be computed using the HA technique.

1.2 Research Objectives

The primary objective of this research is to analyse the spatial and temporal variability of the Earth's gravity field provided by five years (April 2002 to May 2007) of monthly GRACE static gravity field solutions. This is done by applying HA and PCA to the residual (with respect to the five year average) of the GRACE gravity field solutions. The results are used to analyse the most dominant spatial and temporal patterns of variability of the Earth's gravity field.

In particular, the objectives of the research are:

1. Analysing the global variability of the Earth's gravity field by deriving statistical values (e.g., RMS) and applying the HA (e.g., trend and annual signal).
2. Performing a global analysis of the spatial and temporal variability of the Earth's gravity field using the PCA. This will use five years of GRACE data covering nearly the whole globe. The results of this analysis will be global patterns of the Earth's gravity field variability and all dominant signals that appear in the PCA results.
3. Performing localized studies in areas of high variability and/or with interesting geophysical processes. This will be done by applying PCA and/or harmonic analysis including the determination of linear trends only over those areas.
4. Analysing anomalous (a-periodic) behavior by removing geophysically meaningful signals such as trend and annual signals.

1.3 Thesis Outline

This thesis consists of seven chapters. Chapter 1 (this chapter) describes the objectives of the research and provides some elementary information of the GRACE satellite mission and the PCA. Detailed information on the GRACE satellite mission is presented in Chapter 2, which includes the objectives and techniques used by this mission. Various applications of the GRACE data in Earth sciences studies are also described here.

In Chapter 3, theories, studies and highlights related to spatial and temporal variations of the Earth gravity field are reviewed. The past and historical studies about the dynamic Earth's underlie this chapter. The Earth's mass redistribution that causes the changes in the Earth's gravity field are explained. Some selected research of the time-variable gravity field will also be presented to give a broad overview of the subject.

Techniques for analysing spatial and temporal variability such as HA and PCA are described in Chapter 4. HA is used to deduce some patterns within the gravity signals that have physical meaning such as trend and annual signal. Statistical techniques to analyse the spatial and temporal variability of the Earth's gravity field are briefly illustrated here. Chapter 5 provides the basic theory of PCA and how it can be used to analyse the spatial and temporal variability of the Earth's gravity field. In this chapter also some other applications of PCA in meteorology and hydrology are presented.

All numerical results of this research are presented and discussed in Chapter 6. This chapter also includes the data and methodology that have been used. The GRACE data are described and the whole analysis process is clearly presented. Analyses are performed on the global and local scale. However, local scale analyses are only performed in areas that have interesting signals. Some analyses are also performed by considering geophysical processes; for instance in-depth analyses are performed in some areas that presume to have strong influences from geodynamic event (e.g., Mikhailov et al., 2004), such as the big Sumatra-Andaman earthquake in late 2004. A summary of the most important results and some conclusions of the thesis are provided in Chapter 7. This chapter also provides an outlook and recommendation for future research.

2. THE GRACE SATELLITE MISSION

This chapter describes the GRACE satellite mission; the technology and techniques that are used to measure the Earth's gravity field, and the GRACE data applications in Earth sciences. Section 2.1 expounds on the GRACE satellite and technology applied by the mission. How the GRACE maps the Earth's gravity field will be explained in Section 2.2. The GRACE data products and errors are described in Sections 2.3 and 2.4, respectively. The Earth's gravity field models, derived from GRACE data, are presented in Section 2.5 and followed by GRACE's data applications in Earth sciences in Section 2.6. Section 2.7 presents other dedicated gravity satellite missions before and after GRACE.

2.1 GRACE Satellites and Technology

The GRACE satellite mission, which is a joint partnership between the National Aeronautics and Space Administration (NASA) in the United States and Deutsche Zentrum Für Luft und Raumfahrt (DLR) in Germany, was launched on 17 March 2002 from the Russian Plesetsk cosmodrome (UTCSR, 2008; JPL NASA, 2008; GFZ Postdam, 2008). Initially, the mission's lifetime was anticipated to be five years (e.g., Tapley et al., 2004a; Wahr et al., 2004; Kusche and Schrama, 2005; Fengler et al., 2006; Hinderer et al., 2006). Recently, the operation has been extended until early 2010 (e.g., Chen et al., 2006a). GRACE is the second satellite mission, after CHAMP, that is dedicated to Earth's gravity mapping (e.g., Rummel et al., 2002; Rummel, 2005) and the first mission that has continuously mapped the static and time-variable part of the Earth's gravity field over several years, with a near-global coverage.

The scientific objective of the GRACE satellite mission is the determination of the global Earth's gravity field with 30 days (monthly) temporal resolution and spatial resolution of $\sim 200 - 500$ km (e.g., Wahr et al., 1998; Nerem et al., 2003; Ramillien et al., 2004; Han et al., 2004; Tapley et al., 2004b). GRACE has now continuously observed both the static

and time-variable part of the Earth's gravity field for over five years. The extension of the GRACE mission which is until 2010, will improve information about the Earth's gravity field.

The GRACE satellite constellation consists of two identical satellites (called GRACE A and GRACE B) on near-polar orbits at initially 500 km altitude and 89.5° inclination. The orbit was chosen in order to get a homogeneous and global coverage of the Earth that is necessary for a precise estimate of the gravitational geopotential (GFZ Postdam, 2008). The initial 500 km altitude was chosen in order to guarantee a multi-year mission duration even under severe solar activity conditions and to get a good compromise between gravity field solutions (better gain from lower altitude) and atmospheric/ionospheric applications (better gain from higher altitude). The predicted natural decay of the GRACE's orbit for the five year mission, which depends on the magnitude of the actual solar activity cycle, is illustrated in Figure 2.1. The decay may amount to more than 200 km for a high activity scenario or only 50 km for a low activity scenario (GFZ Postdam, 2008). Up until January 2007, GRACE had lost approximately 27 km of its altitude (UTCSR, 2008); thus, according to Figure 2.1, the mission's life-time will be well extended beyond the anticipated five years.

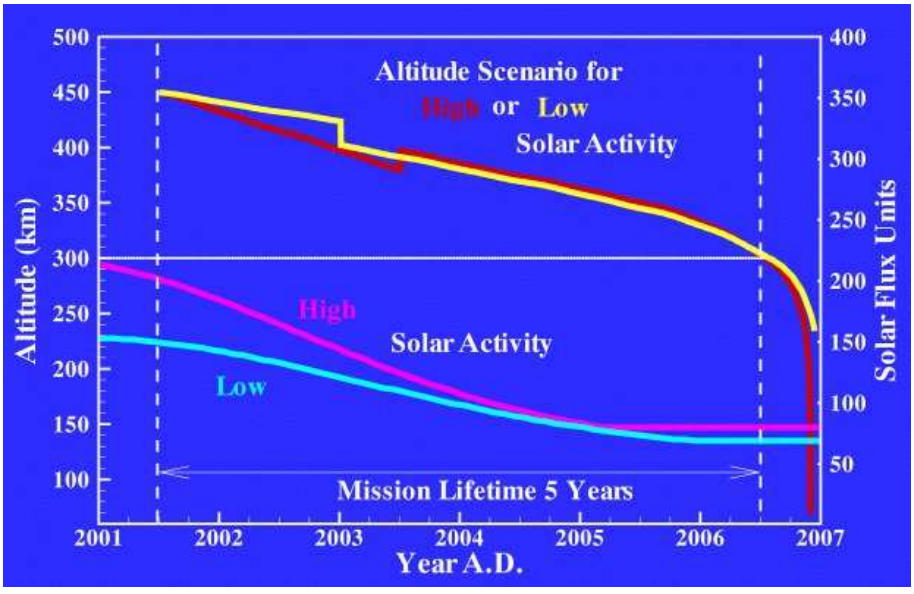

Figure 2.1: GRACE's altitude decay scenario (GFZ Postdam, 2008)

GRACE's twin satellites are separated from each other by approximately 220 km along-track distance, and linked by a highly accurate inter-satellite K-band microwave ranging system (KBR). The flight configuration of the GRACE satellite can be seen in Figure 2.2. Each satellite, in addition to the internal ranging system, also carries global positioning system (GPS) receivers and attitude sensors (e.g., Tapley et al., 2004b). The payload instruments, which are identical for the two satellites, are summarised in Table 2.1 and the technical components of GRACE spacecraft are presented in Figure 2.3. Detailed explanations about the GRACE spacecraft can be obtained from http://www.gfz-potsdam.de/pb1/op/grace/.

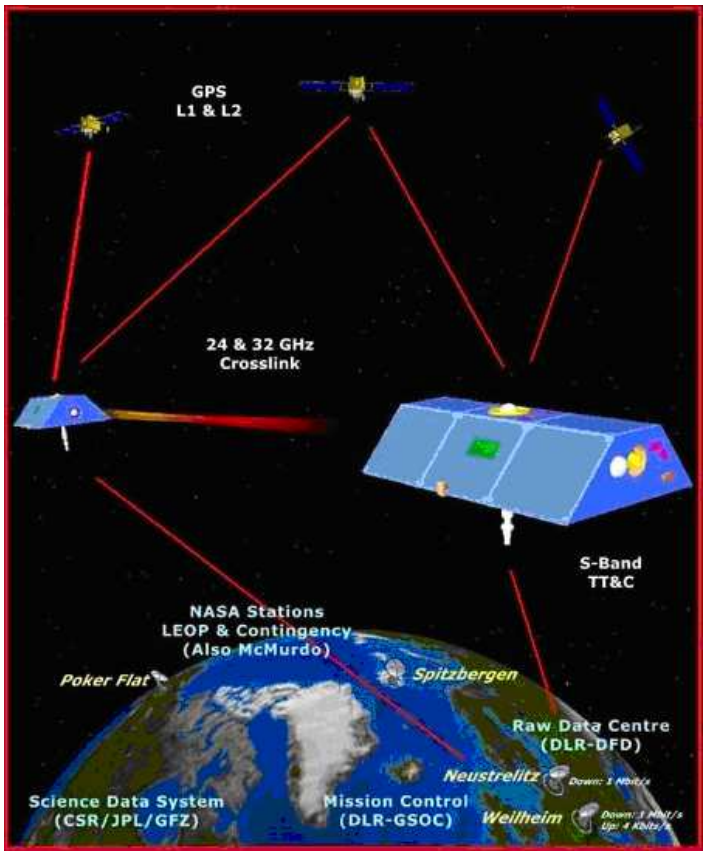

Figure 2.2: GRACE: Flight configuration
(http://www.csr.utexas.edu/grace/mission/flight_config.html)

The KBR is an essential instrument to measure the precise change in distance between the two GRACE satellites with a 1 μms^{-1} precision. The KBR obtains the range at a sampling rate of 10 Hz. The KBR system consists of:

– a single horn antenna for transmission and reception of the dual-band K-band and Ka-band microwave signals (24 and 32 GHz respectively);

– an ultra stable oscillator serving as a frequency reference;

– a microwave assembly for up-converting the reference frequency, down-converting the received phase from the other satellite to approximately 2 MHz and for implying and mixing the received and the reference carrier phase;

– an instrument processing unit that is used for sampling and processing the digital signal from the K-band carrier phase signals and data from the GPS space receiver, the accelerometer and the star camera assembly.

The frequencies of the KBR on each satellite are shifted by 500 KHz to avoid cross-talk between transmitted and received signals and to offset the down-converted signal from zero frequency. Each satellite also transmits carrier phase signals on two frequencies, allowing for ionospheric corrections. Multipath effects are reduced by sharp spacecraft pointing requirements (<1 μrad) and representative antenna on the spacecrafts' front panel.

Table 2.1: GRACE science payload status (Tapley et al., 2004b)

Instrument	Measurements (Precision)	Collection rate	Status
Ranging system	K- & Ka-band phase (<10 μm)	10 Hz	In-flight calibration precisely aligned K-band antenna phase centre relative to attitude precisely
Accelerometer	Linear accelerations (10^{-11} g)	10 Hz	In-flight calibration precisely aligned accelerometer with attitude sensors. The satellite CG is within $\sim 50\mu$m of the accelerometer proof-mass
Star cameras	Quaternions (80 - 200 μrad)	1 Hz	Routine dual-head/1-Hz operation since Feb 2003
GPS receiver	L1 & L2 phase (7 mm)	1 Hz for L1 & L2	
	CA & P1 pseudo-range (20 cm)	0.1 hz for CA & P1	

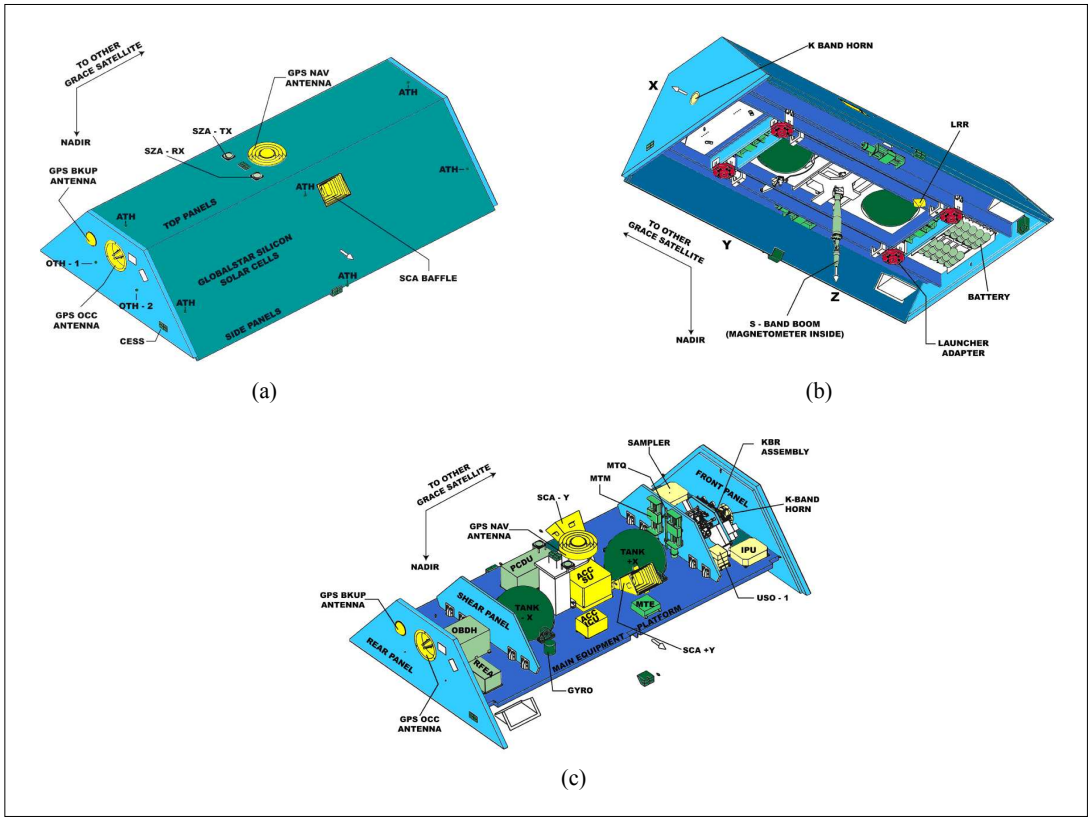

Figure 2.3: The GRACE satellite (a) front view, (b) bottom view, (c) internal view (http://www.gfz-potsdam.de/pb1/op/grace)

The accelerometer measures all non-gravitational accelerations due to atmospheric drag, solar radiation pressure and attitude control activator impulses initiated by the attitude and orbit control system. In combination with the sub-millimeter inter-satellite distance observed by the KBR and the accurate satellite position measured by the onboard GPS receiver, the potential difference accuracy can be determined in the level of 10^{-3} m^2s^{-2} (Han et al., 2003).

By satellite-to-satellite tracking between GPS and GRACE satellite, the onboard GPS receiver gives a precise orbit determination (POD) of the GRACE satellite with several centimeter accuracy and provides data for atmospheric and ionospheric profiling. A navigation solution which is comprised of position, velocity and a time mark is derived on board as it is required for the satellite attitude and orbit control system. The GPS receiver assembly consists of two omnidirectional POD-antennas (one primary in zenith, and one backup in the aft-direction), one high-gain helix antenna with 45° field of view in the aft-direction and a receiver electronics and processing box. The GPS receiver uses up to 16 channels, of which up

to 12 channels are for precise orbit determination and the remaining four are for occultation measurements.

The zenith-pointing POD-antenna is used for the simultaneous tracking of up to 12 individual GPS satellites to derive the onboard navigation solution and to collect the tracking data for on-ground precise orbit determination. To derive the orbital positions of the GRACE satellites, the position, velocity and time mark, both the carrier phases, and the pseudo ranges from the GPS satellites are tracked. The aft-pointing POD antenna serves as a redundant source for orbit determination in case of a failure of the zenith antenna.

The aft-pointing helix-antenna is Earth-limb pointing. Usually, the signals of one GPS satellite will be tracked with high time resolution during the last phases of its occultation by the Earth's atmosphere while the non-occulted GPS satellite serves as a reference and will be tracked in parallel. This allows for the derivation of atmospheric parameters such as pressure, temperature and humidity with high vertical resolution by observing the signal deceleration and attenuation of the carrier phases of the occulted satellite under the influence of the neutral layers of the atmosphere. Using both GPS satellite frequencies (L1 and L2), the ionospheric effects, which are superimposed on the influence of the neutral atmosphere, can be separated.

The laser retro reflector is a passive payload instrument used to reflect short laser pulses of visible or near-infrared wavelengths transmitted by committed laser ground stations. The direct distance between the GRACE satellite and the ground station can be measured with an accuracy of 1-2 cm. The laser retro reflector data will be used for precise orbit determination in combination with GPS tracking data for gravity field recovery and calibration of the onboard GPS receiver.

The star camera assembly is used for the precise orientation of the satellite within the attitude and orbit control system and for the correct interpretation of the accelerometer measurements. The instrument consists of two simultaneously operated DTU star cameras with a field of view of 18° by 16° and one data processing unit (DPU). The star camera will measure the spacecraft's attitude to an accuracy better than 0.3 μrad (with the goal of 0.1 μrad) by autonomous detection of star constellations using an onboard star catalog. The coarse Earth

and Sun sensor (CES) system provides an omni-directional, reliable and robust, coarse state of the Sun and the Earth for initial acquisition and safe mode. One CES sensor is mounted on each of the six sides of the satellite. The resulting Earth vector has an accuracy of $\sim$5-10°and the Sun vector $\sim$ 3-6° (there is a dependence upon orbit geometry).

An ultra stable oscillator system is used to generate the frequency of the K-band ranging system. It needs to have a long term stability of better than $1\text{x}10^{-10}$ per day after 30 days. The centre of mass trim assembly (CMT) is used to adjust the offset between the satellite's centre of mass (COM) and the centre of the accelerometer's proof-mass. In order to reach less than 50 m in all three axes, the CMT will adjust the COM with a step size of 10 m or less over a total range of ±2 mm in each axis.

The technology and instrumentation implemented in the GRACE satellite mission are dedicated to obtain high accuracy in geoid heights. The anticipated geoid height errors of GRACE are presented in Table 2.2.

Table 2.2: The anticipated geoid height errors derived from monthly GRACE data (GFZ Postdam, 2008)

Harmonic degree	Geoid height error [mm] (per degree)	Cumulative geoid height error [mm] (from n=3)
n=2	< 0.10	-
$3 \leq n \leq 10$	< 0.01	< 0.02
$10 \leq n \leq 70$	< 0.15	< 0.40
$70 \leq n \leq 100$	< 1.50	< 3.50
$100 \leq n \leq 150$	< 65.0	< 200.0

2.2 GRACE Gravity Field Measurement Concept

GRACE maps the gravity field by sensing spatial and temporal mass variation on the Earth's surface as the two satellites pass over the surface. It is well known that gravity is a function of mass distribution according to Newton's Law of Gravitation (cf. Equation 3.1). Mass is also related to density; thus, the amount of materials located in any one place affects gravity as well. For example, rock is denser than water, and water in its liquid form is denser than in its solid form. Since the Earth has various topographic features such as mountains, valleys, and underground caverns, the Earth's mass is not evenly distributed and different physical features can be distinguished. There are lumps observed in the Earth's gravity field resulting from this uneven distribution of mass on the Earth's surface, and GRACE will map these anomalies.

GRACE measures the changing Earth's gravity field by the measurement of the changing distance between the two satellites using very precise KBR. As the GRACE satellites orbit the Earth, the precise speed of each satellite and the distance between them are constantly monitored via the microwave KBR instrument. As the gravitational field changes beneath the satellites - correlating to changes in mass distribution on and beneath the Earth's surface - the distance between the two satellites changes. This is the fundamental quantity used to solve for the Earth's global (static and temporal) gravity field (Han et al., 2004). Figure 2.4 illustrates how GRACE measures the Earth's gravity field.

Combining the tracking data from the KBR and GPS (e.g., Tapley et al., 2004a,b), global gravity field solutions are produced. The KBR provides information on the relative motion of the GRACE satellites. GPS receivers tie each GRACE satellite to the terrestrial reference frame (e.g., Luthcke et al., 2006) and also record the orbit information for data processing purposes.

GRACE gravity field solutions can also be derived only from inter-satellite range measurements, as has been done by Rowlands et al. (2005) and validated by Luthcke et al. (2006). According to Luthcke et al. (2006), gravity field solutions derived from inter-satellite range data are very similar with the GRACE project gravity field solutions from degree 5 through

degree 12. They even have two significant improvements; namely, more realistic recovery of information at the very lowest degrees and fewer problems above degree 14, especially at order 15 and 16 (the source of striping error in standard GRACE models).

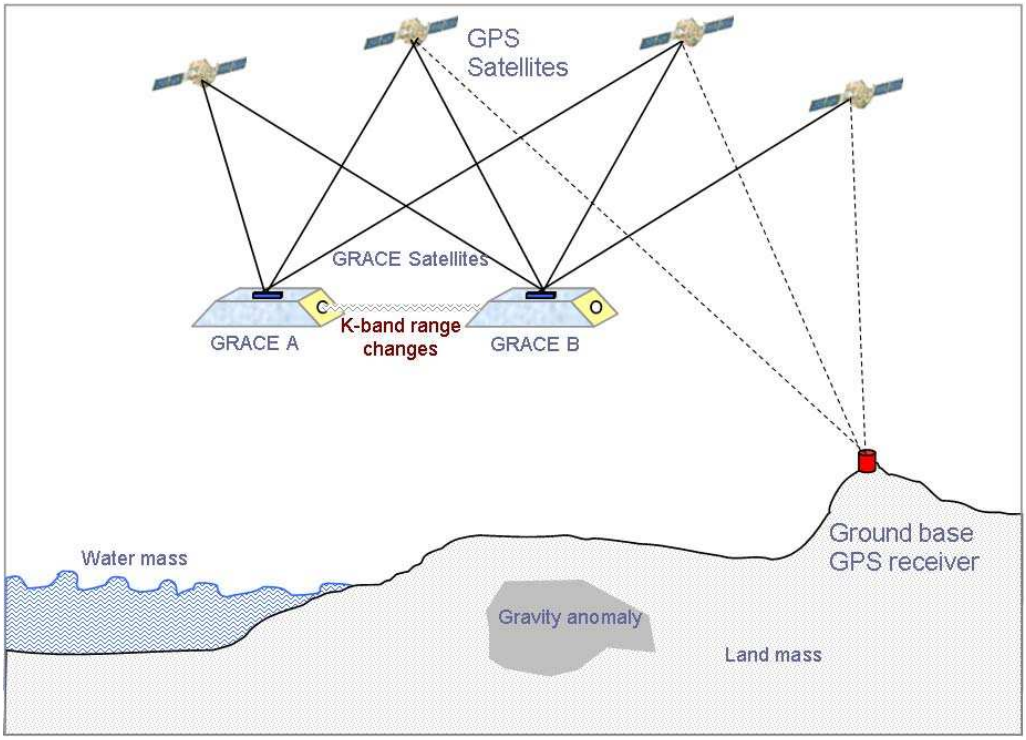

Figure 2.4: GRACE gravity field measurement [adapted from UTCSR (2008)]

2.3 GRACE Science Data System

The GRACE science data system (SDS) is a distributed data system. The SDS development, data processing and archival is shared between Centre for Space Research (CSR) University of Texas, GeoForschungsZentrum Postdam (GFZ) and the Jet Propulsion Laboratory (JPL) (Bettadpur, 2007). The SDS is designed to perform all tasks for gravity field processing through the production of monthly gravity field solutions. The general data flow for the GRACE data processing is presented in Figure 2.5. Based on the information and processing method, the GRACE SDS provides three basic levels of data: GRACE level-0 data, GRACE level-1 data and GRACE level-2 data.

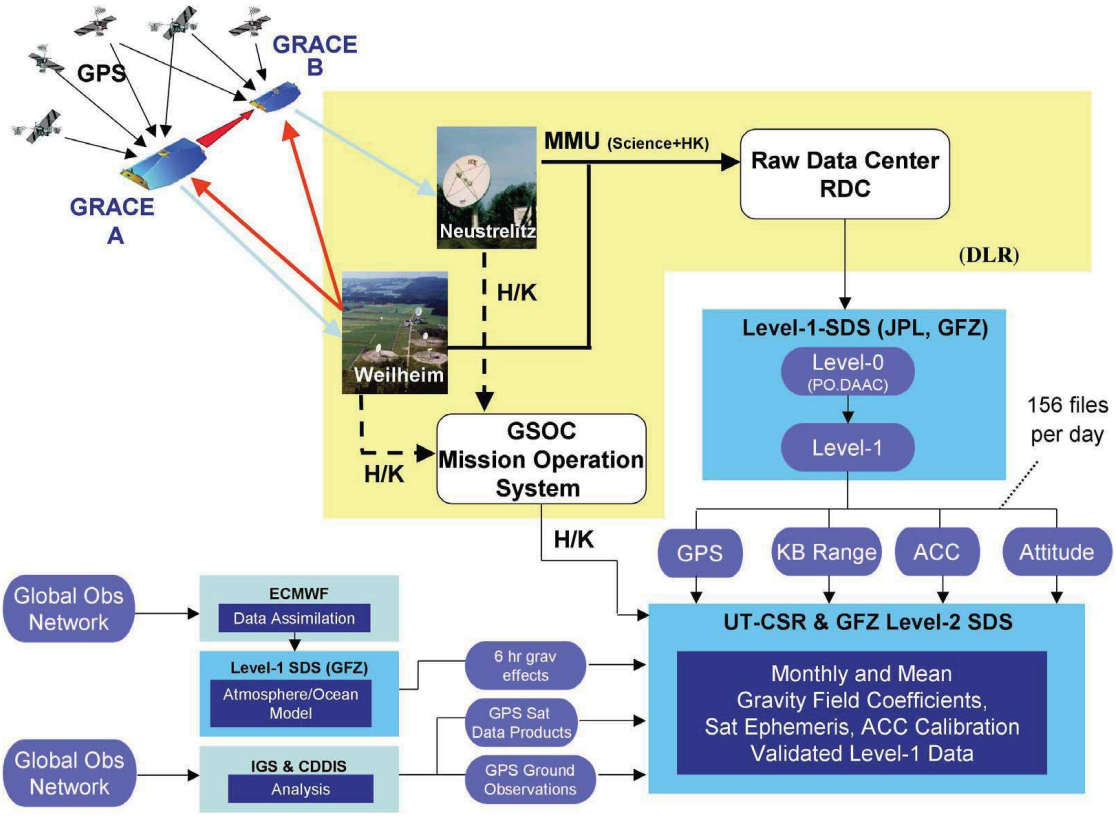

Figure 2.5: GRACE science data flow (UTCSR, 2008)

2.3.1 GRACE Level-0 Data

The level-0 data products are the results of telemetry data reception, collection and decommutation by the GRACE raw data centre (RDC) at DLR in Neustrelitz (Bettadpur, 2007; GFZ Postdam, 2008). From each pass, from each satellite, the data streams are separated into two files, one containing the science data and the other containing the housekeeping data. These two files are defined as the level-0 data products and stored in the rolling archive at RDC. The SDS retrieves the data files and extracts and reformats the corresponding instruments and ancillary housekeeping data such as GPS navigation solutions, space segment temperatures or thruster firing events. Level-0 products are available 24 hours after data reception.

2.3.2 GRACE Level-1 Data

The level-1 data are the preprocessed, time-tagged and normal-pointed instrument data. These are the K-band ranging, accelerometer, star camera and GPS data of both satellites. Additionally, the preliminary orbits of both GRACE satellites are generated. Level-1 data processing software is developed by JPL with support from GFZ (e.g., accelerometer data preprocessing). Processing of level-1 products is done primarily at JPL. An identical processing system (hardware/software) is installed at GFZ to serve as a backup system in case of hardware or network problems. This double implementation is necessary to guarantee the envisaged level-1 product delay of five days. All level-1 products are archived at JPL's Physical Oceanography Distributed Active Data Centre (PODAAC) and at GFZ 's Integrated System Data Centre (ISDC). Both archives are harmonized on a sub-daily time interval.

The GRACE level-1 data are divided into two types, namely GRACE level-1A and GRACE level-1B. The level-1A data are the result of non-destructive processing applied to the level-0 data. These data are generally reversible to level-0 except for bad data packets. Level-1B data are the result of possibly destructive or irreversible processing applied to both level-1A and level-0 data. For further scientific analysis the data will be edited and decimated from the high sample rate of the instruments to the low sample rate.

2.3.3 GRACE Level-2 Data

Level-2 data include the short term (30 day) mean gravity field derived from calibrated and validated GRACE level-1B data products. This level also includes ancillary data sets (temperature and pressure fields, ocean bottom pressure, hydrological data) which are necessary to eliminate time variabilities in the gravity field solutions. Additionally, the precise orbits of both GRACE satellites are generated. All level-2 products are archived at JPL's PODAAC and at GFZ 's ISDC and are available 60 days after the observation took place. The level-2 occultation processing systems at JPL and GFZ are not part of the GRACE SDS, but both are linked to the SDS archives for retrieval of level-1 products and ancillary ground data and for archiving of their level-2 products (total electron content, temperature and water vapour).

The level-2 processing software is developed independently by all three processing centres using already existing but completely independent software packages which are upgraded for GRACE specific tasks. Common data file interfaces guarantee a strong product validation. Routine processing is done at UTCSR and GFZ, while JPL only generates level-2 products at times for verification purposes. Even though they use many similar background models, UTCSR, GFZ and JPL use different algorithms to compute the gravity field coefficient from the raw GRACE observations (e.g., Chambers, 2006a). For recovery of temporal gravity fields (e.g., Han et al., 2004; Bettadpur, 2007), ocean tides and atmosphere, which are the two largest systematic and high (temporal) frequency signals, are assumed to be known and removed from the GRACE data.

The latest available GRACE level-2 data (by January 2008) products in the three GRACE centres are shown in Table 2.3. Each GRACE's monthly gravity field solution consists of a set of Stokes coefficients, C_{lm} and S_{lm}, complete to degree and order $\leqslant 120$. The subscript l and m are the degree and order of the spherical harmonic expansions and the horizontal scale is defined as $\sim 20,000/l$ km.

Table 2.3: Available Level-2 data at GRACE data centres (JPL NASA, 2008)

Centre	Release	Data availability	Total
CSR	R04	All months from April 2002 to October 2007, except June and July 2002 and June 2003	64 monthly solutions
GFZ	R04	All months from August 2002 to June 2007,except September and December 2002; January and July 2003; January 2004	57 monthly solutions
JPL	R04	April/May 2002 plus all months from September 2002 to July 2007, except June 2003	59 monthly solutions

Apart from those three levels of GRACE data products, several GRACE users have developed new data by putting together resources to create and distribute value-added products from the GRACE project data products. These kind of data are often called GRACE level-3 data (UTCSR, 2008). An example of level-3 data are global surface mass density changes provided by GRACE Tellus (http://gracetellus.jpl.nasa.gov/). These data are available as

user-friendly data grids, with most corrections applied, to analyse changes in the mass of the Earth's hydrologic components.

2.4 GRACE Data Limitations, Errors and Filtering Methods

According to Schrama et al. (2007) the spatial and temporal resolution of a surface mass signal observed by GRACE are limited. These limitations are the presentation of specific noise characteristics in the observations which the gravity field is derived from, the observations that are collected at 500 km above the Earth surface, the required time for the GRACE satellites to map the gravity field over the entire globe and the KBR data that are acquired along the satellite flight path. The time that is needed by GRACE to cover the entire globe (10 days) also causes an uneven distribution of the tracking data (e.g., Tapley et al., 2004a); therefore recovery process is necessary for a gravity field determination.

In addition to the limitations in GRACE data resolutions, the accuracies of GRACE measurements are also affected by various errors, including system-noise error and orbital error (e.g., Wahr et al., 1998). System noise error comprises of the error in the satellite-to-satellite microwave ranging measurements, accelerometer error and error in the ultrastable oscillator. The expected effect of these errors can be calculated and used to reformulate the accuracy of the GRACE data. Wahr et al. (2004) defined the GRACE error as the total error in the monthly gravity solutions, caused by a combination of measurement errors; these are processing errors and errors in the geophysical models that are used to de-alias the GRACE measurements before the constructing of gravity field solutions.

The aliasing error refers to the difference between the measured mean values of the gravity signal over a month and the true mean value. This error is dependent on temporal and spatial variations of the signal and the sampling provided by the satellite orbit track (e.g., Han et al., 2004; Seo and Wilson, 2005; Thompson et al., 2004). When the signals are rapidly changing in space and time, the aliasing error may be larger. GRACE data are severed from this error because it measures the change of time-varying gravity along the satellite orbit track.

Each processing of GRACE science data, in order to reduce the aliasing error, estimates are made up of updates to an *a priori* best-known geopotential model (Bettadpur, 2006). The GRACE data flow (cf. Figure 2.5) shows that in order to remove atmospheric effects from the raw data before constructing the gravity field solutions, ECMWF (European Centre for Medium-Range Weather Forecasts) meteorological fields are used. However, the errors contained in the ECMWF also contribute to the error in the GRACE mass estimates. According to Thompson et al. (2004), the magnitude of the aliasing error is strongly correlated with the power of the high-frequency variability of the geophysical model used.

GRACE time-varying gravity also affected by the short term variations in the oceans (e.g., Flechtner, 2007), even though they are much smaller that the atmospheric effects. Both the atmospheric and oceanic effects have to be removed for the (GRACE level-2) gravity field determination process. To do this, GRACE level 1-B product called AOD1B (atmosphere and ocean de-aliasing level-1b) are used and they have provided in each GRACE data center. This atmosphere and ocean mass variation models are calculated using different atmospheric fields (e.g., ECMWF) and a (barotropic) ocean model (e.g., Bettadpur, 2006; Flechtner, 2007).

The GRACE high-degree Stokes coefficients (short wavelength components) are dominated by errors that are related to the near-polar orbit ground track (e.g., Wahr et al., 1998; Chen et al., 2005). These so called correlation errors (because they imply correlations in the gravity field coefficients) and presence in the GRACE monthly solution as linear features (i.e. stripes) are generally oriented north to south (the orientation of the satellite ground tracks) (e.g., Swenson and Wahr, 2006). This error reflects a weakness in the GRACE recovery of the cross-track gravity signal (e.g., Wahr et al., 2004). In order to reduce the appearance of stripes in the maps, spatial averaging or smoothing is usually applied to the GRACE data.

Methods to smooth the GRACE data have been proposed by several authors; these are: an isotropic Gaussian filter (e.g., Wahr et al., 1998), a non-isotropic filter (e.g., Han et al., 2005c; Kusche, 2007), optimal filters based on a priori estimates of signal and measurement error variances (e.g., Swenson and Wahr, 2002; Seo and Wilson, 2005), global optimized variance-dependent smoothing (e.g., Chen et al., 2006b), and spectral-domain filtering (e.g., Swenson

and Wahr, 2006).

Isotropic filtering, also known as Gaussian smoothing, was introduced by Wahr et al. (1998) and based on Jekeli's Gaussian averaging function (e.g., Jekeli, 1981). This function was constructed to improve the estimates of the Earth's gravity field to compensate for the poorly known, short-wavelength components of the spherical harmonic coefficients. This is the common method to reduce the high degree noise in the GRACE gravity field (e.g., Wahr et al., 1998; Chen et al., 2005) for global and large scale applications. For small scale applications, e.g., small river basins, the Gaussian smoothing is less appropriate. According to Chen et al. (2006b), this is due to two main limitations of the method; namely, (i) an increased leakage associated error as the effective radius increases and (ii) Gaussian smoothing that only assigns isotropic weights in the spatial domain or only degree-dependent weights in the spectral domain. The leakage error arises from the limited range of GRACE spherical harmonics which are not corrupted by noise (e.g., Seo et al., 2006) and which falsify the spatial interpretation of the gravity field anomaly.

Shum et al. (2004) as cited in Han et al. (2005c) also argue that isotropic smoothing is not optimal for GRACE level-2 products as they inherit the spherical harmonic degree-dependent and order-dependent error characteristics associated with the high inclination of the GRACE orbit. Han et al. (2005c) introduced a non-isotropic filtering that has a degree-dependent and order-dependent spectrum. Applying the non-isotropic filtering yields improved correlation of the smoothed GRACE gravity field, which also improves resolution in latitude direction.

The global optimized variance-dependent smoothing method proposed by Chen et al. (2006b) is assumed to be more effective in recovering global surface mass changes from GRACE time-variable gravity compared to Gaussian smoothing. This method maximizes the variance ratio of mass changes over the land relative to the ocean and also produces lower levels of leakage associated with limited a range of spherical harmonics and improved spatial resolution. Like the non-isotropic filtering introduced by Han et al. (2005c), the method also assigns the degree and order dependent weights differently.

Due to different levels of errors for some local regions, it is also important to treat the error in specific regions differently. Swenson and Wahr (2002) and Swenson et al. (2003) proposed a method to minimize the sum of satellite errors and leakage errors through the construction of an optimal averaging kernel for each region. As stated in Swenson and Wahr (2002), there are four methods for constructing the averaging kernel; namely, choosing an exact (block) average, Gaussian convolution, the use of Lagrange multipliers, and minimization of the sum of satellite and leakage errors.

Research has investigated how to choose the most optimal smoothing radius (e.g., Chen et al., 2005; King et al., 2006). Chen et al. (2005) point out that the effective smoothing radius may be studied from two approaches. First is the comparison of the GRACE results with estimates from advanced geophysical models. In this case, the model prediction acts as a "ground truth" to evaluate at what spatial radius GRACE yields the best agreement with the model. Second, an optimum smoothing radius can be examined from the representation of some residuals over the ocean as the GRACE level-2 data have been de-aliased from oceanic influences. From their study, Chen et al. (2005) concluded that a 800 and 600 km Gaussian smoothing radius can efficiently remove the high-degree errors from GRACE-estimated global mass changes and geoid height changes, respectively.

2.5 GRACE Gravity Models

The Earth's gravity field is derived by the observed gravity value at every single position on the Earth's surface. Before GRACE, the long-wavelength path of the Earth's gravity field from space was determined from various tracking measurements of Earth orbiting satellites. However, the accuracy and resolution of the Earth's gravity field models derived from these measurements were limited, with most of the satellite contributions limited to wavelengths of 700 km or longer. At shorter wavelengths, the data errors were too large to be useful. Furthermore, only broad geophysical features of the Earth's structure could be detected. Consequently, improvements of the Earth gravity models at medium and short wavelengths had to be added from terrestrial and/or marine gravity observation; which were also of varying epoch, quality, and geographic coverage.

The GRACE gravity models are determined using the principle explained in Reigber et al. (2003). First, the two GRACE satellite orbits, which are based on an initial force field (Earth gravity, third bodies, observed SuperSTAR sense accelerations), are numerically integrated. Then, the linearized observation equations of the GPS-GRACE and KBR tracking data are set up, leading after accumulation over the evaluation period to a normal equation system, in a least squares sense, to be solved by matrix inversion. GPS-GRACE and KBR tracking data provide the relationship of various unknowns such as the gravity field spherical harmonic coefficients, the orbit state vector at epoch per-arc and sensor-specific parameters.

To sum up, the solution of the gravity field parameters using GRACE tracking data is based on a two-step approach (Reigber et al., 2005b):

1. Adjustment of the high GPS constellation orbits and clock parameters from ground-based tracking data;
2. GRACE orbit determination and computation of observation equations with fixed GPS spacecraft positions and clocks as from step 1.

According to Wahr et al. (2004), the accuracy of a gravity model can be described as degree amplitudes of geoid error. Following Wahr et al. (1998), the error on the average geoid heights due to degree amplitudes error is given by equation (2.1),

$$\delta N_l = a\sqrt{\sum_{m=0}^{l}(\delta C_{lm}^2 + \delta S_{lm}^2)} \tag{2.1}$$

where δC_{lm} and δS_{lm} are the errors in the GRACE geoid coefficients. δN_l^2 is the contribution to the geoid height error variance per degree l, which is a measure of the spatial scale of a spherical harmonic (cf. Section 3.1). Hence, δN_l^2 is also a measure from all terms of a given spatial scale to the variance.

A study by Wahr et al. (2004) concluded that a monthly GRACE solution has lower error than EGM96, both at low degree, where EGM96 (Lemoine et al., 1998) is constrained by decades of satellite tracking, and at degrees as high as 90 or 100, where EGM96 is constrained by

surface gravity and altimetry data. The comparison between EGM96S, EIGEN-CHAMP and EIGEN-GRACE model resolution is shown in Figure 2.6. Figure 2.7 shows the spatial appearance differences between GRIM5-S1 (Biancale et al., 2000) geopotential model, EIGEN-CHAMP and EIGEN-GRACE. However, it should be considered that those three models are based on different degree resolution.

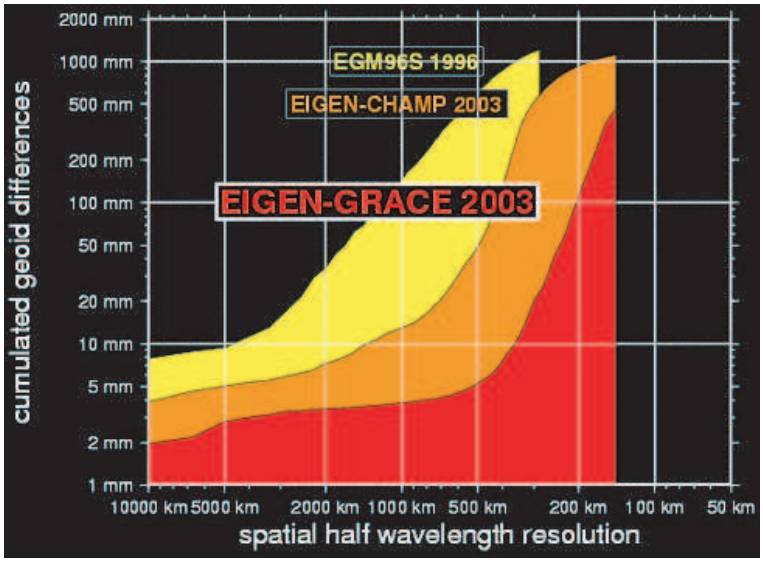

Figure 2.6: Gravity model resolutions (GFZ Postdam, 2008)

The Earth's gravity field data observed by GRACE have been used to develop better and more accurate geoid models (at the low-frequency part) to represent the Earth's physical model. The GRACE gravity models have been developed by the Centre of Space Research, University of Texas (UTCSR) and GFZ Postdam as Global Geopotential Model (GGM) and EIGEN-GRACE respectively. Initial GRACE gravity models, designated as GGM01S (UTCSR) and EIGEN-GRACE01S (GFZ), were determined using GRACE measurements (e.g., Tapley et al., 2004b, 2005). Brief description of other available global geopotential models generated by the two centres are presented in Table 2.4 (GFZ Postdam, 2008; UTCSR, 2008).

Table 2.4: Global geopotential models derived from GRACE data

Model	Max degree	Year	Developer	Description
GGM01S	120	2003	UTSCR	Estimated from 111 days (spanning April trough November 2002) of GRACE K-band range-rate, attitude, and accelerometer data.
EIGEN-GRACE01S	140	2003	GFZ	Estimated from 39 days (August and November 2002) of GRACE GPS, K-band range-rate, accelerometer and attitude data.
EIGEN-GRACE02S	150	2004	GFZ	Calculated from 110 days of GRACE tracking data.
GGM02S	160	2004	UTCSR	Based on the analysis of 363 days (April 2002 - December 2003) of GRACE in-flight data, unconstrained by any other information.
GGM02C	200	2004	UTCSR	Based on the analysis of 363 days (April 2002 - December 2003) of GRACE in-flight data, constrained by with terrestrial gravity information.
EIGEN-CG01C	360	2004	GFZ	Combined CHAMP (860 days), GRACE (200 days) and 0.5°×0.5° surface data (gravimetry and altimetry).
EIGEN-CG03C	360	2005	GFZ	Combined CHAMP (860 days), GRACE (376 days out of February to May 2003, July to December 2003 and February to July 2004) and 0.5°×0.5° surface data (gravimetry and altimetry).
EIGEN-GL04C	360	2006	GFZ	Combined GRACE and LAGEOS mission plus 0.5°×0.5° gravimetry and altimetry surface data.
EIGEN-GL04S1	150	2006	GFZ	Combined GRACE and LAGEOS mission data

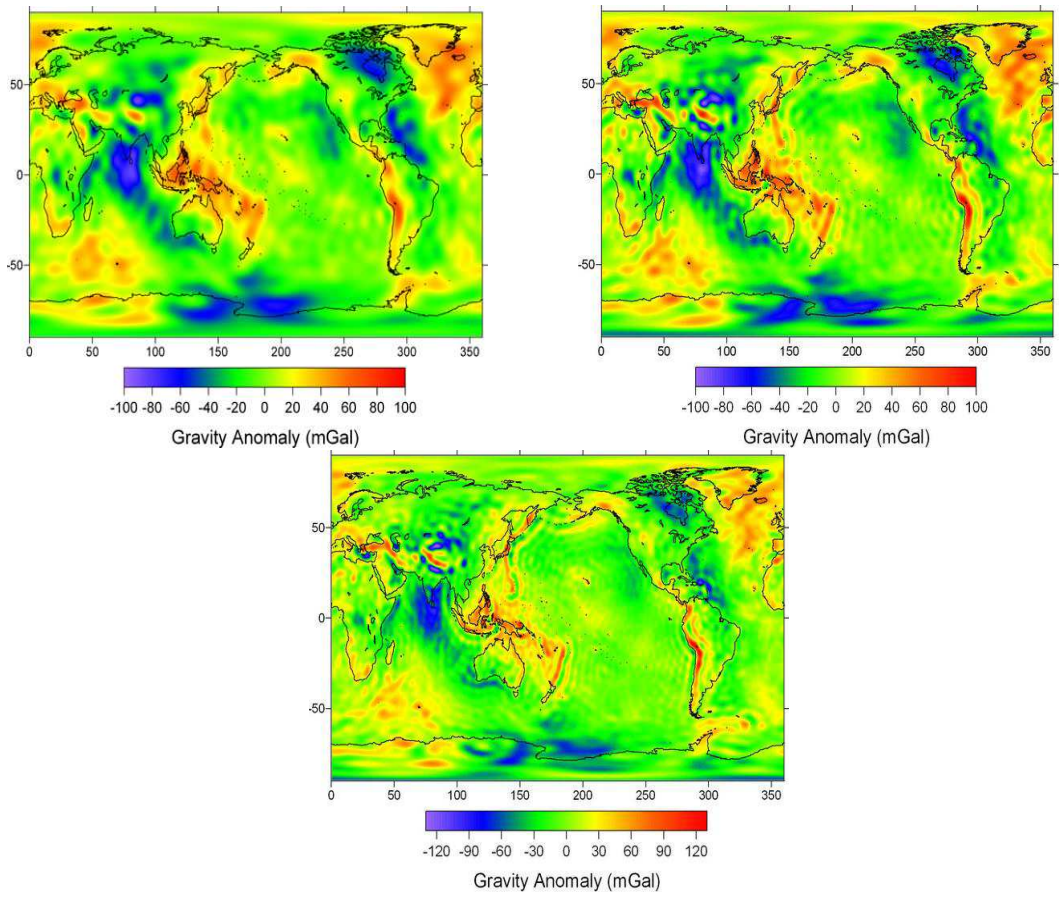

Figure 2.7: GRIM5-S1 model(top left), EIGEN-CHAMP02S model (top right) and EIGEN-GRACE01S model (bottom)

2.6 GRACE Data Applications in Earth Sciences

According to Rummel et al. (2002) and Rummel (2003), there are three types of applications of the gravity field in Earth's sciences. First, as the temporal variations of the Earth's gravity field is affected by any redistributions and exchange of mass in the Earth's system, its measurement will serve the analysis of global mass transports. Second, the gravity field variations can be directly related to ocean mass surface circulations as the geoid corresponds to the surface of a hypothetical ocean at rest. Third, geoid and gravity anomalies reflect un-modeled dynamic processes in the oceanic and continental lithosphere and in the upper mantle as they measure the deviation of the actual mass distribution from the Earth model.

The operation of the GRACE satellite mission has improved the knowledge of the Earth's gravity field for both static and time-variable aspects. Today, GRACE data has been used by scientists from various Earth sciences such as Geodesy, Geophysics, Oceanography and Meteorology.

2.6.1 Time-variable Gravity

Changes in gravity can be used to study processes involving changes in the Earth's mass distribution (e.g., Wahr et al., 2004). According to Ramillien et al. (2004), the GRACE time-variable gravity can also be useful to detect changes as a result of surface and deep currents in the oceans, change in soil and ground water storage on land, mass changes of the ice sheets and glaciers, air and water vapor mass change within the atmosphere and variations of mass within the solid part of the Earth. A study by Fengler et al. (2006) shows that GRACE time-variable data are capable of sensing signals related to high-frequency geophysical, geodetic, magnetic, and oceanographical phenomenon.

Hinderer et al. (2006) showed that seasonal changes in the gravity field detected by GRACE include large scale continental hydrological cycles. For example, the interannual gravity changes over Europe which were detected in summer 2003 can be related to the heatwave which occurred then. Interannual gravity changes from GRACE also have been studied by Andersen and Hinderer (2005) in relation to changes in continental water storage.

2.6.2 Geodynamics

A geophysical phenomena occurring during the GRACE operational period that attracted many Earth scientists is the Sumatra-Andaman earthquake in late December 2004. Bao et al. (2005), using a numerical tsunami model, assumed that the tsunami generated by Sumatra-Andaman earthquake would be detectable in the range of measurements from the GRACE satellite. This is intensified by other studies that have shown the capability of GRACE to capture earthquake signatures (e.g., Sun and Okubo, 2004; Sabadini et al., 2005; Han et al., 2006a; Ogawa and Heki, 2007; Han and Simons, 2008; Chen et al., 2007). In another area of

geophysics, the postglacial rebound and Earth's viscosity structure detected by GRACE has been studied by Velicogna and Wahr (2002) and Wahr and Velicogna (2003).

2.6.3 Hydrology

The ability of GRACE data to detect water mass variation in the atmosphere, oceans and continents has been assessed by several scientists (Wahr et al., 1998; Rodell and Famiglietti, 1999; Rodell et al., 2004; Woodworth and Gregory, 2003; Baur et al., 2007; Chambers, 2006a,b; Chambers et al., 2007; Han et al., 2005b; Ramillien et al., 2004; Schmidt et al., 2006; Seo et al., 2006; Swenson et al., 2003). Schmidt et al. (2006) state that the time-variable gravity field measured by GRACE has provided a novel data source for measuring the variation of continental water storage from space.

The GRACE capability of measuring continental water storage includes monitoring river basin variability. This is due to the resolution of GRACE gravity field is high enough to determine mass variations corresponding to hydrological signal for large river basin (e.g., Wahr et al., 1998; Swenson et al., 2003). For instance, according to Tapley et al. (2004a), the spatial resolution of GRACE is sufficient to measure the differences in water level between the Amazon and Orinoco river basin. Other GRACE data applications for water storage monitoring have been studied by several authors (e.g., Swenson and Wahr, 2006; Ramillien et al., 2004; Chen et al., 2005; Tamisiea et al., 2005). The applicationd that specifically address the problem within river basins have been conducted by Swenson and Wahr (2002); Swenson et al. (2003); Rodell et al. (2004).

According to Leuliette et al. (2002), the availability of five year of GRACE data will allow the detection of mass redistribution on the Earth's surface related to climate change, including the mass component of long-term sea level change. Furthermore, the GRACE data can provide an important constraint to develop global climate models (e.g., Nerem et al., 2003). A study about how to extract low frequency climate signals from GRACE data has been conducted by Viron et al. (2006).

2.6.4 Geodesy

In geodesy the requirements of geoid and gravity fields are particularly high (e.g., Flury and Rummel, 2006). Using GRACE, even though the improvement in geoid and gravity field determination is substantial, the requirements in terms of accuracy and spatial resolution are not yet fully met, having been achieved only in the long-wavelength part. However, GRACE and other satellite gravity missions have made significant improvements in the subject of temporal gravity field variations, which is one of the subjects in geodesy science (e.g., Vaníček and Krakiwsky, 1986; Torge, 2001).

2.7 Other Gravity Dedicated Satellite Missions

A mission dedicated to high resolution mapping of the Earth's gravity and magnetic field has been under study in Europe since the early 1980s (e.g., Visser et al., 1994). However, the first missions were just realised in 2000 with the launch of CHAMP satellite. Dedicated gravity satellite missions before and after GRACE, include ARISTOTELES, CHAMP and GOCE, a brief description of which follows.

2.7.1 ARISTOTELES

Application and research involving space techniques to observe the Earth's gravity field from low Earth orbiting satellites (ARISTOTELES) is the European Space Agency (ESA) satellite mission. ARISTOTELES was designed to provide global models of the Earth's gravity and magnetic fields with a spatial resolution of 100×100 km and accuracy less than 5 mGal for gravity anomalies and 10 cm for geoid heights (e.g., Benz et al., n.d.; Visser et al., 1994). ARISTOTELES would measure the Earth's gravity by implementation of on board gravity gradiometer and applied SST techniques with an onboard GPS receiver. The GPS receiver would also support the precise orbit determination for ARISTOTELES and provide additional information to improve the accuracy of low-degree spherical harmonic expansion of the gravity field to a higher level (Visser et al., 1994). The mission was intended to be

launched in 1997 into a 400 km orbit with inclination of 96°, but it was never accomplished. A similar mission proposed by ESA is the GOCE satellite mission.

2.7.2 CHAMP

The CHAMP satellite mission was the first dedicated gravity mapping mission. CHAMP is a German geoscience satellite, initiated by the Geo Forschungszentrum Postdam, that was launched into a near circular, almost polar and low altitude (450 km) orbit on 15 of July 2000. CHAMP adapted the high-low SST by carrying a GPS receiver to track its orbit. The scientific objectives of the CHAMP mission are to gain a better understanding of dynamic processes within the Earth's interior and in its near space (e.g., Reigber et al., 2005a).

2.7.3 GOCE

GOCE is a space gradiometer mission by ESA that is planned to be launched in early 2008 (European Space Agency, 2007). The mission duration is envisaged to about 20 months with six months dedicated to estimate the Earth's gravity field parameters. GOCE is designed to observe the static gravity field of the Earth with an accuracy of several centimeters in geoid height and a minimum spatial resolution of 65 km (e.g., Rummel, 2005; Han et al., 2006b) (cf. Table 1.1). GOCE will use a combination of onboard gradiometer to measure the Earth gravity gradient tensor and GPS receivers to determine the precise orbit. The GRACE and GOCE mission can be considered to be both supplementary and complementary (Visser, 1999).

2.8 Summary

The GRACE satellite mission has orbited the Earth for more than five years and collected informative data that have been used by Earth scientists to study the dynamic nature of the Earth's gravity field. This chapter described the GRACE satellite mission and its applica-

tion to Earth Sciences. Apart from explaining the objective of the mission, this chapter also detailed the technology and methodology used by the GRACE satellite to map the Earth's gravity field. GRACE errors and proposed techniques to reduce the error and increase accuracy have also been discussed. Other satellite missions dedicated to the observation of the Earth's gravity were presented to give a broader overview of the chronicle of the Earth's gravity mapping missions from space.

3. SPATIAL AND TEMPORAL VARIATIONS OF THE EARTH'S GRAVITY FIELD

The study of the Earth's gravity field is the main focus of Geodesy. As explained in the previous chapter, the knowledge of the Earth's gravity field has been significantly enhanced with the launch of the GRACE satellite mission. Since its first campaign in 2002, GRACE has provided valuable information about both the static and time-variable part of the Earth's gravity field and now with more than five years of continuous data it is possible to study the spatial and temporal variability of the Earth's gravity field. Importantly, the spatial and temporal variability of the Earth's gravity field can be associated to the redistribution of the Earth's masses over time (e.g., Cazevane and Nerem, 2002; Chao, 2005; Cox and Chao, 2002; Dickey et al., 2002; Wahr et al., 1998). This chapter will present basic information of the Earth's gravity field and its spatial and temporal variations.

3.1 Theoretical Foundation of the Earth's Gravity field

The fundamental concept of gravity was introduced by Newton's law of gravitation (cf. Equation 3.1), that describes the relationship between the force of gravitation (F) and point masses (m_1 and m_2) (e.g., Heiskanen and Moritz, 1967; Hofmann-Wellenhof and Moritz, 2005; Torge, 1989, 2001; Kaula, 2000) expressed by

$$F = G\frac{m_1 m_2}{r^2} \tag{3.1}$$

with $G = 6.673 \times 10^{-11}\mathrm{m}^3\mathrm{kg}^{-1}\mathrm{s}^{-2}$ being Newton's gravitational constant and r is the distance between the two point masses (the attracting mass and the attracted mass) . In the case of the Earth's gravity field the Earth acts as an attracting mass, therefore the force of the Earth's gravitation is mainly due to the masses within and on the surface of the Earth. In a simplistic view the attracted mass is set to unity and denote the attracting mass as M, the

Equation 3.1 becomes

$$b = G\frac{M}{r^2} \tag{3.2}$$

In Equation 3.2, b is represent the gravitational acceleration of the unit mass due to the attracting mass. The gravitational potential (cf. Equation 3.3) indicates the work that must be done by gravitation in order to move the unit mass from infinity $(V = 0)$ to a point with distance r from the attracting mass, M. This property is expressed by

$$V = G\frac{M}{r} \quad \text{with} \quad \lim_{r\to\infty} V = 0 \tag{3.3}$$

While the above equations (Equation 3.1 to Equation 3.3) only hold for point masses (or homogenous sphere) the simplistic formula have to be replaced by an integral over all point masses of any arbitrarily shaped body (e.g., Heiskanen and Moritz, 1967).

A gravity field can be geometrically described by its surfaces of constant gravitational potential (e.g., Torge, 1989); they are also known as equipotential surfaces or level surfaces (cf. Figure 3.1). The properties of the Earth's gravity field are closely related to the so called figure of the Earth (e.g., Bursa and Pec, 1988). The Earth's equipotential surface that coincides most closely with mean sea level presented the figure of the Earth and is called geoid.

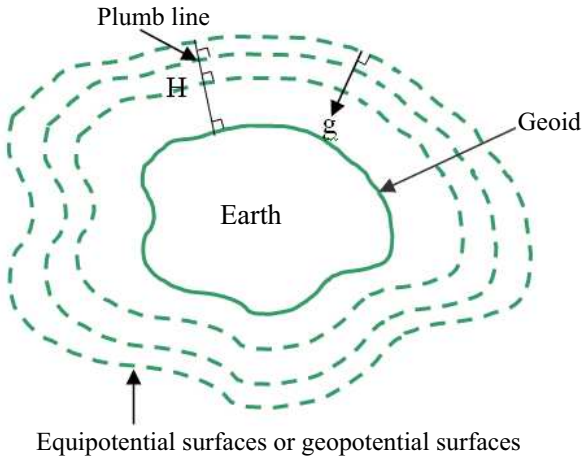

Figure 3.1: Equipotential surface and plumb lines near the Earth's surface [adapted from Torge (1989)]

According to Heiskanen and Moritz (1967), the Earth's gravitational potential (V) at any point exterior to the Earth surface ($r \geqslant R$) can be expressed by an infinite spherical harmonic series. For the point of interest specified by the geocentric radius (r), geographic latitude (ϕ) and longitude (λ) the Earth's exterior potential can be represented as:

$$V(\phi, \lambda, r) = \frac{GM}{R} \sum_{l=0}^{\infty} \sum_{m=0}^{l} \left(\frac{R}{r}\right)^{l+1} \bar{P}_{lm}(\sin\phi) \left[\bar{C}_{lm}(t) \cos m\lambda + \bar{S}_{lm}(t) \sin m\lambda\right] \quad (3.4)$$

with the fully normalized Legendre functions $\bar{P}_{lm}$ of degree l and order m, the Earth's gravitational constant G, the total mass of the Earth M, the mean radius of the Earth R, and the fully normalized spherical harmonic coefficients (SHC) $\bar{C}_{lm}$ and $\bar{S}_{lm}$. The infinite series is usually truncated at the maximum resolvable degree $L = l_{max}$, which can be translated into a corresponding spatial-scale D (half wavelength given in km).

$$D = \frac{\pi R}{L} [\text{km}] \quad (3.5)$$

Based on the spherical harmonic representation of the gravitational potential (cf. Equation 3.4) the geoid heights (measured above the adopted reference ellipsoid) can be obtained by

$$N(\phi, \lambda) = R \sum_{l=2}^{L} \sum_{m=0}^{l} \bar{P}_{lm}(\sin\phi) \left[\bar{C}_{lm}(t) \cos m\lambda + \bar{S}_{lm}(t) \sin m\lambda\right] \quad (3.6)$$

and the gravity anomaly by

$$\Delta g(\phi, \lambda) = \gamma \sum_{l=2}^{L} (l-1) \sum_{m=0}^{l} \bar{P}_{lm}(\sin\phi) \left[\bar{C}_{lm}(t) \cos m\lambda + \bar{S}_{lm}(t) \sin m\lambda\right] \quad (3.7)$$

with γ is the mean value of gravity on the adopted reference ellipsoid. The three equations above hold only on a spherical approximations.

In geodesy, the knowledge of the Earth's gravity field is important for the determination of the Earth's shape; specifically gravimetric geoid . This objective is accomplished by solving the geodetic boundary value problems (GBVP), which allows the determination of the Earth's shape from measurements upon its surface (e.g., Heiskanen and Moritz, 1967; Torge, 2001). Global models of the Earth's gravity field that represent the figure of the Earth (e.g, geoid models) are commonly called Global Geopotential Models (GGMs). They are given by the values of the fully normalized spherical harmonic coefficients $\bar{C}_{lm}$ and $\bar{S}_{lm}$ for all degrees and orders from $l = 2$ up to $L = l_{max}$. The actual values of the coefficients are determined from real data (e.g., satellite and terrestrial gravity data).

There are essentially three classes of GGMs (e.g., Torge, 2001): satellite-only GGMs, combined GGMs and tailored GGMs. Satellite-only GGMs are derived solely from the analysis of the orbits of artificial Earth satellites whereas Combined GGMs are derived from the combination of satellite orbit data, land and ship track gravity observations, and marine gravity anomalies derived from satellites radar altimetry, and more recently airborne gravimetry data. While the GGMs have a global view, tailored GGMs are mainly developed in order to better approximate the gravity field over a particular region. Such models are constructed by adjusting a satellite-only or combined GGMs using gravity data that optimally have not been used before to better reproduce high resolution gravity anomalies in the region (e.g., higher degree coefficients).

3.2 Spatial and Temporal Variations of the Earth's Gravity field

Spatial and temporal variation of the Earth's gravity field are the result of an ever changing mass redistribution within the Earth and on or above its surface (e.g., Wahr et al., 1998; Rummel, 2005). Conversely, the Earth's gravity field reflects the composition and structure of the planet (cf. Figure 3.2), including the distribution of the atmosphere and the water mass on and below its surface (e.g., Tapley et al., 2004a). While the composition and structure of the solid Earth is changing by processes that occur within longer periods (cf. Figure 3.3), Chen et al. (2005) argue that for periods of several years or shorter, the main driving forces behind these temporal variations of the Earth's gravity field are the atmosphere, ocean

circulation and changes in continental water storage (in liquid and solid form).

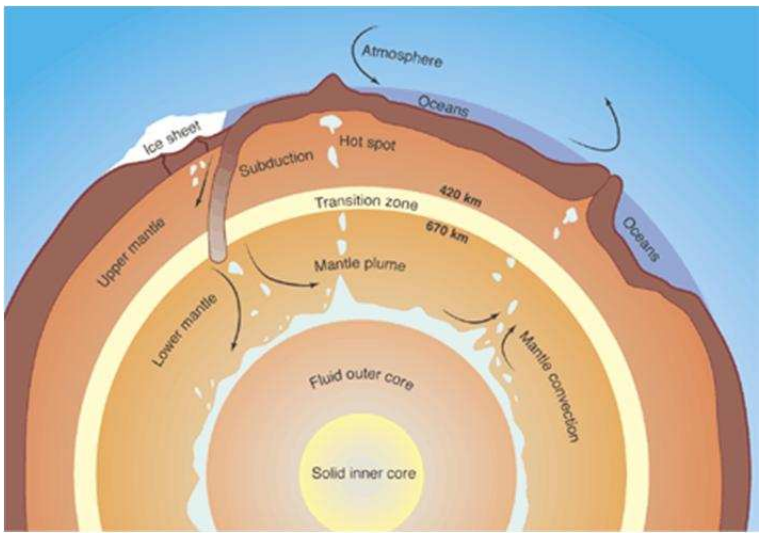

Figure 3.2: Mass redistribution beneath and on the Earth's surface (from Cazevane and Nerem, 2002)

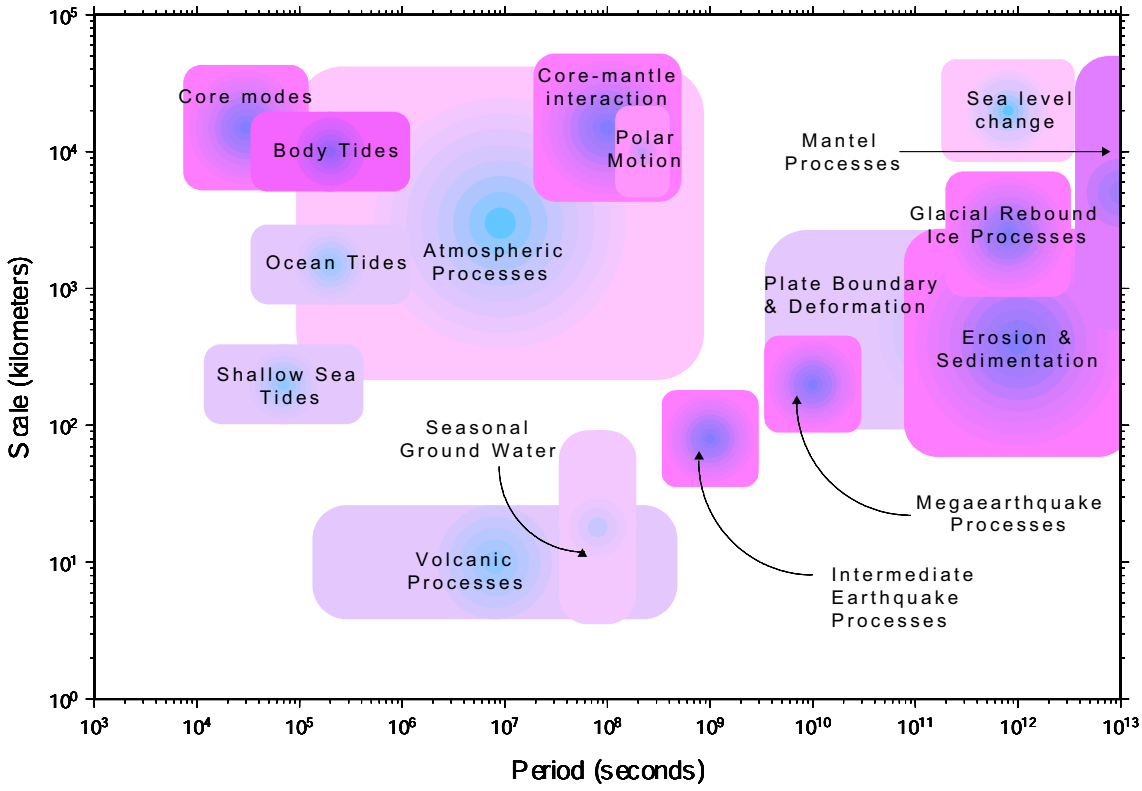

Figure 3.3: The space-time spectrum of principal geodynamic processes that are expected to cause temporal variations in the Earth's gravity field. [adapted from Lambert et al. (1995)]

According to Lambert et al. (1995), the geodynamic processes that cause the changes in gravity can be specified in terms of their principal frequencies (period) and spatial scale (wavelengths) (cf. Figure 3.3). The processes influencing the gravity field are composite of primary and secondary effects; one process can be triggered by another process. For instance, sea level change can be constituted by ice-mass melting and postglacial rebound. The processes occurring within periods more than 100 years generally appear as secular variations with rates of $\leq$10 μGal (cf. Table 3.1).

Figure 3.3 shows that the Earth's gravity changes are caused by geodynamic processes that are occurred within short-term to long-term periods covering spatial scales from few kilometers to thousands of kilometers. The effect (magnitude) of these geodynamic processes in terms of gravity and geoid height according to their spatial and temporal resolution, as given in Rummel et al. (2002), are presented in Table 3.1. Vice versa, the table also shows the requirements for the spatial and temporal resolutions that are needed to detect various geodynamic processes from gravity measurements.

Table 3.1: Time variable gravity field, scientific requirements [Beutler et al. (2003)]

Geodynamic Effect	Magnitude		Spatial Resolution (km)	Main Periods
	Geoid (mm)	Gravity (μgal)		
Tides (oceans, solid earth)	100-150		50-5000	Daily, semi-daily, semi-monthly
Atmosphere (IB, NIB, vertical integration)	15		200-2000	Annual, seasonal, daily, others
Oceans (Sea level, currents)	10-15		100-2000	Seasonal, secular
Hydrology (snow, rain, runoff, precipitation, evaporation, reservoir, ground water)		10	10-1000	Daily to annual
Postglacial rebound		10	1000-10000	Secular
Polar ice and glaciers		5	100 -1000	Secular
Solid Earth				
-Earthquake	0,5		10 - 100	Single events
-Volcanism	0,5		10 - 100	Single events
-Tectonics	?		$>$ 500	Secular
-Core and Mantle	?		$>$ 500	Secular

3.3 Inferring Changes in the Earth's Mass Distribution from Time-variable Gravity

The time-variable gravity signal is produced by mass redistributions varying with time. Consequently, global time-variable gravity signals detected from space (e.g., by the GRACE mission) contain information about mass redistributions within the Earth system. According to Chao (2005), time-variable gravity is the sum of the gravitational signals originating from all geophysical sources at work at any given time. Therefore, by sorting out physical meaningful signal such as trend and an annual signal, a-periodic or geophysically unreasonable signals can be revealed from time-variable gravity. Furthermore, recently it is also becoming a new data type for the monitoring of climatic and geophysical changes.

More than five years GRACE gravity mapping mission observations has made it possible to continuously measure the time-variable gravity over the whole globe. Some studies (e.g., Tapley et al., 2004a; Wahr et al., 2004; Andersen and Hinderer, 2005; Han et al., 2005a; Rowlands et al., 2005) have shown that GRACE data are capable to measure large-scale mass redistributions within the Earth's system. A method for constructing surface mass estimates from time-variable gravity was developed by Wahr et al. (1998). They showed that a local change in surface mass density, $\Delta\sigma(\phi,\lambda)$, can be related to the change in gravity, given by the corresponding changes in spherical harmonic coefficients (time-varying SHC) ΔC_{lm} and ΔS_{lm} (cf. Equation 3.8 and Equation 3.9) with the assumption that the density redistribution, $\Delta\rho(r,\phi,\lambda)$, is concentrated to a thin layer with the surface mass density given by

$$\Delta\sigma(\phi,\lambda) = \int_{\text{thin layer}} \Delta\rho(r,\phi,\lambda)dr \tag{3.8}$$

$$\begin{aligned}\begin{Bmatrix}\Delta C_{lm}\\ \Delta S_{lm}\end{Bmatrix} &= \frac{3}{4\pi a\rho_{ave}(2l+1)}\int \Delta\rho(r,\phi,\lambda)\bar{P}_{lm}(\cos\phi)\\ &\quad\times\left(\frac{r}{a}\right)^{l+2}\begin{Bmatrix}\cos(m\lambda)\\ \sin(m\lambda)\end{Bmatrix}\sin\ \phi\ d\phi\ d\lambda\ dr\end{aligned} \tag{3.9}$$

with ρ_{ave} is the average density of the Earth (= 5517 kg/m^3).

The contribution of the direct gravitational attraction of the surface mass changes and the elastic deformation of the solid Earth due to the surface mass load changes are described by Equation 3.10 and 3.11, respectively. The total change in the Earth's gravitational potential is expressed by the sum of the corresponding spherical harmonic coefficients.

$$\begin{Bmatrix} \Delta C_{lm} \\ \Delta S_{lm} \end{Bmatrix}_{\text{surf mass}} = \frac{3}{4\pi a \rho_{ave}(2l+1)} \int \Delta\sigma(\phi,\lambda) \times \bar{P}_{lm}(\cos\phi) \begin{Bmatrix} \cos(m\lambda) \\ \sin(m\lambda) \end{Bmatrix} \sin\ \phi\ d\phi\ d\lambda \tag{3.10}$$

$$\begin{Bmatrix} \Delta C_{lm} \\ \Delta S_{lm} \end{Bmatrix}_{\text{solid E}} = \frac{3k_l}{4\pi a \rho_{ave}(2l+1)} \int \Delta\sigma(\phi,\lambda) \times \bar{P}_{lm}(\cos\phi) \begin{Bmatrix} \cos(m\lambda) \\ \sin(m\lambda) \end{Bmatrix} \sin\ \phi\ d\phi\ d\lambda \tag{3.11}$$

with the love numbers k_l representing the elastic response of the Earth due to the changing surface loads, where for $l = 1$ it is assumed that the origin of the coordinate system is the centre of figure of the solid Earth's. The love numbers are taken from Wahr et al. (1998) and given in Table 3.2.

To summarise, the changes of surface mass density as the result of the time-variable gravity is given by

$$\Delta\sigma(\phi,\lambda) = a\rho_w \sum_{l=0}^{\propto} \sum_{m=0}^{l} \bar{P}_{lm}(\cos\phi)(\Delta\bar{C}_{lm}\cos(m\lambda) + \Delta\bar{S}_{lm}\sin(m\lambda)) \tag{3.12}$$

with ρ_w is the density of fresh water (= 1000 km/m^3) and included here so that $\Delta\bar{C}_{lm}$ and $\Delta\bar{S}_{lm}$ are dimensionless.

A simple relation between un-normalised spherical harmonic coefficients (ΔC_{lm} and ΔS_{lm}) and fully-normalised coefficients ($\Delta \bar{C}_{lm}$ and $\Delta \bar{S}_{lm}$) is shown in Equation 3.13

$$\begin{Bmatrix} \Delta \bar{C}_{lm} \\ \Delta \bar{S}_{lm} \end{Bmatrix} = \frac{a\rho_{\text{ave}}}{3\rho_w} \frac{2l+1}{1+k_l} \begin{Bmatrix} \Delta C_{lm} \\ \Delta S_{lm} \end{Bmatrix} \tag{3.13}$$

Finally, inserting (3.13) in (3.12) gives

$$\Delta\sigma(\phi,\lambda) = \frac{a\rho_{ave}}{3} \sum_{l=0}^{\infty} \sum_{m=0}^{l} \frac{(2l+1)}{(1+k_l)} \bar{P}_{lm} \cos(\phi) \{\Delta C_{lm} \cos m\lambda + \Delta S_{lm} \sin m\lambda\} \tag{3.14}$$

Table 3.2: Elastic love numbers taken from Wahr et al. (1998)

l	k_l
0	+0.000
1	+0.027
2	-0.303
3	-0.194
4	-0.132
5	-0.104
6	-0.089
7	-0.081
8	-0.076
9	-0.072
10	-0.069
12	-0.064
15	-0.058
20	-0.051
30	-0.040
40	-0.033
50	-0.027
70	-0.020
100	-0.014
150	-0.010
200	-0.007

One of the drawbacks of inferring mass changes from time-variable gravity is the non-unique solution(gravitational inverse problem). It states that the external gravity field, even if completely and exactly known, cannot uniquely determine the density distribution of the body that produces the gravity field (e.g., Chao, 2005). This is a natural character of the field that obeys the Laplace equation (e.g., Hofmann-Wellenhof and Moritz, 2005). The uniqueness

problem of the gravitational inversion in terms of spherical harmonic has been examined by Chao (2005). He proved that using a 2-D spherical shell without radial dependence, the gravitational inversion for the (surface) density function proves to be unique. This is applicable for many real geophysical situations as the gravity signals are often derived from the Earth's surface which can be approximated by a spherical shell. Therefore, by assuming the density redistribution is concentrated in a thin layer, the inversion of time-variable gravity to mass changes is unique (e..g., there is only one mass layer that can produce a given gravity signal).

3.4 The Earth's Gravity field Data Sources

There are three main data sources of the Earth's gravity field (e.g., Rummel et al., 2002). First, mean gravity anomalies which are derived from terrestrial gravity observation combined with height measurements and from shipborne gravimetry. This type of observation typically covers areas of 100 x 100 km² or 50 x 50 km². The second source is from satellite altimetry, which over ocean areas provide a direct observation of the geoid surface. The third source comes from geopotential models that are determined from satellite orbit analysis, such as from the GRACE satellite mission.

Satellite and terrestrial measurements can be combined in a complementary way so to provide an optimum representation of the spatial variations of the Earth's gravity field (e.g., Rapp, 1994). Temporal variation of the gravity field are now also being studied by both satellite and terrestrial methods. However, in case of spatial variations, satellite measurements are best suited for the determination of very-long wavelength changes (e.g., Lambert et al., 1995). Other advantages of the space based gravity field measurement are (near-) global coverage that does not depend on geographical and geopolitical boundaries; and continuous observation.

3.5 Summary

This chapter described the basic theory of the Earth's gravity field starting from the Newton's Law of Gravitation. The relationship between the Earth's mass redistribution and variations in the Earth's gravity field has been given. Some basic formulae for inferring the mass distribution from time-variable gravity (e.g., GRACE data) were presented as it will be used later in the data processing stage. The different sources of the Earth's gravity field have been explained as well.

4. TECHNIQUES FOR SPATIAL AND TEMPORAL SIGNAL ANALYSIS

This chapter describes some common techniques used to analyse any spatial and temporal signal (e.g., the GRACE gravity field data). Brief explanation of the spatial and temporal system is given in Section 4.1. Some common techniques used to analyse the spatial and temporal signal are described in Section 4.2.

4.1 Spatial and Temporal Systems

Spatial and temporal systems, often called spatio-temporal systems, are systems that gradually change over both space and time. The systems are often used to represent environmental and geophysical processes that are characterised by spatial and temporal variability such as precipitation, climate and ocean changes (e.g., Gneiting et al., 2006). In statistics, the spatio-temporal data set is regarded as a realisation of random variables spread out in space and evolving in time (e.g., Finkenstadt et al., 2006).

The spatio-temporal systems comprise of two domains; namely, the space domain and time domain. Each domain constitutes of multivariate processes so that the system becomes a complex multivariate system. The Earth's gravity field, as it is changing in both space and time, can be regarded as a spatio-temporal system.

4.2 Techniques for Analysing Spatio-temporal Signal

The spatio-temporal data sets comprise of multivariate processes. Therefore methods to analyse the system must be able to account for multiscale dynamical variability across different dynamical variables in space and time, account for various source of error, and provide efficient dimension reduction (Wikle, 2002). In this section some analytical and statistical

techniques for analysing the spatio-temporal systems will be presented. However, only some common techniques will be briefly discussed, that are: Harmonic analysis, Wavelets and Empirical Orthogonal Function (EOF).

4.2.1 Harmonic Analysis

Harmonic (or frequency) analysis (HA) has been commonly used for time series analysis. This method is based on a Fourier analysis of a spatial process (Fuentes et al., 2006), which is a decomposition of the process into sinusoidal components (sine and cosine waves). The coefficients of the sinusoidal components are often called the Fourier transform of the process. To analyse the space-time system, however, the HA method is only best suited for gridded data that show some regular behaviour over the entire region of observation (stationary).

The illustration of a harmonic signal is presented in Figure 4.1 whereas the representation of the signals as sine and cosine function are given by Equation 4.1 and Equation 4.2, respectively.

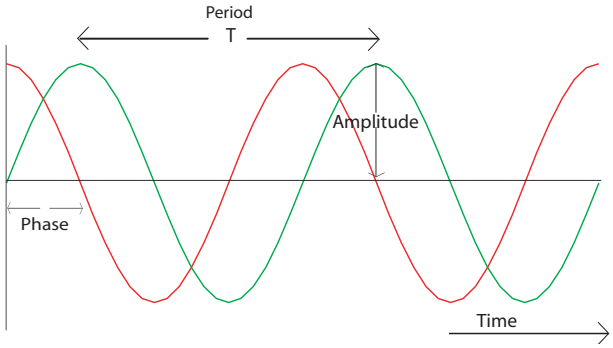

Figure 4.1: Harmonic oscillation illustrated as wave

$$y = A\sin(2\pi\omega + \phi) \tag{4.1}$$

$$y = A\cos(2\pi\omega - \phi) \tag{4.2}$$

The functional model for harmonic oscillation of the time series (h_i) in grid-point i is given by

$$h_i(t_k) + v_{ik} = d_i t_k + \sum_{r=1}^{R} A_{ir} \cos(\omega_r t_k - \Phi_{ir}) \tag{4.3}$$

with the amplitude A_i, phase, Φ_i, frequency ω_r and the period $T_r = \frac{2\pi}{\omega_r}$. Using Equation (4.3), the linear trend $d_i t_k$ of the time series in grid-point i (h_i) is also determined.

4.2.2 Wavelets

Wavelets are mathematical functions that divide data into different frequency components, and then study each component with a resolution matched to its scale or resolution. Wavelet analysis attempts to decompose the variability of the spatio-temporal process both in time and frequency. This is in contrast to the frequency (harmonic) analysis such as the Fourier analysis that only deals with frequency. According to Gneiting et al. (2006), there are some advantages of the wavelet analysis compared to the Fourier analysis. First, the wavelet analysis aims at handling nonstationary processes by allowing the frequency (scale) decomposition to change over time. Second, the wavelet theory can handle long-term memory process, where Fourier theory breaks down.

Wavelets attempts to represent general function of large data sets. Therefore, recently this method is widely used in Earth sciences as the satellite missions have the ability to collect millions of data covering the whole globe (e.g., Fengler et al., 2006).

4.2.3 Empirical Orthogonal Function or Principal Component Analysis

Empirical orthogonal functions (EOFs) are the manifestation of the classic eigenvalue or eigenvector decomposition of a covariance matrix usually used by geophysicists (e.g., Wikle, 2002). For the discrete formulation, this technique is called principal component analysis

(PCA). The EOFs are usually used for: (1) finding principal (in terms of explanation of variance) spatial structures together with their corresponding time variations, and (2) reducing the dimension (spatially) in large data sets while simultaneously reducing errors (noises).

One of the advantages of the EOF is its ability to compress the complicated variability in large data sets onto a relatively small set of eigenvectors. Unfortunately, such an EOF analysis only detects spatial structures that do not change position in time. To extend the EOF analysis to the study of spatial structures that can propagate over time, one can perform a complex principal component analysis within the frequency domain. The technique involves the computation of complex eigenvectors from cross-spectral matrices.

PCA is another term used for EOF. This technique is commonly used is Meteorology and Oceanography (Preisendorfer, 1988). The PCA analyse the spatio-temporal system by decomposing the system to space functions and time functions. The time function is called principal component (PC) which represents the system's time series and the space function is called EOF which represents the spatial pattern of the system.

4.3 Summary

The spatial and temporal systems and some techniques that are commonly used to analyse the systems have been discussed. However, here only some techniques based on transform methods, namely Harmonic Analysis, Wavelets and EOF, have been expounded as these techniques are often used in Earth sciences. The PCA which is the technique predominantly used in this study will be discussed in more detail in the next chapter.

5. PRINCIPAL COMPONENT ANALYSIS

As mentioned before in Chapter 4 PCA, also known as empirical orthogonal function (EOF) analysis (e.g., Wang, 2001), is one of the statistical methods that can be applied to analyse spatial and temporal variation of the Earth's gravity field. This chapter gives a brief history of the PCA , theoretical background and application of the PCA in Earth sciences.

5.1 History of Principal Component Analysis

The PCA was introduced for the first time by Pearson in 1901 , however the modern use of PCA was developed by Hotelling in 1933 (e.g., Jolliffe, 2002; Manly, 1986; Preisendorfer, 1988). The basic idea of the PCA is to reduce the dimension of data by transforming them to a new set of uncorrelated variables called principal components (PCs) (e.g., Jolliffe, 2002). The method decomposes a space-time field into spatial patterns called EOF and associated time indices called PCs. In meteorology, PCA techniques were first used in the late 1940s (Hannachi et al., 2006).

However, even though the PCA decompositions are forced to be correlated to the original field, they may not capture interesting aspects of temporal variations (Kooperberg and O'Sullivan, 1996) and sometimes are difficult to interpret because of their geometrical properties and their orthogonality in space and time (Hannachi et al., 2006). Therefore, spatial interpretation of the EOF should be done carefully.

5.2 Theoretical Background of the PCA

The original aim of the PCA was to achieve a decomposition of a space-time field $X(t,s)$, where t and s denote time and spatial position respectively, as

$$X(t,s) = \sum_{k=1}^{p} c_k(t)u_k(s) \tag{5.1}$$

where p is the number of modes contained in the field, using an optimal set of basis functions in space $u_k(s)$ and expansion function in time $c_k(t)$. In practice the PCA technique aims at finding a new set of variables that capture most of the observed variance from the data through linear combinations of the original variables.

5.2.1 Data Preparation

Suppose a gridded data set is composed of a space-time field $X(t,s)$ representing the value of the field X, such as gravity field, at time t and spatial position s. The value of the field at discrete time t_i and grid point s_j is denoted by x_{ij} for $i = 1, ..., n$ time elements and $j = 1, ..., p$ positions. The observed field is then represented by the space-time matrix

$$X = (\mathbf{x}_1, \mathbf{x}_2, ..., \mathbf{x}_n)^T = \begin{bmatrix} x_{11} & x_{12} & \cdots & x_{1p} \\ x_{21} & x_{22} & \cdots & x_{2p} \\ \vdots & \vdots & \ddots & \vdots \\ x_{n1} & x_{n2} & \cdots & x_{np} \end{bmatrix} \tag{5.2}$$

where $\mathbf{x}_t = (x_{t1}, x_{t2}, ..., x_{tp})^T$, $t = 1, ..., n$ represents the map, or the value of the field at time t. Denote by $\bar{x}_{.i}$ the time average of the field at the ith spatial grid point. This time average is given by

$$\bar{x}_{.i} = \frac{1}{n} \sum_{k=1}^{n} x_{ki.} \tag{5.3}$$

Based on Equation 5.3, the average of the field is defined by:

$$\bar{\mathbf{x}}_{.i} = (\bar{x}_{.1}, ..., \bar{x}_{.p}) = \frac{1}{n} 1_n^T X \tag{5.4}$$

where $1_n = (1, ..., l)^T$ is a (column) vector of length n containing only ones. The anomaly field, or departure from the average is defined at $(t, s_k), t = 1, ..., n$, and $k = 1, ..., p$ by

$$x_{tk}^{'} = x_{tk} - \bar{x}_{.k} \tag{5.5}$$

or in matrix form:

$$X^{'} = X - 1_n \bar{\mathbf{x}} = \left(I_n - \frac{1}{n} 1_n 1_n^T \right) X = HX \tag{5.6}$$

where I_n is the $n\mathbf{x}n$ identity matrix, and H is the centering matrix of order n (Hannachi et al., 2006).

5.2.2 Formulation and Computation of EOFs and PCs

Procedures to obtain EOFs and PCs are explained clearly in some references such as Jolliffe (2002). It is summarised as follow. Once the anomaly data matrix (cf. Equation 5.6) is determined, the sample covariance matrix is then defined by:

$$S = \frac{1}{n} X^T X^{'} \tag{5.7}$$

which contains the covariances s_{ij}, $i, j = 1, ..., p$, between the time series of the field at any pair of grid points (s_i, s_j), i.e.

$$s_{ij} = [S]_{ij} = \frac{1}{n} \sum_{t=1}^{n} x_{ti} x_{tj.} \tag{5.8}$$

The aim of PCA is to find uncorrelated linear combinations of the different variables that explain maximum variance, that is to find a unit-length direction $\mathbf{u} = (u_1, ..., u_p)^T$ such that $X\mathbf{u}$ has maximum variability. This readily yields:

$$\max(\mathbf{u}^T S\mathbf{u}) \tag{5.9}$$

where $\mathbf{u}^T\mathbf{u} = 1$

The EOFs are therefore obtained as the solution to the eigenvalue problem:

$$S\mathbf{u} = \lambda^2\mathbf{u} \tag{5.10}$$

The k[th] EOF is simply the k[th] eigenvector $\mathbf{u}_k$ of S. The corresponding eigenvalue λ_k^2, $k = 1, ..., p$ is then

$$\lambda_k^2 = \mathbf{u}^T - kS\mathbf{u}_k = \frac{1}{n}\|X\mathbf{u}_k\|^2 \tag{5.11}$$

and hence gives a measure of the variance of the data accounted for in the direction $\mathbf{u}_k$. After finding the eigen elements of the sample covariance matrix S in Equation 5.9, the eigenvalues are normally sorted in decreasing order as $\lambda_1^2 \geq \lambda_2^2 ... \geq \lambda_p^2$. It is usual to write the variance accounted for in percentage as:

$$\frac{100\lambda_k^2}{\sum_{k=1}^{p}\lambda_k^2}\% \tag{5.12}$$

The projection of anomaly field X onto the k[th] EOF $\mathbf{u}_k = (u_{k1}, u_{k2}, ..., u_{kp})^T$, i.e. $\mathbf{a}_k = X\mathbf{u}_k$ is the k[th] PC whose elements a_{tk}, $t = 1, ..., n$, are given by:

$$a_{tk} = \sum_{j=1}^{p} x_{tj}u_{kj} \tag{5.13}$$

So the kth eigenvalue λ_k^2 represents the variance of the kth PC $a_k = (a_{1k}, a_{2k}, ...a_{nk})^T$. The relationship between Equation 5.13 and Equation 5.1 can now be noted. The time function $c_k(t)$ and the space function $u_k(s)$ in Equation 5.1 are represented in Equation 5.13 by x_{tj} and u_{kj} respectively. In various literatures the EOFs are also known as PC loadings. The PCs on the other hand also known as EOF expansion coefficients, EOF amplitudes, PC time series, and PC scores. In this study the terminology EOFs and PCs represent the spatial and temporal patterns of the space-time systems, respectively.

5.3 PCA in Earth Sciences

The PCA technique is commonly used in Meteorology, Climatology and Oceanography. However, lately, this technique also has been applied in gravity field analysis, particulary GRACE data analysis (e.g. Rangelova et al., 2007; Rangelova and Sideris, 2007; Viron et al., 2006). For these fields, which have both spatial and temporal variations and also contain of large data sets, the PCA is a suitable tool to be applied. In Meteorology, the PCA is applied not only for reducing the large data set, but also as a prediction tool (e.g., Hannachi et al., 2006).

The application of PCA in Meteorology was developing since the late 1940s by the study of Obukhov (1947) and Lorenz (1956). In Oceanography, the PCA was applied for the first time by the study of Trenberth (1975) that related the sea surface temperature with southern hemisphere atmospheric oscillation. Since then, a large number of PCA application have been performed to various oceanographic data sets. Theory and applications of the PCA that specifically address Meteorology and Oceanography are comprehensively discussed in Preisendorfer (1988).

For the gravity field analyses, the PCA has been applied to the GRACE data. For example, a study by Rangelova et al. (2007) which applied the PCA for analysing 44 GRACE monthly gravity field solutions. The purpose of their study was to extract and validate regional hydrology signals from GRACE data. Another application of the PCA to GRACE data was conducted by Viron et al. (2006), which used this method to extract low frequency climate

signals from four years of GRACE gravity data.

5.4 Summary

The basic theory of the PCA has been explained in this chapter. From this chapter it was shown that the PCA would be a suitable tool to analyse the spatio-temporal variation of the Earth gravity field. Application of the PCA to the Earth's gravity field derived by GRACE will be presented in Chapter 6, including the analysis and results from the data processing.

6. SPATIO-TEMPORAL VARIABILITY OF GRACE GRAVITY FIELD

This chapter presents the processing stage of the research. GRACE level-2 data developed by UTCSR are analysed using the HA and PCA to investigate the most dominant spatial and temporal variations of the Earth's gravity field over the five year period (April 2002 to May 2007, inclusive). The data used in this research will be explained in Section 6.1. In this study the variability of the Earth gravity field is expressed by surface mass changes, thus the GRACE gravity field in the form of spherical harmonic coefficients is converted into equivalent water thickness (EWT) value. The corresponding procedure will be expounded in Section 6.2. The HA and PCA techniques will be presented in the same section and the results and analysis will be given in Section 6.3 of this chapter. The analysis will be performed for the whole globe as well as for the local areas: Sumatra-Andaman, Australia, Africa, Antarctica, South America, Arctic, Greenland, South Asia, North America and Central Europe.

6.1 GRACE Data Used

In this study, GRACE level-2 RL04 data generated at CSR University of Texas Austin are used. Up to February 2008, 64 GRACE's monthly gravity field solutions are available for download at the UTCSR data centre (cf. Figure 6.1). However, this study is based only on the data period from April 2002 to May 2007. Each monthly CSR GRACE level-2 data set consists of a set of fully normalized spherical harmonic coefficients complete up to degree and order 60. Here, the static field geopotential coefficient data estimated from GRACE only data (GSM) have been used.

The CSR RL04 data used in this research comprises 59 GRACE gravity monthly solutions inclusive from April 2002 to May 2007 (cf. Figure 6.1), excluding June and July 2002; and June 2003 when the gravity recovery was not fully resolved due to degradations of the

GRACE satellite orbit (e.g., Wagner et al., 2006). However, these gaps are insignificant as the data are still capable to show the full five year cycle of the gravity signal. For the purpose of the PCA, the data gaps were ”filled in” by linear interpolation during the data preparation stage.

Table 6.1: CSR RL04 GRACE Level-2 data, gray (no): no observation; red (nd) : no data; green (du) : data are used ; yellow (dnu) : data available but not be used

CSR RL04	Jan	Feb	Mar	Apr	May	Jun	Jul	Aug	Sep	Oct	Nov	Dec
2002	no	no	no	du	du	nd	nd	du	du	du	du	du
2003	du	du	du	du	du	nd	du	du	du	du	du	du
2004	du	du	du	du	du	du	du	du	du	du	du	du
2005	du	du	du	du	du	du	du	du	du	du	du	du
2006	du	du	du	du	du	du	du	du	du	du	du	du
2007	du	du	du	du	du	dnu	dnu	dnu	dnu	dnu	nd	nd

6.2 Method and Processing

Generally the processing stage consists of three main stages, namely: data preparation, HA and PCA. The data preparation stage is mainly dealing with inferring mass changes from the GRACE monthly gravity field solutions in the form of a spherical harmonic expansion of the Earth’s gravity potential. Chen et al. (2005) argued that at periods of several years or shorter, atmosphere, ocean circulations and continental water storage changes are the main driving forces behind the temporal variations of the gravity field (cf. Chapter 3). As the GRACE gravity field solutions have been reduced from atmospheric and oceanic influences, the surface mass density changes derived from GRACE are mainly formed from continental water storage changes. Therefore, here the surface mass density changes expressed as equivalent water thickness (EWT) will be used for both the HA and PCA. The HA and PCA are performed to analyse the temporal and spatial variations of the gravity field, which is the main objective of this research. The different processing stages are summarised as flowchart in Figure 6.1 and explain in more detail in the following section.

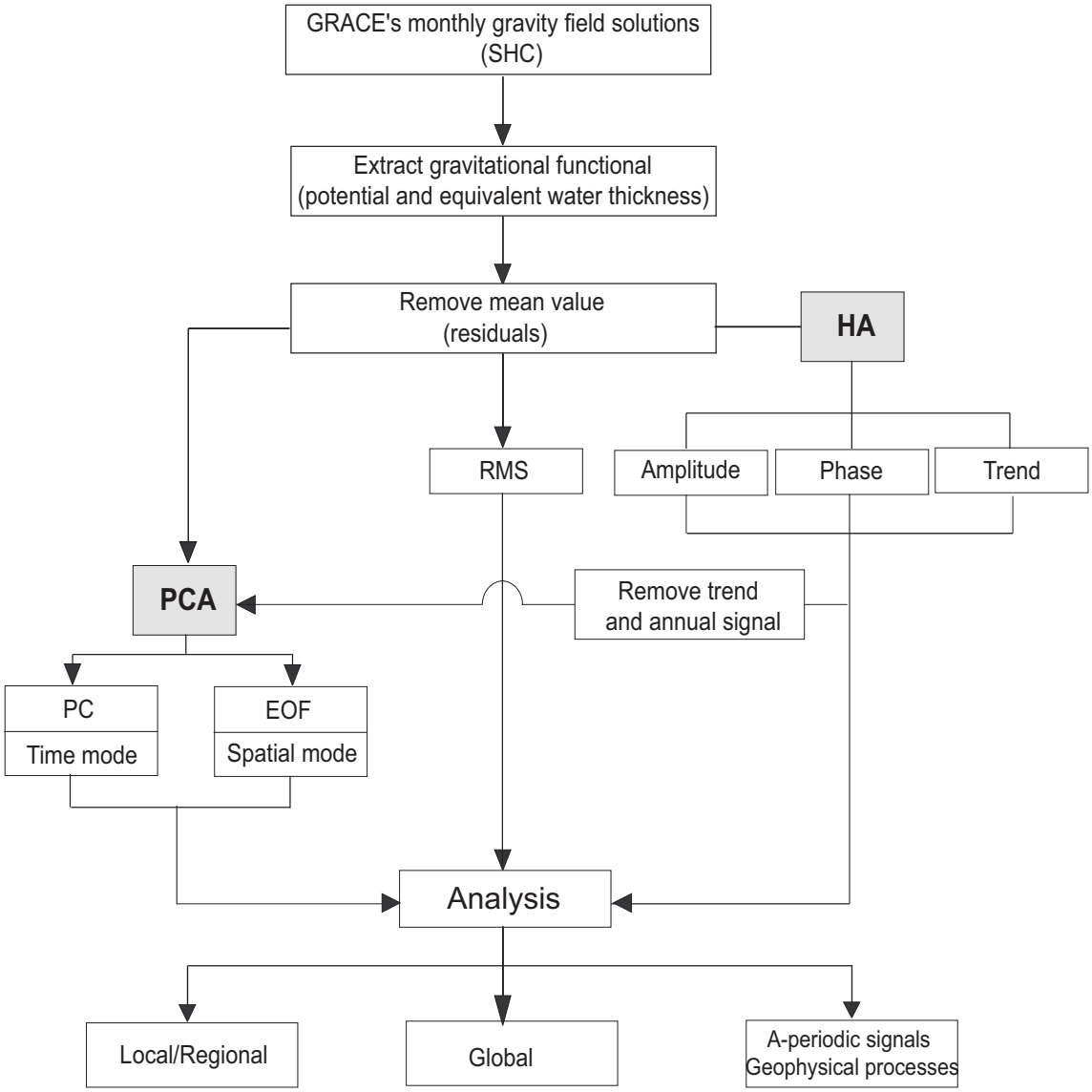

Figure 6.1: Flowchart on GRACE gravity field analysis using HA and PCA

6.2.1 Data Preparation

GRACE level-2 data represent the Earth's gravity field by fully normalized spherical harmonic coefficients, $\bar{C}_{lm}$ and $\bar{S}_{lm}$ of the gravity potential. As GRACE measure the change in gravity potential over time, they are represented here as $\Delta\bar{C}_{lm}$ and $\Delta\bar{S}_{lm}$. The surface mass estimates are developed from the GRACE level-2 data on a spatial resolution 1 degree by 1 degree, up to degree and order 60. Here, the method proposed by Wahr et al. (1998) is used, where the surface mass density is expressed by

$$\Delta\bar{\sigma}(\phi,\lambda) = \frac{2\pi a\rho_{ave}}{3}\sum_{l=0}^{L}\frac{2l+1}{1+k_l}W_l\sum_{m=0}^{l}\bar{P}_{lm}(\sin\phi)(\Delta\bar{C}_{lm}\cos(m\lambda) + (\Delta\bar{S}_{lm}\sin(m\lambda)) \tag{6.1}$$

The average mass density of the solid Earth, ρ_{ave}, is 5517 kg/m^3 (e.g., Wahr et al., 1998). The degree-dependent load Love numbers, k_l as listed in table 3.2 are taken from calculated love numbers for a unit mass load on the surface of a Gutenberg-Bullen Earth model as explained by Farrell (1972). Equation 6.1 also accounts for spatial averaging based on Gaussian smoothing as presented in Wahr et al. (1998). The coefficients W_l, which downweight the high-degree frequency errors, are computed with the recursive relations as follow (e.g., Jekeli, 1981):

$$\begin{aligned} W_0 &= \frac{1}{2\pi} \\ W_1 &= \frac{1}{2\pi}\left[\frac{1+e^{-2b}}{1-e^{-2b}} - \frac{1}{b}\right] \\ W_{l+1} &= -\frac{2l+1}{b}W_l + W_{l-1} \end{aligned} \tag{6.2}$$

with $b = \frac{\ln(2)}{(1-\cos(R/a))}$ and R is referred to as the averaging (smoothing) radius. The surface mass density is transformed to EWT ($\Delta\bar{v}(\phi,\lambda)$) by a simple formula as follows (e.g., Wahr

et al., 1998):

$$\Delta\bar{v}(\phi,\lambda) = \frac{\Delta\bar{\sigma}(\phi,\lambda)}{\rho_w} \tag{6.3}$$

with ρ_w = 1000 kg/m^3 is the density of fresh water and $\Delta\bar{v}(\phi,\lambda)$ is given in the unit meter. In this research a 500 km smoothing radius has been chosen, based on the study of Swenson et al. (2003) that showed that the minimum accumulative errors usually occurs for smoothing radius between R = 200 km and R = 600 km (cf. Chapter 2). Dealing with correlations errors, the spectral-domain filtering method as explained in Swenson and Wahr (2006) is used. The filtering is restricted to the spherical harmonic degrees $8 \leq l \leq 50$ as for $l < 8$ no correlation errors occur and as the spectral components $l > 50$ and $m > 50$ do not affect the spatially averaged results with $R \leq 500$ km (Chambers (2006b) as cited in Baur et al. (2007)). For further analysis the EWT values are reduced by the average value over the complete data period as is also needed for the PCA.

6.2.2 Harmonic Analysis

The HA is applied to gain two kind of information. Firstly it is applied here to find the areas with high annual variabilities or significant trends. Secondly it is applied to identify geophysical meaningful signals within the GRACE data. The HA is also expanded with the calculation of RMS values to provide an impression on the overall variability. The variations and trend of the global gravity field over five years will be presented by the spatial distribution of RMS values, the amplitude of the annual signal and the linear trend. As most places in the Earth's temporal gravity field variation is constituted of an annual and trend signal the HA is used to determine both the linear trend and the amplitude and phase of the annual signal. This is done by a least squares fit to a given time series (e.g., Kuhn et al., 2005). The functional model for harmonic oscillation of the time series (h_i) in grid-point i is given by Equation 4.3. The amplitude A_i, and phase, ϕ_i are the parameters to be examined and the period T, is equal to 1 year as the analysed signal is assumed to be an annual (yearly) signal. Using Equation (4.3), the linear trend $d_i t_k$ of the time series in point i (h_i) is also determined.

6.2.3 PCA

As mentioned before, there were some data gaps in the original GRACE data (cf. Section 6.1 and Table 6.1). As the PCA requires continuous spatial and temporal data as input, these gaps should be filled in and here linear interpolation method is used. The data gaps can be considered as not really critical (the largest gap is 2 months) based on the fact that the PCA results do not show any anomalous behaviour around these data gaps (see the results from PCA).

The basic equation used in the PCA is taken from Preisendorfer (1988) and applied to a space-time signal. The PCA uses the covariance matrix of a given signal (e.g., space-time signal) to construct a set of eigenvectors, u_{kj}, called empirical orthogonal functions (EOFs). Here this The expansion coefficients of time from the signal, are then used to construct the principal components (PCs), a_{tk} of the data set using analysis formula in Equation 5.13.

The PCs and the EOFs represent the time series or temporal modes and spatial modes of the data set, respectively. Both together are used to construct an alternative representation of the space-time signal, $x(tj)$, by the synthesis formula as follow:

$$x(tj) = \sum_{j=1}^{p} a_{tk} u_{kj} \tag{6.4}$$

$t = 1, ..., n$; $k = 1, ..., p$ and p is the number of modes.

The PCA is performed in two stages. First it is applied to the original data, which are the GRACE monthly solutions in terms of equivalent water thickness that have been already reduced by the mean value. This stage is performed to analyse all dominant signals captured in the GRACE gravity signal. In the second stage, the geophysically meaningful signals of a linear trend and annual signal are removed from the original GRACE data in order to possibly isolate or enhance further signals. Then, the PCA is applied once again to the new reduced data set. It is expected that the remaining signals captured in the reduced data will be long-periodic or a-periodic signals, noise or even peculiar signals from geodynamic events.

6.3 Results and Analysis

This section provides the results from the HA and the PCA. For the sake of simplicity, from now on the PCA that is applied to the data only reduced by the mean value will be called the unreduced PCA. The PCA that is applied to the data reduced by mean, annual signal and linear trend, on the other hand, will be called the reduced PCA. The analysis will be performed over the whole globe and some local areas. The results from the global analysis is also taken into account for choosing the local areas that will be analysed separately. In this chapter only some selected results are presented. Whereas, the annual and seasonal plots of GRACE's EWT values and also all the PCA results are presented in the appendices.

6.3.1 Global Analysis

A global PCA is performed to study the general spatial and temporal pattern of the gravity field changes over the whole globe. The global global grids have 360 longitude values with 1-degree incereement (0.5,1.5,2.5,...,359.5), and 180 latitude values with the same increement (-89.5, -88.5, ..., -0.5, +0.5, ...+89.5). Apart from the PCA results, results from the HA and RMS values are also presented here. However, the HA is only performed to the unreduced signals (only reduced by the mean value) as it was only used to gain some general information of the GRACE gravity signal.

Spatial Pattern of the RMS and Annual Signal

The spatial pattern of the RMS value shows the variations of the gravity field in every locations of the space-time signal over the five year period. Figure 6.2 shows that high variations are present in some areas of: South America, Africa, South Asia, North Australia-Indonesia, Alaska, Greenland and Antarctica. The highest variations is found in South America in the area where Amazon and Orinoco basin are located. The spatial distribution of the amplitude of the annual variation (cf. Figure 6.3) also shows that the highest amplitude of the GRACE gravity signal occurs over the Amazon basin . As such, the PCA will be performed locally

in those areas to look at the most dominant spatial and temporal signals present in each area.

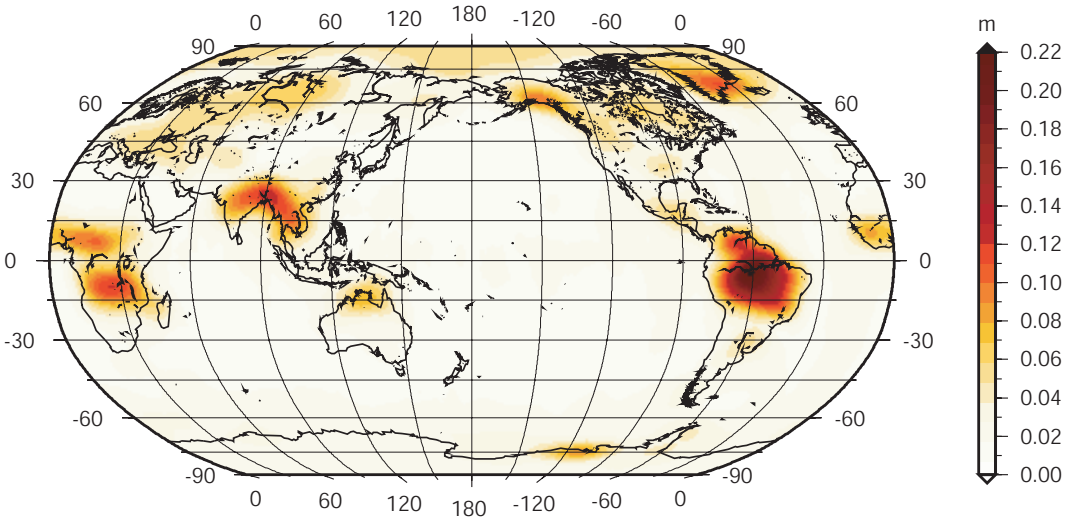

Figure 6.2: Global distribution of (EWT) RMS value. Robinson projection

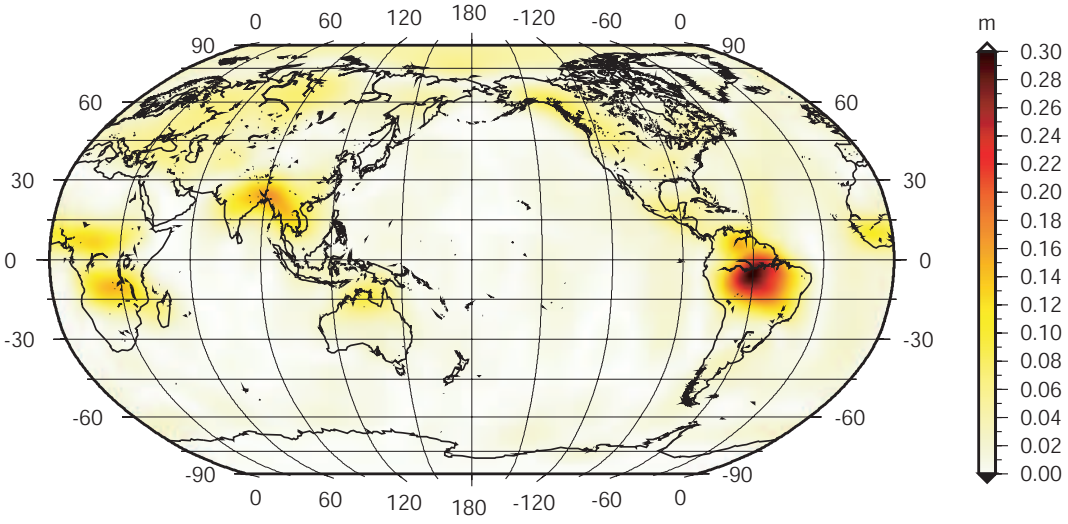

Figure 6.3: Global distribution of (EWT) amplitude of the annual signal. Robinson projection

Global Trend

The spatial pattern of the linear trend over the five year period is shown in Figure 6.4. The figure shows that significant trends are present in the areas of: Greenland, Alaska, Antarctica,

Sumatra-Andaman and North America. The PCA also will be performed locally over these areas to examine the most dominant spatial and temporal signals. Some minor trends also can be seen over the continental basins e.g., Lake Victoria, Ganges, Parana-Uruguay, Ob, Chao Phraya and Wisla (e.g., Rodell and Famiglietti, 1999)

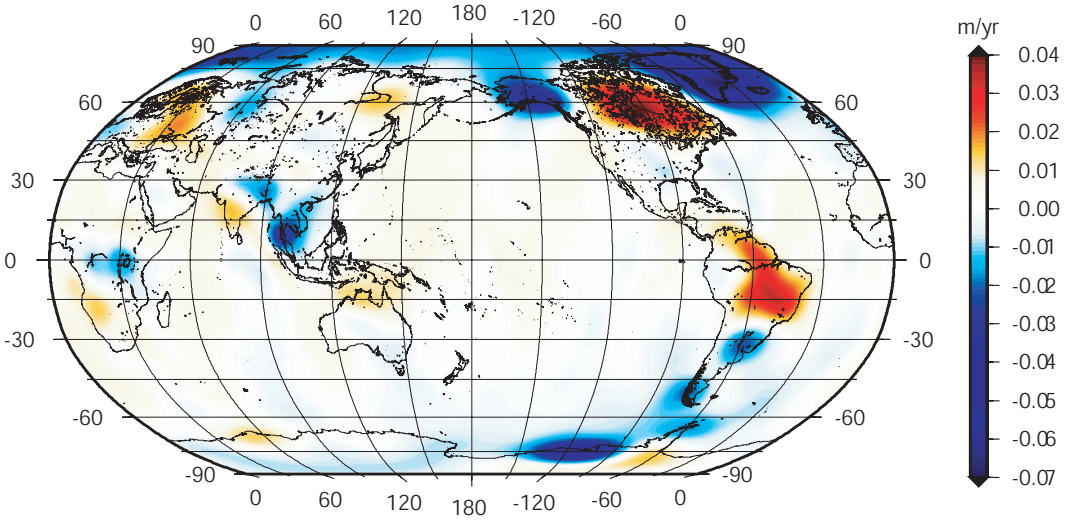

Figure 6.4: Global trend distribution of EWT between April 2002 and May 2007. Robinson projection

Results from PCA

The results for the unreduced PCA show that the most dominant temporal variations for the global coverage is an annual signal. Annual signals are mostly present in the PCs of mode 1 and mode 4 (cf. Figure 6.5) and together taking up about 50% of the total variability. In Figure 6.5 and all subsequent figures showing PCA results, the time series always show the PCs and the spatial distribution represents the EOF of the indicated mode. Furthermore, the relative amount in percentage of overall variability that is taken up by a particular mode is given together with the number of the mode.

From Figure 6.5 it can be seen that the annual signal is mostly present along the tropical regions, such as South America, Africa, South Asia and North Australia-South Indonesia. A phase shift of six months is present between the northern and southern hemisphere, showing

the seasonal differences between them. This perfectly shows that a great part of the temporal variability of the Earth's gravity field is seasonal, which is nicely captured by GRACE (see Figure 6.5, Appendix A, and Appendix B).

The most dominant annual signal is present over the Amazon basin. Even though in agreement with the spatial distribution of the amplitude of the annual signal from the HA, the maximum amplitude found in the PCA result is located slightly south of the centre of the basin. This could be caused by spatial leakage of the annual signal over the Orinoco basin which has a phase shift of half year. To confirm this finding, however, independent in-situ data are needed. The strong annual signals that are found over the tropics are mostly the result of strong wet and dry seasons.

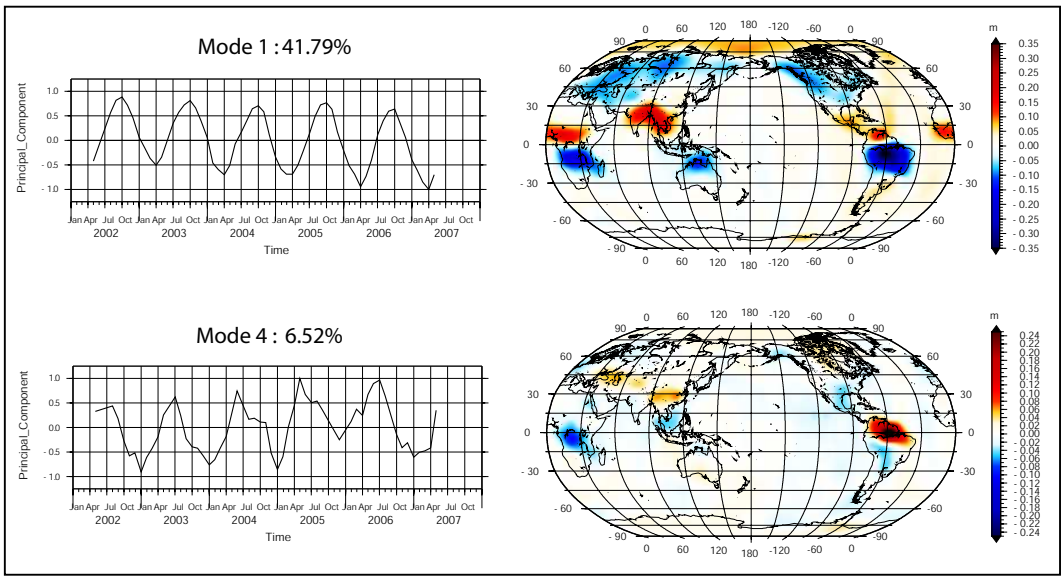

Figure 6.5: The unreduced data show that more than 50% signal variability is captured in mode 1 and mode 4 of the PCA result is an annual signal

Apart form the rather strong annual signal over the tropical region, weaker annual signals also appear in mid and higher latitude regions on the northern hemisphere such as Alaska (and Rocky mountains range), North and Central Europe and the Arctic. The annual signal in those regions is more likely related to the variations in snow and ice cover. On the southern hemisphere, a weak annual signal is present in small regions over the Antarctic continent (cf. Figure 6.5).

Trends with some inter-annual variability are shown in mode 2 and mode 3 of the unreduced PCA (cf. Figure 6.6). In tropical regions, trend signals are present in Africa (Lake Victoria) and Amazon basin showing that during the five years period those areas experienced mass loss. Beside the trends over the tropical regions, the most dominant trend signals are present over the polar regions such as Greenland, Alaska and Antarctica. The trend in those areas indicate considerable ice-mass loss over the five year period. However, to cautiously infer exact ice-mass changes, the post glacial rebound (PGR) signal has to be removed first from the gravity signal in these areas (e.g., Velicogna and Wahr, 2002; Swenson et al., 2003; Baur et al., 2007). Further dominant trend signals showing mass gain are revealed over great parts of Canada (the Canadian shield) and Fennoscandia (the Scandinavian shield) mostly related to crustal uplifting caused by PGR (e.g., Johnston and Lambeck, 1999).

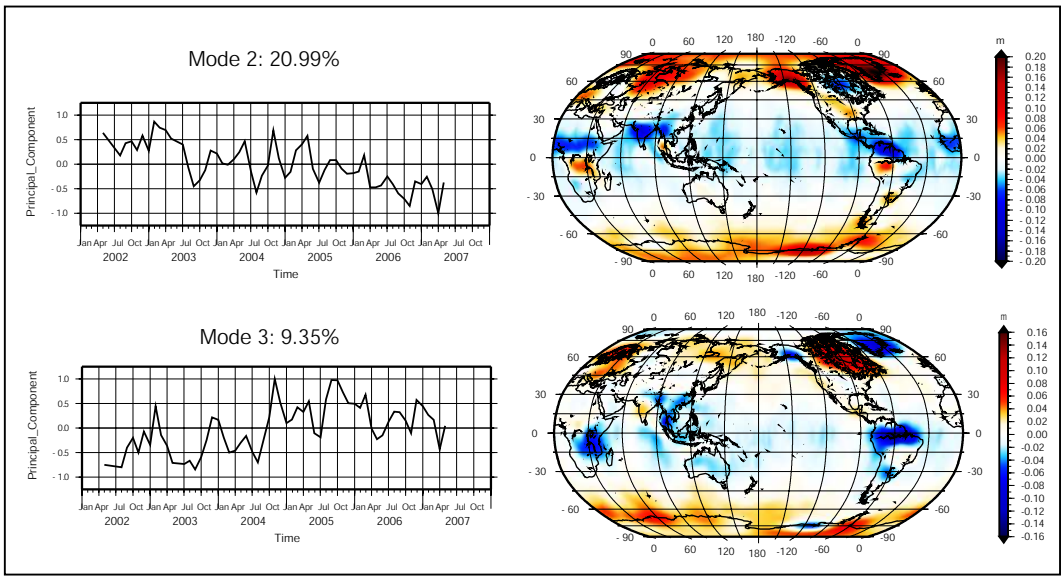

Figure 6.6: Trends are shown in mode 2 and mode 3 of the PCA results of the unreduced data

In the global analysis it can also be seen that in some areas the annual signal is slightly disturbed, such as in the Sumatra-Andaman region, which is the result of a massive earthquake that happened in December 2004. To study the gravity signal of this phenomena in more detail, a PCA over this region will be performed. A possible long-periodic signal is shown in the PC of mode 5 of the PCA, this could be related to a geophysical signal, or is only an artefact of the GRACE data (cf. Figure 6.8). Altogether, as indicated in Figure 6.5, 6.6 and

6.8 the first five modes take up more than 81% of the overall variability.

To better show remaining signals apart from trend and annual signal, the reduced PCA is performed. After reduction of the original GRACE data by the trend and annual signal (cf. Figure 6.3 and 6.4), the PCA results show that there are semi-annual signals as well. Performing a Fourier analysis on the PC, it is revealed that the semi-annual signal captures most of the energy in the first mode (cf. Figure 6.7) in the reduced signal. The inter-annual signal of mode 1 of the reduced PCA is mostly present in the tropical and polar regions with also a considerably magnitude over the oceans.

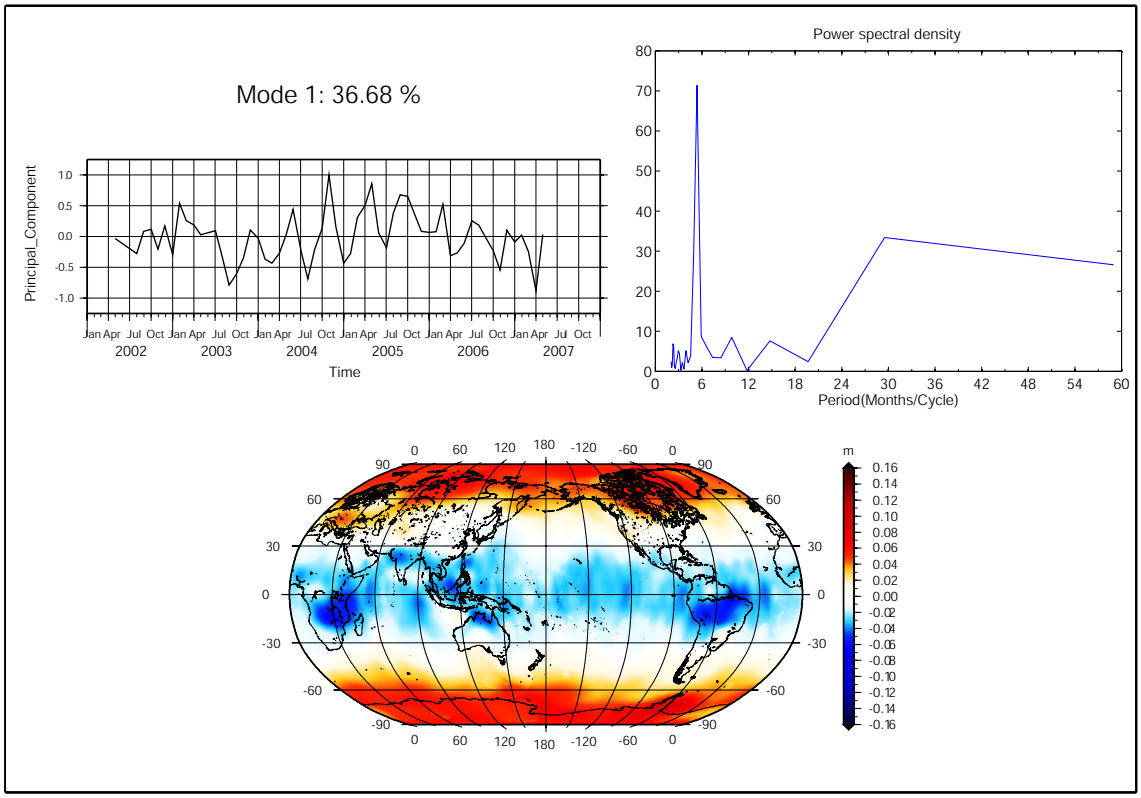

Figure 6.7: Power spectral density of the PCA shows that most energy in mode 1 of the reduced PCA for the global coverage is captured by a semi-annual signal.

Long-periodic changes as shown in mode 5 of the unreduced PCA appear now in mode 2 of the reduced PCA (cf. Figure 6.8). Again, it is not clear whether the signal is related to a real geophysical signal or an artefact of the GRACE data. The remaining mode (mode 3 and higher) of the reduced PCA becomes more difficult to interpret and considering the rather low contribution to the overall variability (more than 50% has been already reduced

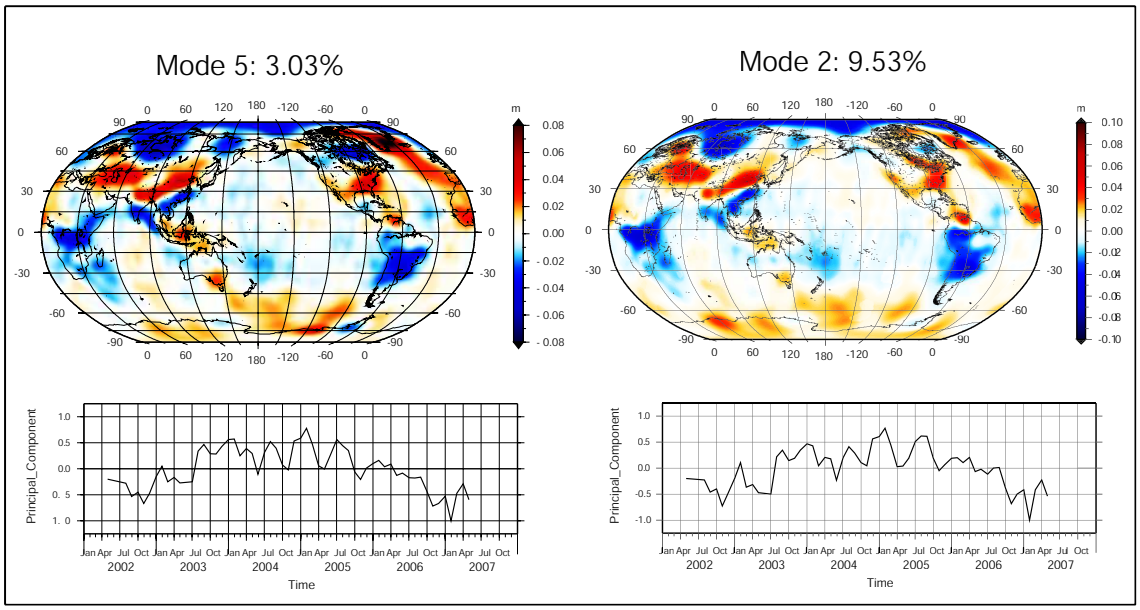

Figure 6.8: A long term changes found in mode 5 of the unreduced PCA (left) and mode 2 of the reduced PCA (right).

by annual signal and trend) no interpretation attempt has been made here. However, for completeness the PCA results for these modes are presented in Appendix C and a summary of the five most dominant signals variabilities is presented in Table 6.2.

Table 6.2: Variability of the five most dominant signals for global coverage of the unreduced PCA and the reduced PCA.

	Variability(%) of mode				
PCA	1	2	3	4	5
Unreduced	41.79	20.99	9.35	6.52	3.03
Reduced	36.68	9.53	4.96	4.44	3.86

6.3.2 Localized Analysis

The results from the global analysis indicate some locations with interesting signals and those area will be locally analysed using again a PCA. These areas are : Sumatra-Andaman, Australia, Africa, Antarctica, South America, Arctic, Greenland, North America, South Asia and Central Europe. The local analysis is performed in order to clearly examine geophysical signals as their gravity signals tend to be concentrated to specific locations. Both the unreduced PCA and the reduced PCA will be performed over these local areas. Comparing the unreduced PCA and reduced PCA results, the variability with respect to the overall variability expressed by the RMS value taken by trend and annual signal in the different study areas are summarised in Table 6.3.2. From this table it can be seen that in most region the annual signal takes up most of the overall variability except over Antarctica, Arctic and Greenland, where the trends are the most dominant signals.

Table 6.3: Overall variability taken up by trend and annual signal in each region.

Region	RMS Value				Variability taken by (%)		
	Unreduced	Reduced					
		trend	annual	both	trend	annual	both
1. Global	0.0388	0.0373	0.0234	0.0211	3.86	37.37	45.61
2. Sumatra-Andaman	0.0453	0.0399	0.0316	0.0246	11.92	30.24	46.00
3. Australia	0.0340	0.0329	0.0212	0.0201	3.24	37.65	40.88
4. Africa	0.0503	0.0496	0.0279	0.0266	1.39	44.53	47.12
5. Antarctica	0.0327	0.0271	0.0292	0.0256	17.12	10.70	21.71
6. South America	0.0930	0.0774	0.0346	0.0298	16.77	62.80	67.96
7. Arctic	0.0516	0.0394	0.0429	0.0292	23.64	16.86	43.41
8. Greenland	0.0573	0.0303	0.0558	0.0275	52.73	2.62	52.00
9. South Asia	0.0579	0.0417	0.0243	0.0220	27.98	58.03	62.00
10.North America	0.0387	0.0321	0.0303	0.0220	17.05	21.71	43.15
11.Central Europe	0.0420	0.0400	0.0274	0.0251	4.76	34.76	40.24

a. Sumatra-Andaman

The GRACE gravity signal is presumed to reflect geodynamic signatures. According to Gross and Chao (2001), the static displacement field generated by an earthquake can redistribute the Earth's mass. Due to the time span of the GRACE mission which is from April 2002 to June 2007, it is considered that the effect of the 2004 Sumatra-Andaman earthquake can be detected by GRACE. Studies of GRACE data application to analyse the track of earthquake signals have been conducted by several Earth's scientists such as Sun and Okubo (2004); Bao et al. (2005); Sabadini et al. (2005); Han et al. (2006a); Ogawa and Heki (2007); Chen et al. (2007); Sabadini et al. (2007).

During five years of the GRACE satellite mission to map the Earth's gravity field, USGS (US Geological Survey) has recorded several big earthquakes with magnitudes larger than five on the Richter scale around the Sumatra-Andaman region (cf. Table 6.4). These geophysical phenomena, should contribute to local gravity changes and GRACE should be able to detect these changes. The results of the PCA in this study area generally have a good agreement with other related studies (Bao et al., 2005; Sabadini et al., 2005; Han et al., 2006a; Ogawa and Heki, 2007; Chen et al., 2007; Sabadini et al., 2007). It has been proved that GRACE is capable to detect geophysical phenomena, in this case the earthquake. It also shows that by removing known geophysical meaningful signals, PCA can be used to analyse anomalous (a-periodic) signals of the gravity field.

The PCs of mode 1 and mode 2 of the unreduced PCA in the Sumatra-Andaman area show generally annual signals which are slightly disturbed around December 2004 - January 2005 coinciding with the great Sumatra-Andaman earthquake (cf. Figure 6.9). While the disturbance in the PC of mode 1 manifest mostly as a change in amplitude of the annual signal, in the PC of mode 2 it is shown as a complete interruption (shift) of the signal. As the Sumatra-Andaman region lies on the tropics most of the overall variability is taken up by the annual signal (mode 1 and mode 2 sum up to more than 84% of the overall variability) related to the annual cycles of wet and dry seasons.

Table 6.4: More than 5M earthquakes in Sumatra-Andaman region between April 2002 and May 2007 compiled from USGS.

Date	Location		Magnitude
	Epicenter	Depth (km)	(Richter)
2 November 2002	3.020°N 96.180°E	33	7.5
25 July 2004	2.455°N 103.977°E	576	7.3
26 December 2004	3.316°N 95.854°E	30	9.1
1 January 2005	5.090°N 92.300°E	12	6.7
28 March 2005	2.074°N 97.013°E	30	8.6
10 April 2005	1.660°S 99.540°E	19	6.7
14 May 2005	0.586°N 98.401°E	34	6.7
19 May 2005	1.965°N 96.976°E	30	6.9
5 July 2005	1.836°N 97.034°E	21	6.7
19 November 2005	2.220°N 96.763°E	30	6.5
16 May 2006	0.081°N 97.073°E	16.2	6.8
6 March 2006	0.512°S 100.524°E	19	6.4

In the unreduced PCA, the spatial structure of the earthquake is visible in the EOF (spatial variability) of mode 2 and mode 3 (cf. Appendix C). Higher modes of the PCA show inter-annual variations with some disturbances around the time of the earthquake. By performing Fourier analysis on the PCs of mode 4 and mode 5, it is shown that most energy of the inter-annual signal is semi-annual (cf. Figure 6.11), however modes beyond mode 2 of the unreduced PCA only contribute little to the overall variability. The five most dominant signal variabilities over this region are presented in Table 6.5.

Table 6.5: Variability of the five most dominant signals in the Sumatra-Andaman region of the unreduced PCA and the reduced PCA.

	Variability(%) of mode				
PCA	1	2	3	4	5
Unreduced	71.84	12.81	8.87	2.01	1.35
Reduced	63.86	18.32	7.20	3.04	2.17

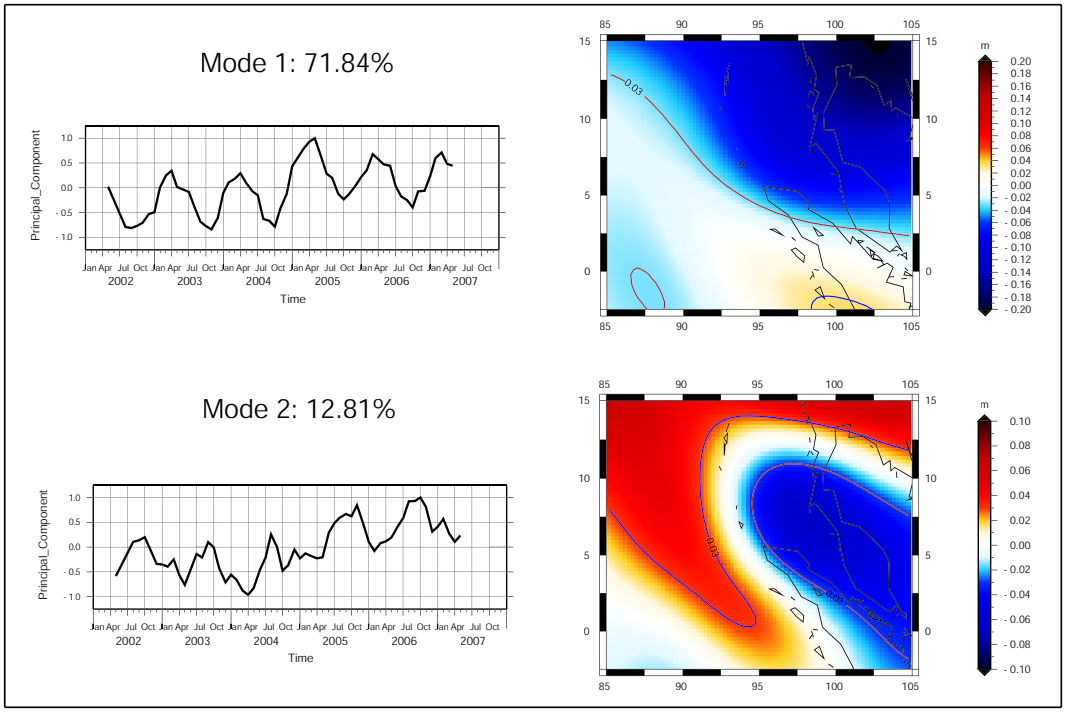

Figure 6.9: Annual signals with disturbances around December 2004-January 2005 are shown in mode 1 and mode 2 of on the unreduced PCA.

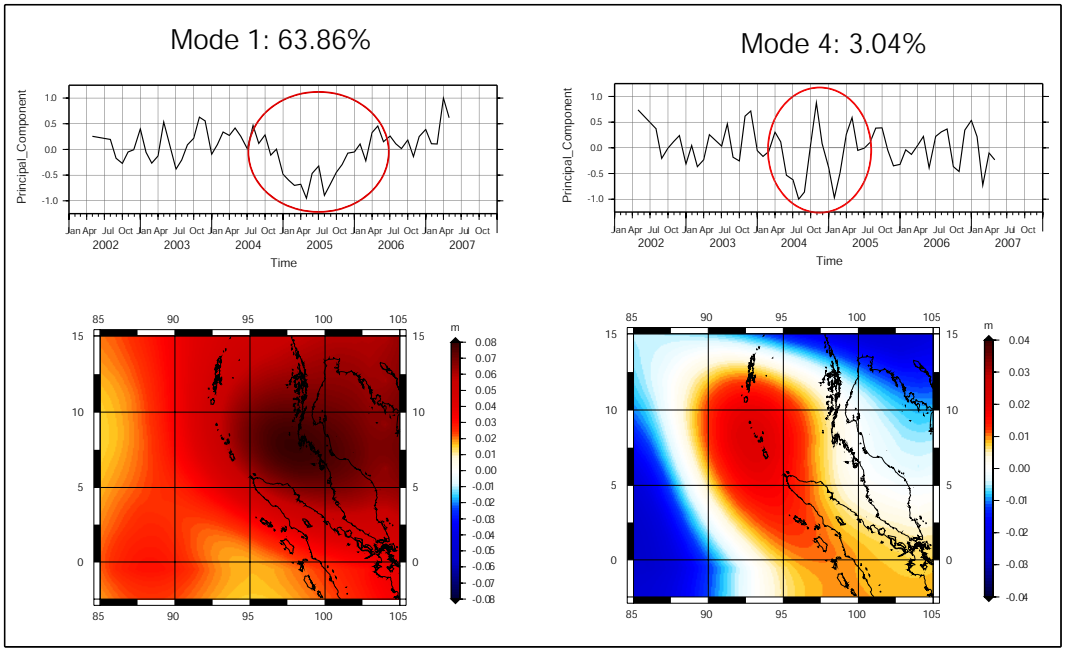

Figure 6.10: The anomalous signals are clearly shown in mode 1 and mode 4 of reduced PCA in Sumatra-Andaman region.

All of the PCA results of the reduced signal show a clear anomalous behavior at the time of the Sumatra-Andaman earthquake (cf. Appendix C). The anomalous signals related to the Sumatra-Andaman earthquake are clearly displayed in the PCs of mode 1 and mode 4 of the reduced PCA (cf. Figure 6.10). These signals are presumably related to the pre-seismic, coseismic and post-seismic signals of the earthquake. The spatial structure of the earthquake is once again shown in the EOFs of mode 2 and mode 3 of the reduced signal (cf. Appendix C). Apart from the anomalous behavior, all five modes also show inter-annual variations.

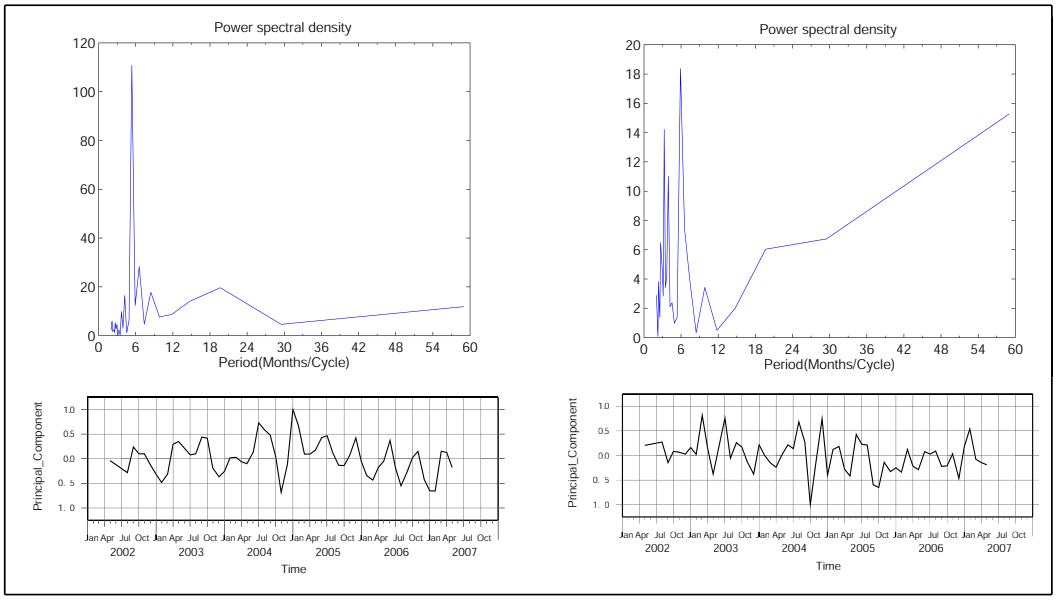

Figure 6.11: Power spectral density of the PC of mode 4 (left) and mode 5 (right) of the unreduced PCA in the Sumatra-Andaman region.

Even though it is obvious that the PCA results can reflect the signature of the Sumatra-Andaman earthquake, the EOFs can not clearly show the exact position of the earthquake's location (e.g., the epicenter). This is probably be caused by the resolution of the GRACE data and/or the type of PCA that used, e.g., it might better to use the rotation PCA in this case . Regarding to the resolution and error within the GRACE data, the leakage error is suspected falsifying the spatial interpretation as well.

b. Australia

The global PCA has shown a strong annual signal in the northern part of Australia related to the wet and dry season in the tropics. The unreduced PCA over the Australia continent shows quite similar results, especially as shown by the EOF of mode 1. Both mode 1 and mode 2 of the unreduced PCA are dominated by an annual cycle, which sum up to more than 77% of the total variability in this region. Interestingly the annual signal in mode 1 is clearly disturbed during the time of the Sumatra-Andaman earthquake. This can be interpreted as the effect of spatial leakage from the gravity signal produced by the "near by" Sumatra-Andaman earthquake.

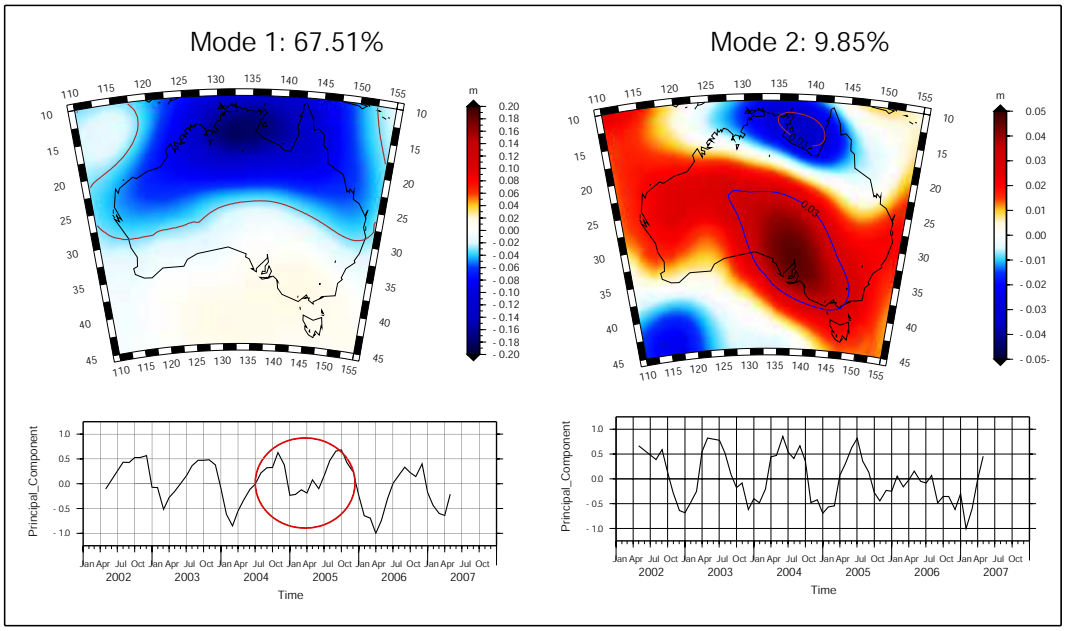

Figure 6.12: Annual signals are shown in mode 1 and mode 2 of the unreduced PCA over Australia. Disturbance is visible in mode 1 coinciding with the Sumatra-Andaman earthquake event.

The EOF of mode 2 shows a weaker annual signal across most of Australia with maximum magnitudes around the Murray-Darling river basin. Recent study of the application of GRACE data for hydrological monitoring over this are have been made by Awange et al. (2007). The annual signal is disturbed during the year 2006 that can be related to the Australian drought in 2006, indicating less rainfall than usual [e.g., shown by the precipitation

anomalies on the Bureau of Meteorology (www.bom.gov.au)]. The remaining modes show clear inter-annual variations of mostly semi-annual nature in the PCs of mode 3 and mode 4 (cf. Figure 6.13). The semi-annual signal is more likely the artefact of an a-symmetric annual cycle represented by a rapid mass gain in the first months of January, February and March and slower mass loss in the remaining months of the year.

All modes of the reduced PCA show clearly inter-annual signal variations with mode 4 exhibiting a semi-annual signal. Anomalous behavior appear once again likely a spatial leakage effect of the Sumatra-Andaman earthquake (cf. Appendix C). The five most dominant signal variabilities over the Australian are presented in Table 6.6.

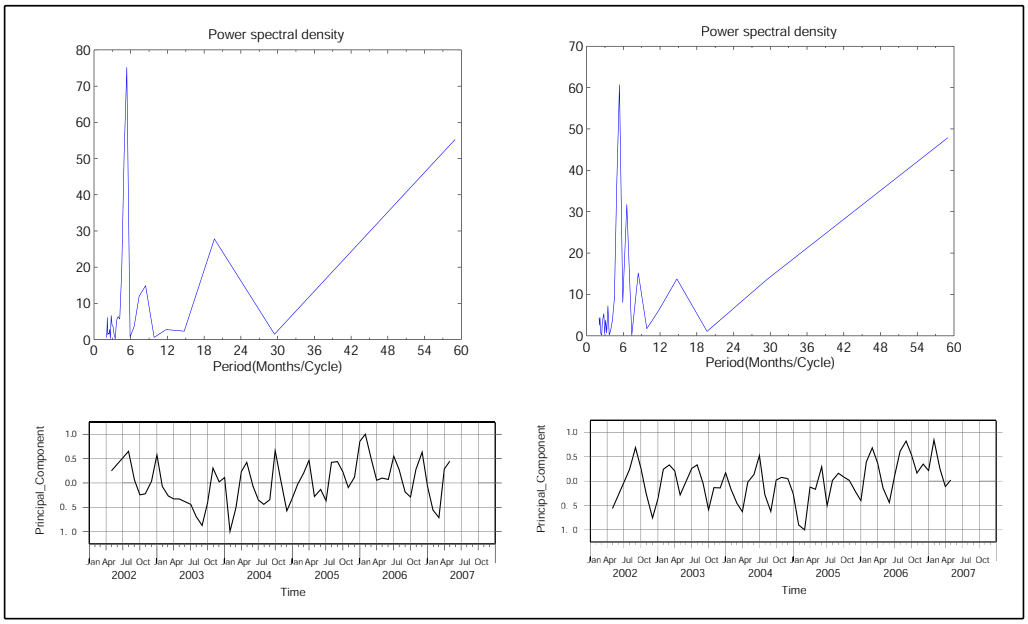

Figure 6.13: Power spectral density of the PCs of mode 3 (left) and mode 4 (right) of the unreduced PCA in Australia region

Table 6.6: Variability of the five most dominant signals for the Australia region of the unreduced PCA and the reduced PCA.

	Variability(%) of mode				
PCA	1	2	3	4	5
Unreduced	67.51	9.85	6.80	3.26	2.81
Reduced	38.28	17.88	9.40	8.04	5.97

c. Africa

The global analysis has shown strong variations of Earth's gravity field over the African continent, which occur as the result of water storage variation in some river basins such as the Lake Victoria region. The unreduced PCA performed over this area also indicates that the strongest temporal variation is annual ($> 77\%$) shown by mode 1. The EOF of mode 1 also shows the inverted season between the northern and southern hemispheres with almost no variability along the equator. A small trend with a superimposed inter-annual signal is shown in mode 2 (cf. Figure 6.14). The remaining modes only take up small parts of the overall variability in this region and show no clear geophysical signals.

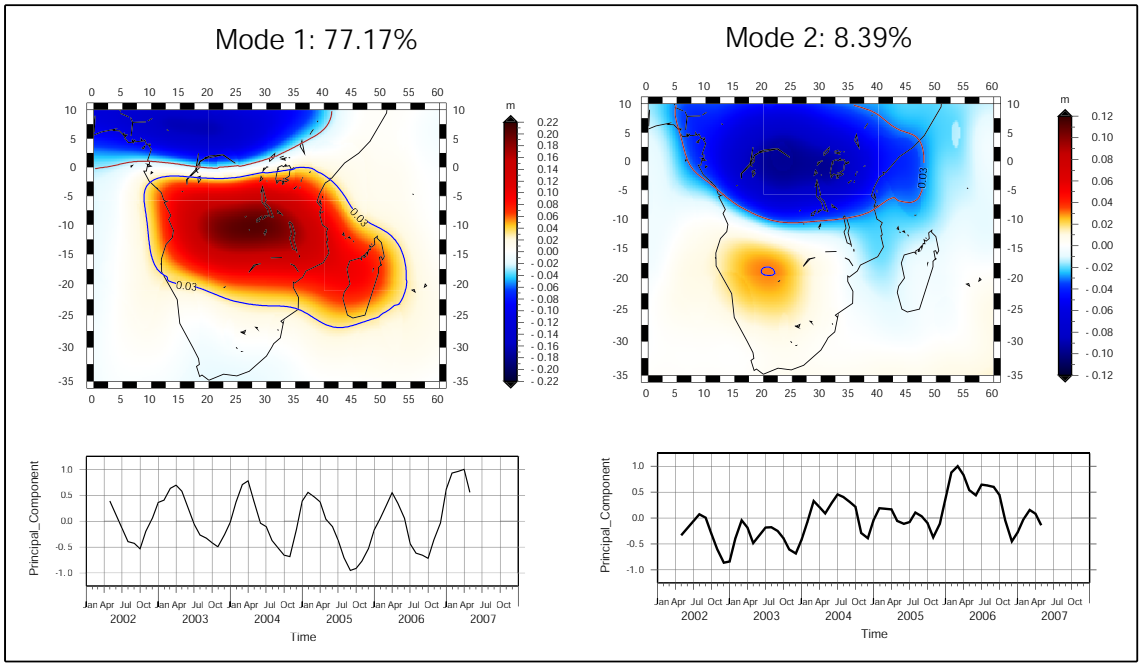

Figure 6.14: The results of the unreduced PCA over Africa. The PC of mode 1 shows clearly an annual signal (left) and the PC of mode 2 shows a small trend with a superimposed inter-annual signal (right).

After removing trend and annual signal from the data the reduced PCA now reveal a semi-annual signal as clearly visible in the PC of mode 2. The PC of mode 1 shows a slow negative trend over the first four years (2002 to 2005) and a rather large positive trend after 2006 which is also visible in the PC of mode 1 of the unreduced signal. Referring to the

EOF (spatial distribution) of mode 1, this behavior is related to a long-term mass loss over the Lake Victoria basin and a rather rapid mass gain in the year 2006. To confirm the finding, additional data such as rainfall data during the five year period are needed. The five most dominant signal variabilities over the Australian are presented in Table 6.7 and all of the PCA results over Africa are presented in Appendix C.

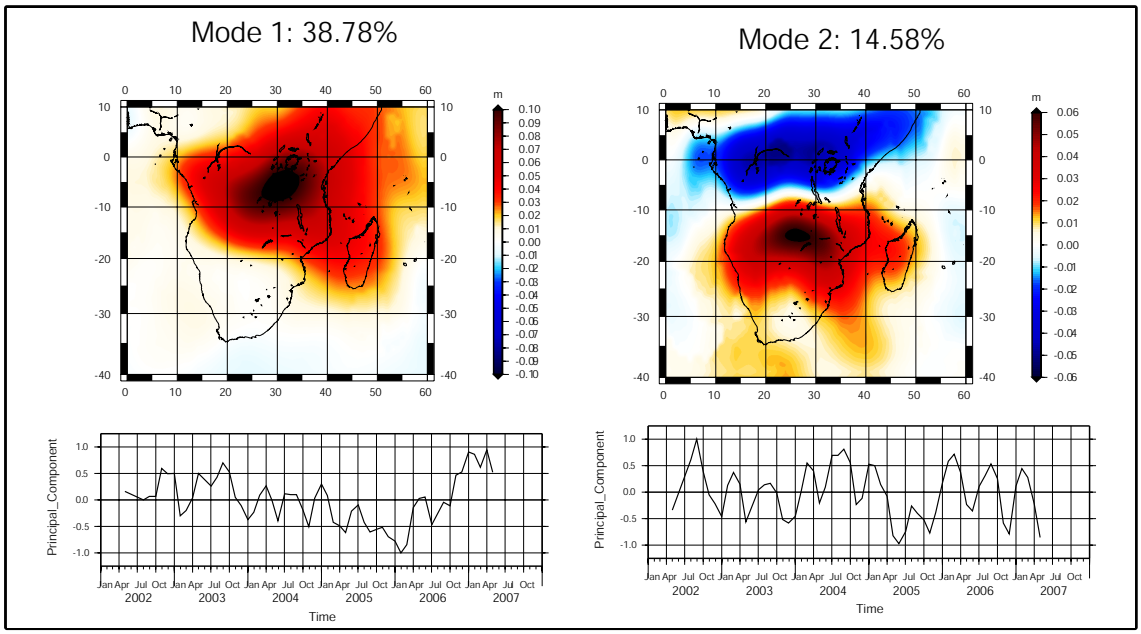

Figure 6.15: Mode 1 of the reduced PCA over Africa shows first a negative and then a positive trend.

Table 6.7: Variability of the five most dominant signals for the Africa region of the unreduced PCA and the reduced PCA.

	Variability(%) of mode				
PCA	1	2	3	4	5
Unreduced	77.17	8.39	4.16	2.84	1.66
Reduced	38.78	14.58	10.31	6.88	5.54

d. Antarctica

Mode 1 and mode 2 of the unreduced PCA capture most of the variability ($> 81\%$) over the Antarctic region and clearly exhibit a trend (cf. Figure 6.16). Mode 1 shows a large-scale mass loss over this region with a maximum over the West Antarctic ice shield and an accelerated mass loss during the last two years. Mode 2 shows mostly mass loss over the West-Antarctic ice shield and mass gain over the East-Antarctic ice shield. The remaining modes show only minor inter-annual variability, which is hard to interpret especially when considering the spatial distribution of the corresponding EOFs.

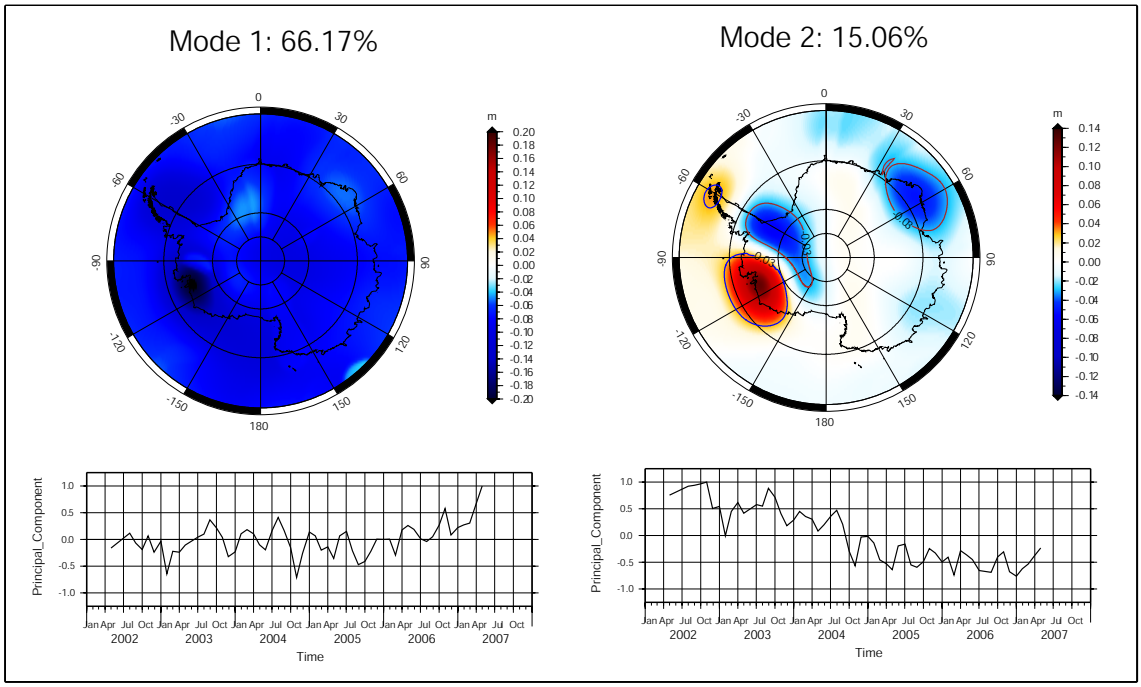

Figure 6.16: The results of the unreduced PCA over the Antarctic region. Mode 1 (left) and Mode 2 (right) show trends related to ice mass loss and gain.

The results of the reduced PCA show that the superimposed semi-annual signal in the first mode of the unreduced PCA now becomes the most dominant overall variability (about 75%). The remaining modes, that mainly show some inter-annual signals, only take up small amounts of the overall variability. The five most dominant signal variabilities over the Antarctic region are presented in Table 6.8 and all of the PCA results are presented in Appendix C.

Table 6.8: Variability of the five most dominant signals for the Antarctic region of the unreduced PCA and the reduced PCA.

	Variability(%) of mode				
PCA	1	2	3	4	5
Unreduced	66.17	15.06	3.46	4.20	1.95
Reduced	76.66	4.20	3.49	2.55	2.08

e. South America

Large gravity variations are found over South America, covering the Amazon and Orinoco basins. The Amazon is the largest drainage basin (5,738 million km^2) in the world according to Rodell and Famiglietti (1999) and has the largest variations in gravity (cf. Figure 6.2). In this region, results from the unreduced PCA show that almost 90% of the overall variability is taken up by the annual signal (shown by mode 1 and mode 2 of the PCA, cf. Figure 6.17).

The EOF of mode 1 shows that the greatest amplitudes of the annual signal occur in the Amazon basin. In the EOF of mode 2, it is shown that the Orinoco basin also contributes to the annual signal, although with a phase shift of a half a year. A study of Tapley et al. (2004a), has shown that it is possible to detect separation of drainage processes between the Amazon watershed and the Orinoco watershed because they are topographically (by the present of Angel Falls) and meteorologically (by the equator) separated. This property is also demonstrated by the PCA results having a clear separation between basins in mode 2 (cf. Figure 6.17).

Trends are shown in the PCs of mode 3 and mode 4, however their contribution to the overall variability are rather small (4.1% and 2.6% respectively). Mode 5 shows some inter-annual variability, however it has to be considered that the contribution to the total variability is very small (1.6 %), thus an interpretation becomes difficult (cf. Appendix C).

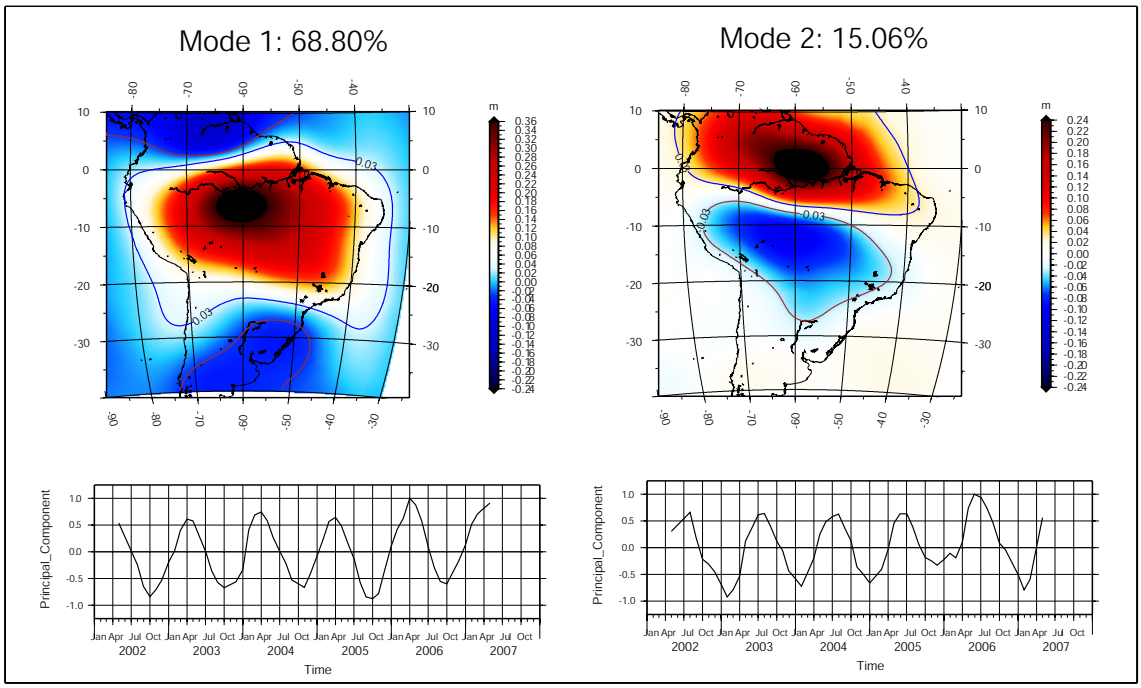

Figure 6.17: Mode 1 (left) and mode 2 (right) of the unreduced PCA show the largest variability in this area is captured by the annual signal.

All of the modes of the reduced PCA show some inter-annual signals without any predominant period, thus being mostly disturbances of the annual signal. Here it has to be considered that most of the variability has been taken up by the annual signal and it has been reduced from the data. The five most dominant signal variabilities over the South American region are presented in Table 6.9 and all of the PCA results are presented in Appendix C.

Table 6.9: Variability of the five most dominant signals for the South America region of the unreduced PCA and the reduced PCA.

	Variability(%) of mode				
PCA	1	2	3	4	5
Unreduced	68.80	18.77	4.08	2.62	1.61
Reduced	32.54	19.64	14.48	6.16	4.82

f. Arctic

Several authors have applied GRACE data to monitor ice-mass changes in the Arctic region (e.g., Chen et al., 2006a; Morison et al., 2004). The HA and global PCA have shown that a strong annual signal, trend (cf. Figure 6.4) and possible long-periodic signal (cf. Figure 6.8) occur in this region. The unreduced and the reduced PCA are applied here in order to investigate possible anomalous or a-periodic signals in this area.

Mode 1 of the unreduced PCA takes up over 50% of the overall variability and mostly shows a trend indicating large-scale mass loss over the Arctic. The EOF of this mode shows that the largest amplitude is located over the south-eastern part of Greenland, indicating that the largest mass loss is occurring over Greenland (more detail analysis will be performed below). Apart from recognizing a trend in mode 1, mode 2 shows an annual signal which captured almost 20% of the total variability. The EOF shows that the annual signal is directly related to the snow cover over Greenland, Alaska and Siberia.

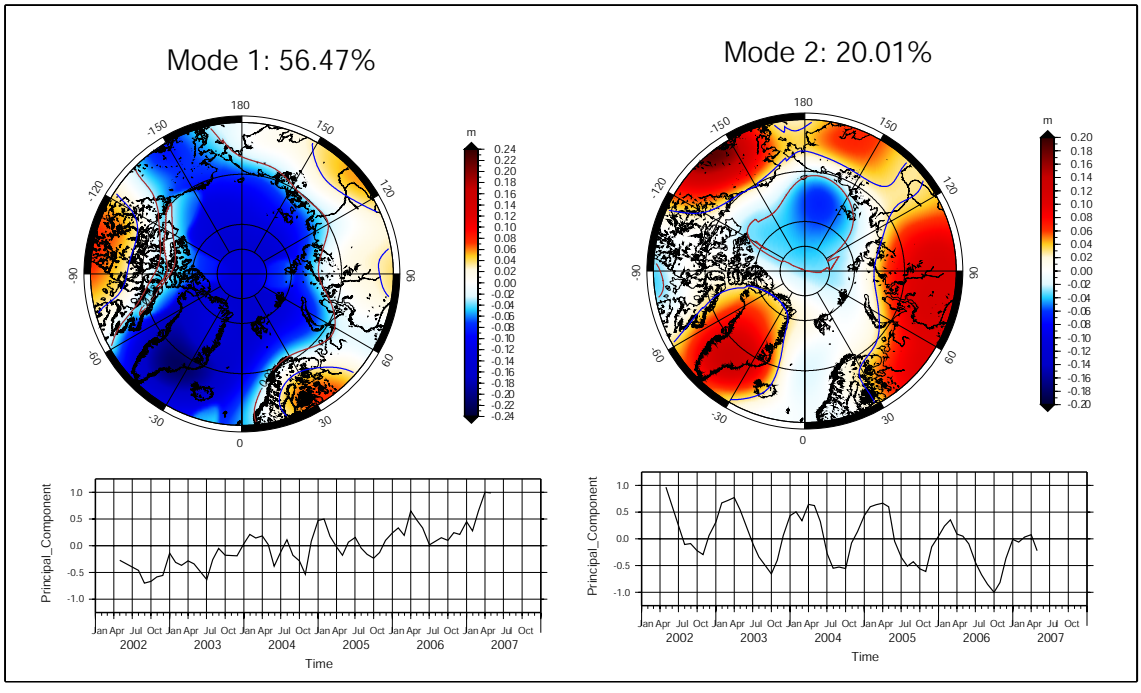

Figure 6.18: The results of unreduced PCA over Arctic region. Mode 1 (left) clearly shows trend and mode 2 (right) shows annual signal.

The maximum of the annual signal is shown in the Northern hemisphere spring, thus referring to the largest snow accumulation. Interestingly, an annual signal is also shown over the Arctic sea even though with a phase shift of a half a year. Considering that it is the North pole area, the phenomena only can be related to ocean water mass or sea ice changes, and it is still not clear what is the reason of the annual signal appearance. However, the study by White et al. (2007) indicates that the environmental changes in this area is believed to be caused by changes in the Arctic freshwater system.

The results of the reduced PCA over the Arctic region generally show that after removing the annual and trend signal, the inter-annual signal becomes dominant. However, interestingly mode 2 of the reduced PCA shows a trend starting in January 2005 and more likely indicating accelerated mass loss has occurred in large parts of the Arctic region (cf. Figure 6.19). The five most dominant signal variabilities over the Arctic region are presented in Table 6.10 and all of the PCA results are presented in Appendix C.

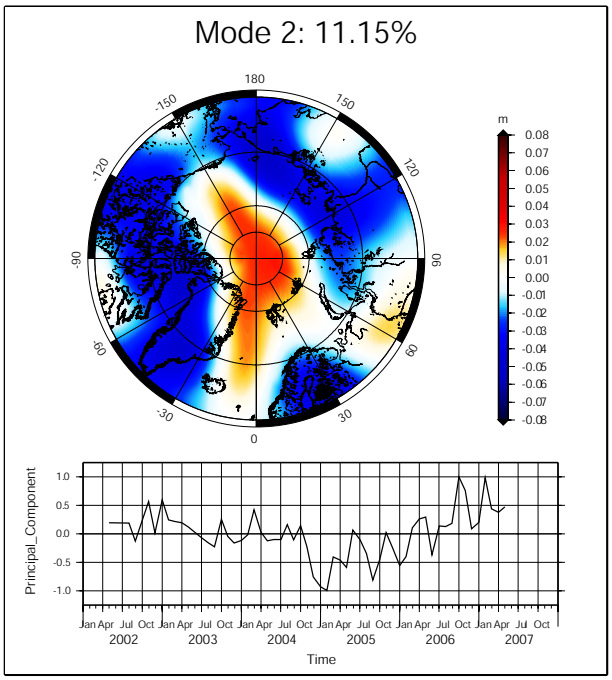

Figure 6.19: Mode 2 of the reduced PCA indicates accelerated mass loss has occurred in large part of the Arctic region over the last two years.

Table 6.10: Variability of the five most dominant signals for the Arctic region of the unreduced PCA and the reduced PCA.

	Variability(%) of mode				
PCA	1	2	3	4	5
Unreduced	56.47	20.01	8.17	4.87	2.40
Reduced	57.69	11.15	7.19	4.90	3.22

g. Greenland

Over Greenland, most of the total variability (about 74%) is taken up by a linear trend indicating large-scale mass loss (e.g., Velicogna and Wahr, 2005; Velicogna et al., 2005; Chen et al., 2006c; Baur et al., 2007). According to the EOF of mode 1, the greatest mass loss occurred over the south eastern part of Greenland, the area where the Gulf Stream passes Greenland. Mode 2 shows an annual signal with some superimposed inter-annual variability. This signal, like the trend in mode 1, is mostly present in the south-eastern part of Greenland (cf. Figure 6.20). This could be associated to the passing Gulf Stream that exhibits an annual signal due to annual temperature changes. In order to confirm this, however, a detailed study of sea surface temperature and sea level change data in this region are needed. The remaining modes have no interesting patterns, even though mode 3 shows some inter-annual variability but with no predominant period.

After removing the trend and the annual signal, mode 1 of the reduced PCA again shows inter-annual variability that is present over the whole region with the highest magnitude over the south-eastern part of Greenland. Mode 2 (cf. Figure 6.21) shows a long-term variation as also shown before in mode 2 of reduced PCA of global analysis (cf. Figure 6.8). It is not clear whether the long-term changes are due to a real geophysical process or an artefact of the GRACE data. The remaining modes show inter-annual variations, however these modes only take up a small part of the overall variability as more than 80% has already been removed by the trend and annual signal. The five most dominant signal variabilities over the Greenland are presented in Table 6.11 and all of the PCA results are presented in Appendix C.

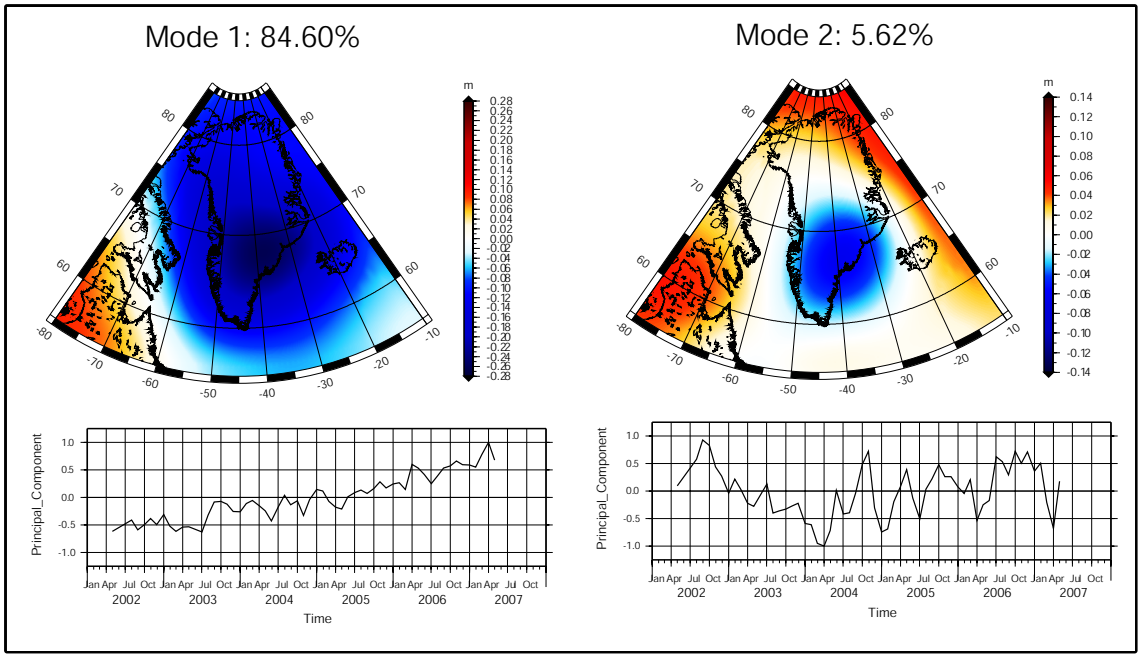

Figure 6.20: The results of the unreduced PCA over Greenland. Mode 1 (left) clearly shows a trend and mode 2 (right) shows an annual signal with trend over the first two years.

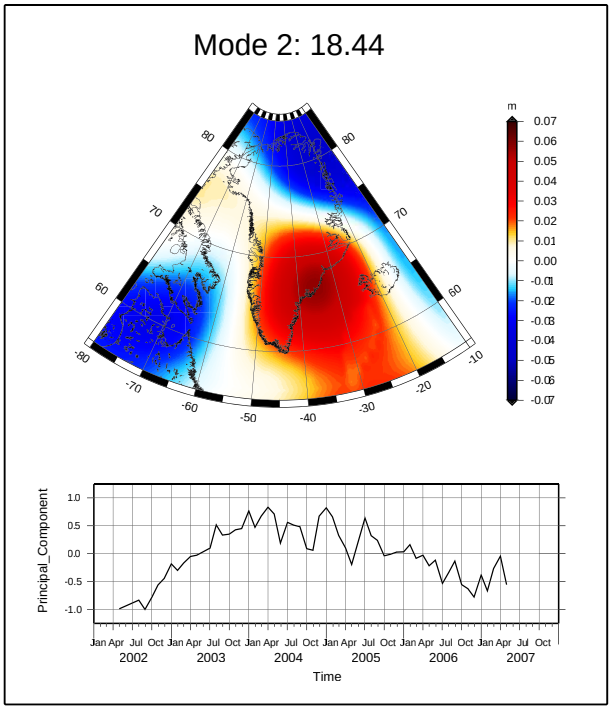

Figure 6.21: Mode 2 of the reduced PCA shows a possible long-periodic mass variations over Greenland.

Table 6.11: Variability of the five most dominant signals for the Greenland of the unreduced PCA and the reduced PCA.

	Variability(%) of mode				
PCA	1	2	3	4	5
Unreduced	84.60	5.62	4.10	2.27	1.51
Reduced	58.90	18.44	8.43	4.39	3.65

h. South Asia

Mode 1 shows that most of the overall variability (almost 70%) in this region is taken up by an annual signal. This signal is mostly present over the Himalayan region including the surrounding basins of the Ganges and Mekong. Therefore, this signal is likely a combination of the seasonal snow cover in the Himalaya and rain season of the surrounding areas. The annual signal is also present over the north part of Australia associated to the rain season (see the Australia region analysis). Mode 2 shows a linear trend with superimposed inter-annual variations. Some larger variations noticeable in 2004 and 2005 can be related to the Sumatra-Andaman earthquake which is also located in this region (cf. Figure 6.22). Annual signals are also shown in mode 3 and mode 4, which are also disturbed by the Sumatra-Andaman earthquake. Mode 5 shows an inter-annual variation with an anomalous large change at the beginning of 2003 (cf. Appendix C).

Mode 1 of the reduced PCA shows inter-annual variation with some larger magnitude in 2004. The corresponding EOF shows that the temporal signal is present over almost the complete region. The semi annual signal is clearly shown in mode 2. The temporal and spatial variability of mode 3 is almost identical with mode 5 of the unreduced PCA. The remaining modes show inter-annual variations with no predominant period. The five most dominant signal variabilities over South Asia are presented in Table 6.12 and all of the PCA results are presented in Appendix C.

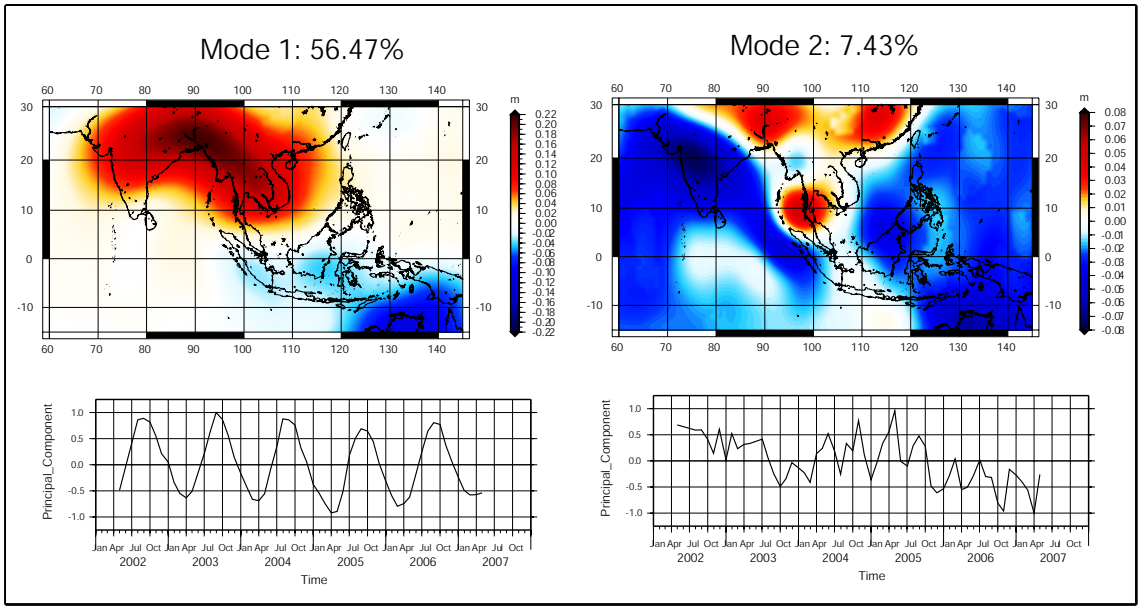

Figure 6.22: The results of the unreduced PCA over South Asia. Mode 1 (left) clearly shows an annual signal and mode 2 (right) shows a trend that presumably is related to the Sumatra-Andaman earthquake.

Table 6.12: Variability of the five most dominant signals for the South Asia region of the unreduced PCA and the reduced PCA.

	Variability(%) of mode				
PCA	1	2	3	4	5
Unreduced	56.47	7.43	6.04	4.80	2.88
Reduced	28.39	14.34	11.61	7.76	6.30

i. North America

A PCA of GRACE data over this area has been performed by Rangelova et al. (2007). Using 59 GRACE monthly solution in the same area, almost the same results as Rangelova et al. (2007) have been obtained here. The highlight in this area is a high variability composed of a trend and a low frequency signal (cf. Figure 6.23). The trend captures 42.62% (mode1) of the total variability in the area, whereas the low-frequency signal captures only 3.03% (mode 5).

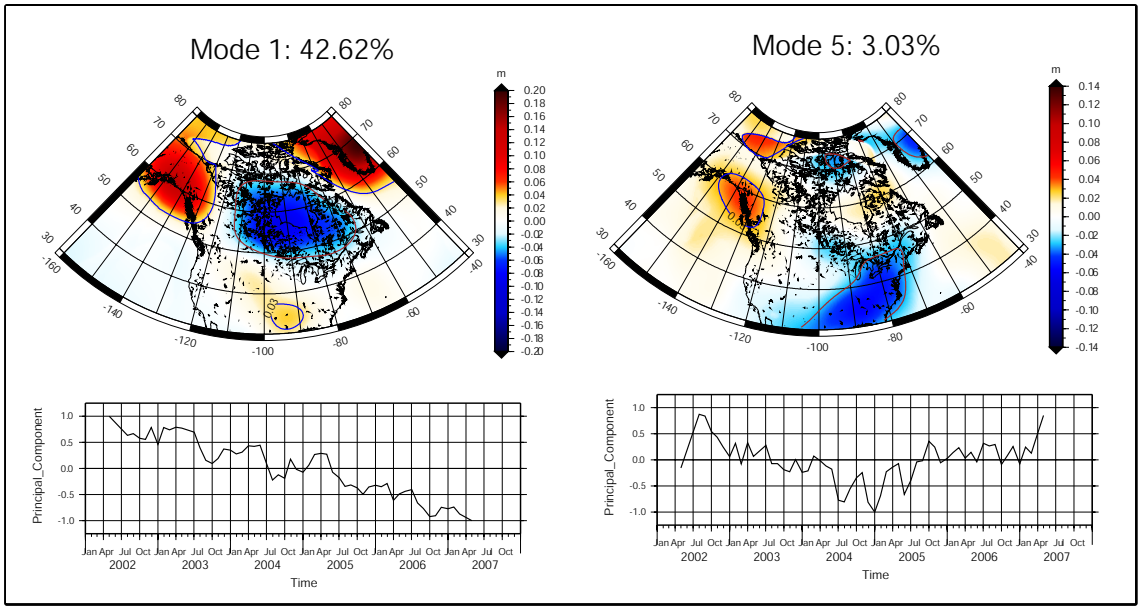

Figure 6.23: The results of the unreduced PCA over North America. Mode 1 (left) clearly shows a significant trend and mode 5 (right) shows low-frequency signal.

The EOF (spatial distribution) of mode 1 of the unreduced signal shows that the linear trend occurs in three major regions: mass loss over Alaska in the west, Greenland in the east and mass gain over large parts of Canada. The former two regions are associated to melting ice masses whereas the latter is the result of crustal uplift caused by postglacial rebound over the Canadian shield. The PC of mode 2 shows an annual signal, which is present over the whole North American continent with the highest magnitude over the Rocky Mountains. This signal is also associated to the seasons in the Northern hemisphere with the higher magnitudes over the Rocky Mountains caused by the changing snow cover. The PC of mode 3 shows an inter-annual signal with no predominant period. Mode 4 shows almost no temporal variability. The PC of mode 5 shows some inter-annual variability with an anomalous behavior in 2004.

By removing trend and annual signal from the original data, high frequency signals dominate the overall variance, even though the low-frequency signal now captures almost 11 %. However, the low-frequency signal is still not clear whether it is related to a real geophysical signal or only an artefact of the GRACE data. Mode 3 to mode 5 show inter-annual signals with no predominant period. The five most dominant signal variabilities over North America are presented in Table 6.13 and all of the PCA results are presented in Appendix C.

Table 6.13: Variability of five most dominant signals for the North America region of the unreduced PCA and the reduced PCA.

	Variability(%) of mode				
PCA	1	2	3	4	5
Unreduced	42.62	26.99	11.43	3.71	3.03
Reduced	43.07	10.72	6.54	5.62	5.00

j. Central Europe

Mode 1 of the unreduced PCA shows an annual signal with similar magnitude over almost the whole area. The annual signal is associated to the seasons in the Northern hemisphere related to the changing snow cover as the maximum of the annual signal is in early spring. A linear trend with some superimposed inter-annual signals is shown in mode 2. This temporal signal are distributed in the western, northern and eastern part but not in the centre of the region. Mode 3 also shows a linear trend but with a superimposed inter-annual variability. In contrary to the EOF of mode 2, this temporal signal is mostly present over Scandinavia and with a phase shift of a half a year in the south-eastern part of the area (cf. Figure 6.24). This signal is a combination of the postglacial rebound signal and snow cover over Fennoscandia. Mode 4 shows almost no temporal variability and a long-term change found in mode 5.

The results of the reduced PCA in this region mainly show high frequency signals, which are difficult to interpret. The five most dominant signal variabilities over Central Europe are presented in Table 6.14 and all of the PCA results are presented in Appendix C.

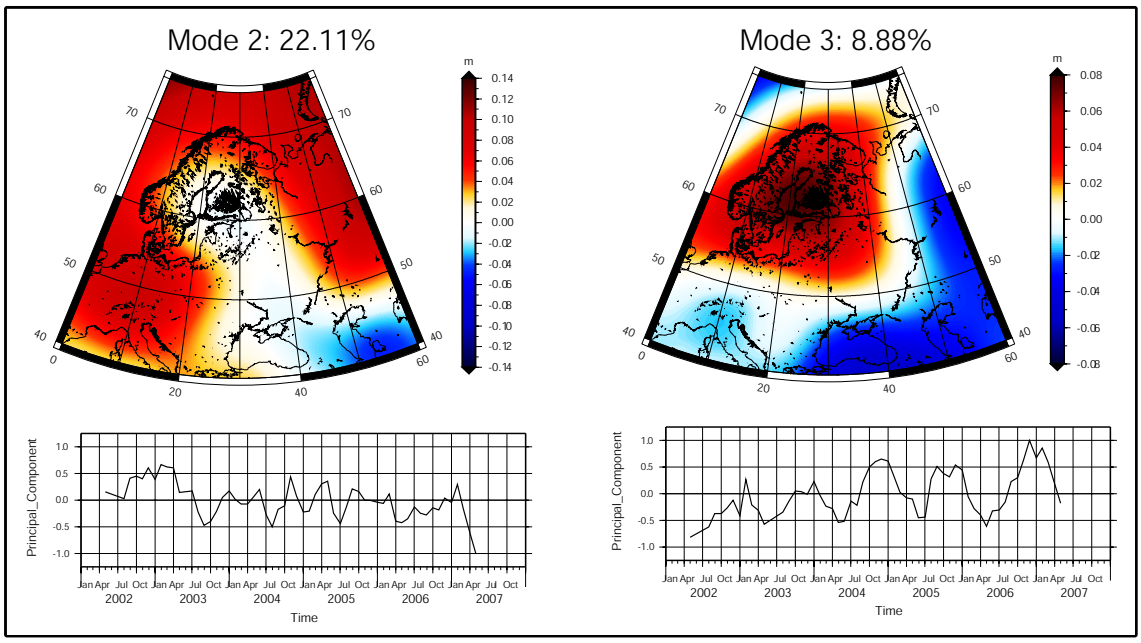

Figure 6.24: Mode 2 and mode 3 of unreduced PCA over Central Europe show the trends that distributed in different part of the region.

Table 6.14: Variability of the five most dominant signals for the Central Europe region of the unreduced PCA and the reduced PCA.

	Variability(%) of mode				
PCA	1	2	3	4	5
Unreduced	50.28	22.11	8.88	5.88	4.91
Reduced	33.95	22.11	17.10	6.06	4.31

6.4 Summary

In this chapter the GRACE data and methods used in this research were described. The analyses and results from the HA and the PCA were presented both on a global scale and a local scale. Based on these results and analysis, a summary and conclusions will be presented in Chapter 7 as well as some outlooks for future research.

7. SUMMARY, CONCLUSION AND OUTLOOK

The significant findings of the study summarised in this chapter are based on the results of applying the HA and PCA to five years of GRACE monthly gravity field solutions. The summary will also include the data and methodology used in this study. From this summary, some conclusions will be derived. Outlook for future research is provided in the last part of this chapter.

7.1 Summary

This study examined 59 GRACE monthly gravity field solutions in order to analyse the spatial and temporal variability of the Earth's gravity field observed by the GRACE satellite mission. The used data cover a complete cycle of five years (from April 2002 to May 2007, inclusive). The GRACE level-2 release four data provided by the UTCSR were used and as they were in the form of spherical harmonic coefficients of the Earth's gravitational potential, a method to infer mass change estimates was applied. Here, the mass change estimates were presented as EWT, and reduced by the mean value for PCA processing.

The general information of the variability of the Earth's gravity field was provided by the HA over the whole globe through the representation of RMS value and global trend. Moreover the results from HA, which are annual signal and linear trend, were then used to reduce the original data in order to isolate remaining geophysical signals apart from the annual and trend signals. The PCA was performed to the data reduced by only the mean (unreduced PCA) and to the data reduced by the mean, annual and trend signals (reduced PCA).

Both the results of the HA and PCA showed that an annual signals is the most dominant variability of the gravity field over most areas over the globe. The unreduced PCA also indicated the dominant annual signals in some local regions. Whereas, trend appeared the

most dominant in some other areas. By reducing the annual signal and trend from the original GRACE data, and performing the so called reduced PCA, it was shown that long-periodic and a-periodic signals were revealed in some regions. The important results of the HA and PCA are summarised below.

a. Dominant Annual signal

The spatial pattern of the RMS showed the areas with high variabilities. These areas are: South America, Africa, South Asia, North Australia-Indonesia, Alaska, Greenland and Antarctica. However this result has not shown what type of variability is present in each area. The results of the unreduced PCA over the whole globe showed that the annual signal captured about 50% of the total variability. The unreduced PCA results also showed the most dominant annual signal over some local areas of: Sumatra-Andaman ($> 80\%$ of total variability), Australia ($> 70\%$ of total variability), Africa ($> 77\%$ of total variability), South America (almost 90 % of total variability), and South Asia (almost 70 % of total variability).

b. Significant Trends in Some Regions

As well as the annual signal, significant trends were also found both on a global and local scale. On the global scale the distribution of the linear trend shown by the HA result illustrated that the significant trends are present in the areas of: Greenland, Alaska, Antarctica, Sumatra-Andaman and North America. Some minor trends also appeared over the continental basins such as the Lake Victoria and Ganges watershed. The global unreduced PCA also showed the trends (captured almost 30% of the total variability) present in the areas of: Greenland, Alaska and Antarctica , which can be related to the ice-mass loss over those areas; and Lake Victoria and Amazon basin, which can be related to water-mass loss. Significant trends showing mass gain were found over the Canadian and Scandinavian shield mostly related to the crustal uplifting caused by PGR.

The local unreduced PCA revealed that the trend is the most dominant signal in the regions of: Antarctica ($> 81\%$ of total variability), Arctic ($> 50\%$ of total variability), Greenland (about 74% of total variability), and North America (about 43% of total variability).

c. Possible Long-periodic Signal

Long-periodic signals found on the global analysis both as the result of unreduced and reduced PCA. However, the spatial representation of this signal (EOF) was hard to interpret and it was not clear whether the signal has real geophysical meaning or is just an artefact of the GRACE data. For the unreduced PCA over Greenland, the long-periodic signal might also indicate a long-term mass change over the Southeast part of Greenland.

d. Detection of Geodynamical Event (A-periodic Signal)

One of the interesting result found in this research is the signature of the Sumatra-Andaman earthquake in late December 2004. Applying PCA to the GRACE data over this region showed that apart from the annual signal and trend in this area, disturbances coinciding with the earthquake were clearly captured in all modes of the unreduced and reduced PCA. The reduced PCA results over this area revealed the earthquake signature more clearly. Geophysical signals related to postglacial rebound also appeared over Canada and Fennoscandia.

7.2 Conclusion

The GRACE gravity data has improved the understanding of both the static and time-variable gravity field. Importantly time-variable gravity data have provided a novel information of the geophysical processes within and on the surface of the Earth. Moreover, this information becomes important for a better understanding of surface mass changes caused by current climate change.

The number of GRACE monthly gravity field solutions (64 as of February 2008 and will increase by the extension of the mission until at least 2010) has made it possible to apply statistical analysis methods to the data. The combination of HA and PCA used in this study has shown significant results. Dealing with the gravity field data as a space-time system, it has been shown that the PCA method is now an appropriate tool to analyse the most dominant spatial and temporal variability of the gravity field signal.

7.3 Outlook

This study has attained interesting results by using the PCA to analyse the spatial and temporal variability of the Earth's gravity field observed by the GRACE mission. Both the global and local analysis has shown that the method is powerful enough to examine the most dominant signals of the GRACE gravity field. The combination of HA and PCA has shown that by reducing geophysical meaningful signals i.e., annual signals and trends (the results of HA), the PCA can detected long-periodic and a-periodic signals due to particular geodynamical events. However, as the PCA is only a mathematical procedure, sometimes the interpretation made on its geometrical properties is difficult. Therefore, for future studies it is recommended to use extended PCA methods such as POPs (Principal Oscillation Patterns) to isolate spatial patterns with strong temporal dependence.

In order to clearly examine the long-periodic signal as found in this study, a longer time series of the data is needed. This will be assisted by the extension of the GRACE satellite mission until at least 2010. The current gravity field data observed by GRACE will be validated by the future GOCE satellite mission. Furthermore, the GOCE mission is expected to enhance both the knowledge and applications of the Earth's gravity field in understanding the dynamics of the Earth.

REFERENCES

Andersen, O. and J. Hinderer. 2005. Global inter-annual gravity changes from GRACE: Early results. *Geophysical Research Letters* 32:L01402.

Awange, J. L., M. A. Sharifi, O. Baur, W. Keller, W. E. Featherstone, and M. Kuhn. 2007. Hydrological monitoring from space: current limitations and future prospects for the GRACE gravimetry mission over Australia. *Journal of Spatial Science* (in-press).

Balmino, G. 2001. New space missions for mapping the Earth's gravity field. *Comptes Rendus de l'Academie des Sciences Series IV Physics* 2(9):1,352–1,359.

Bao, L. F., A. Piatanesi, Y. Lu, H. T. Hsu, and X. H. Zhou. 2005. Sumatra tsunami affects observations by GRACE satellites. *EOS Transactions, AGU* 86:353–356. DOI 10.1029/2005EO390002.

Baur, O., M. Kuhn, and W. E. Featherstone. 2007. GRACE-derived ice-mass variations and their effect on global sea-level change patterns. *Journal of Geophysical Research* (in-press).

Benz, R., M. Langemann, M. Gramolla, and G. Mecke. n.d. ARISTOTELES - Description of the Earth gravity field recovery mission. in-press.

Bettadpur, S. 2006. *Level-2 Gravity Field Product User Handbook*. GRACE 327 - 734. Austin: Centre for Space Research University of Texas.

———. 2007. GRACE product specification document. Tech. Rep. GRACE 327-720, Centre for Space Research University of Texas, Austin.

Beutler, G., R. Rummel, M. R. Drinkwater, and R. v. Steiger, eds. 2003. *Earth gravity field from space - From sensors to Earths sciences*, vol. 17 of *Space Science Series of ISSI*. Dordrecht: Kluwer Academic Publishers.

Biancale, R., G. Balmino, J. M. Lemoine, J. C. Marty, B. Moynot, F. Barlier, P. Exertier, O. Laurain, P. Gegout, P. Schwintzer, C. Reigber, A. Bode, R. König, F. H. Massmann, J. C. Raimondo, R. Schmidt, and S. Y. Zhu. 2000. A New Global

Earths Gravity Field Model from Satellite Orbit Perturbations: GRIM5-S1. *Geophysical Research Letters* 27(22):3611–3614.

Biro, P. 1983. *Time variation of height and gravity*. Karlsruhe: Herbert Wichmann Verlag.

Bursa, M. and K. Pec. 1988. *Gravity field and dynamics of the Earth,*. Berlin: Springer Verlag.

Cazevane, A., F. Mercier, F. Bouille, and J. M. Lemoine. 1999. Global-scale interactions between the solid Earth and its fluid envelopes at the seasonal time scale. *Earth and Planetary Science Letters* 171:549–559.

Cazevane, A. and R. S. Nerem. 2002. Redistributing Earth's mass. *Science* 297(5582):783–784.

Chambers, D. P. 2006a. Evaluation of new GRACE time-variable gravity data over the ocean. *Geophysical Research Letters* 33:L17603.

———. 2006b. Observing seasonal steric sea level variations with GRACE and satellite altimetry. *Journal of Geophysical Research* 111:C03010.

Chambers, D. P., M. E. Tamisiea, R. S. Nerem, and J. C. Ries. 2007. Effects of ice melting on GRACE observations of ocean mass trends. *Geophysical Research Letters* 34:5610–+. Provided by the Smithsonian/NASA Astrophysics Data System.

Chao, B. F. 2005. On inversion for mass distribution from global (time-variable) gravity field. *Journal of Geodynamics* 39(3):223–230.

Chao, B. F. and W. P. O'Connor. 1988. Effect of a uniform sea-level change on the Earth's rotation and gravitational field. *Geophysical Journal* 93:191–193.

Chen, J. L., C. R. Wilson, D. D. Blankenship, and B. D. Tapley. 2006a. Antarctic mass rates from GRACE. *Geophysical Research Letters* 33:L11502. DOI 10.1029/2006GL026369.

Chen, J. L., C. R. Wilson, J. S. Famiglietti, and M. Rodell. 2005. Spatial sensitivity of the gravity recovery and climate experiment (GRACE) time-variable gravity observations. *Journal of Geophysical Research* 110:B08408.

Chen, J. L., C. R. Wilson, and K.-W. Seo. 2006b. Optimized smoothing of Gravity Recovery and Climate Experiment (GRACE) time-variable. *Journal of Geophysical*

Research 111:B06408. DOI 10.1029/2005JB004064.

Chen, J. L., C. R. Wilson, and B. D. Tapley. 2006c. Satellite gravity measurements confirm accelerated melting of Greenland ice sheet. *Science* 313:1958–1960. DOI 10.1126/science.1129007.

Chen, J. L., C. R. Wilson, B. D. Tapley, and S. Grand. 2007. GRACE detects coseismic and postseismic deformation from the Sumatra-Andaman earthquake. *Geophysical Research Letters* 34:L13302. DOI 10.1029/2007GL030356.

Cox, C. M. and B. F. Chao. 2002. Detection of a large-scale mass redistribution in the terrestrial system since 1998. *Science* 297:831–833.

Dickey, J. O. 2001. Time variable gravity : An emerging frontier in interdisciplinary geodesy. In *Gravity, Geoid and Geodynamics 2000*, ed. M. G. Sideris, vol. 123, 1–5. International Association of Geodesy Symposia, Berlin: Springer.

Dickey, J. O., C. R. Bentley, R. Bilham, J. A. Carton, R. J. Eanes, T. A. Herring, W. M. Kaula, G. S. E. Lagerloef, S. Rojstaczer, W. H. F. Smith, H. M. van den Dool, J. M. Wahr, and M. T. Zuber. 1997. *Satellite gravity and the geosphere: Contributions to the study of the solid Earth and its fluid envelopes*. Washington, D.C.: National Academic Press.

Dickey, O. J., S. Marcus, O. d. Viron, and I. Fukumori. 2002. Recent Earth oblateness variations: Unraveling climate and postglacial rebound effects. *Science* 1(298):1975–1977.

European Space Agency. 2007. Gravity field and steady-state ocean circulation mission. http://www.esa.int/esaLP/LPgoce.html (accessed 1 November, 2007).

Farrell, W. 1972. Deformation of the Earth by surface loads. *Review of Geophysics and Space Physics* 10(3):761–797.

Fengler, M. J., W. Freeden, A. Kohlhaas, V. Michel, and T. Peters. 2006. Wavelet modeling of regional and temporal variations of the Earths gravitational potential observed by GRACE. *Journal of Geodesy* 81(1):5–15.

Finkenstadt, B., L. Held, and V. Isham. 2006. *Statistical methods for spatio-temporal system*. Monographs on Statistics and Applied Probability 107. New York: Chapman and Hall.

Flechtner, F. 2007. AOD1B Product Description Document for Product Releases 01 to 04. Tech. Rep. GRACE 327-750, GFZ, Postdam.

Flury, J. and R. Rummel. 2006. Future satellite gravimetry for Geodesy. *Earth, Moon, and Planets* 94(1-2):13–29.

Fuentes, M., P. Guttorp, and P. D. Sampson. 2006. *Using transforms to analyse space-time processes*. Monographs on Statistics and Applied Probability 107. New York: Chapman and Hall.

Garland, G. D. 1977. *The Earth's shape and gravity*. Oxford: Pergamon Press Ltd.

GFZ Postdam. 2008. The GRACE mission. http://www.gfz-potsdam.de/pb1/op/grace/ (accessed January, 2008).

Gneiting, T., M. G. Genton, and P. Guttorp. 2006. *Geostatistical space-time models, stationarity, separability, and full symmetry*. Monographs on Statistics and Applied Probability 107. New York: Chapman and Hall.

Gross, R. S. and B. F. Chao. 2001. The gravitational signature of earthquakes. In *Gravity, Geoid and Geodynamics 2000*, ed. M. G. Sideris, vol. 123. International Association of Geodesy Symposia, Berlin: Springer.

Han, S.-C., C. Jekeli, and C.-K. Shum. 2003. Static and temporal gravity field recovery using GRACE potential difference observables. *Advances in Geosciences* 1:19–26.

Han, S.-C., C. Jekeli, and C. K. Shum. 2004. Time-variable aliasing effects of ocean tides, atmosphere, and continental water mass on monthly mean GRACE gravity field. *Journal of Geophysical Research* 109:B04403.

Han, S.-C., C. K. Shum, M. Bevis, C. Ji, and C.-Y. Kuo. 2006a. Crustal dilatation observed by GRACE after the 2004 Sumatra-Andaman earthquake. *Science* 313(5787):658–662.

Han, S.-C., C. K. Shum, and A. Braun. 2005a. High-resolution continental water storage recovery from low-low satellite-to-satellite tracking. *Journal of Geodynamics* 39(1):11–28.

Han, S.-C., C. K. Shum, P. Ditmar, P. Visser, C. van Beelen, and E. J. O. Schrama. 2006b. Aliasing effect of high-frequency mass variations on GOCE recovery of

the Earth's gravity field. *Journal of Geodynamics* 41(1-3):69–76.

Han, S.-C., C. K. Shum, C. Jekeli, and D. Alsdorf. 2005b. Improved estimation of terrestrial water storage changes from GRACE. *Geophysical Research Letters* 32:L07302. DOI 10.1029/2005GL022382.

Han, S.-C., C. K. Shum, C. Jekeli, C.-Y. Kuo, C. Wilson, and K.-W. Seo. 2005c. Non-isotropic filtering of GRACE temporal gravity for geophysical signal enhancement. *Geophysical Journal International* 163:18–25.

Han, S.-C. and F. J. Simons. 2008. Spatiospectral localization of global geopotential fields from GRACE reveals the coseismic gravity change due to the 2004 Sumatra-Andaman earthquake. *Journal of Geophysical Research* 113:B01405.

Hannachi, A., I. T. Jolliffe, and D. B. Stephenson. 2006. Empirical orthogonal functions and related techniques in atmospheric science: A review. *International Journal of Climatology* 27(9):1119–1152.

Heiskanen, W. A. and H. Moritz. 1967. *Physical Geodesy*. San Francisco: W. H. Freeman and Company.

Hinderer, J., O. Andersen, F. Lemoine, D. Crossley, and J.-P. Boy. 2006. Seasonal changes in the European gravity field from GRACE: A comparison with superconducting gravimeters and hydrology model predictions. *Journal of Geodynamics* 41(1-3):59–68.

Hofmann-Wellenhof, B. and H. Moritz. 2005. *Physical Geodesy*. Vienna: Springer.

Jekeli, C. 1981. Alternative methods to smooth the Earth's gravity field. Tech. Rep. 327, Dept. of Geod. Sci. and Surv., Ohio State Univ., Columbus.

Johnston, P. and K. Lambeck. 1999. Postglacial rebound and sea level contributions in the geoid and the Earth's rotations axis. *Geophysical Journal International* 136:537–558.

Jolliffe, I. T. 2002. *Principal component analysis*. Springer series in statistics, 2nd ed. New York: Springer.

JPL NASA. 2008. GRACE: Gravity Recovery and Climate Experiment. http://podaac.jpl.nasa.gov/grace/ (accessed January, 2008).

Kaula, W. M. 2000. *Theory of satellite Geodesy*. New York: Dover Publications, Inc.

King, M., P. Moore, P. Clarke, and D. Lavallée. 2006. Choice of optimal averaging radii for temporal GRACE gravity solutions, a comparison with GPS and satellite altimetry. *Geophysical Journal International* 166:1–11.

Kooperberg, C. and F. O'Sullivan. 1996. Predictive oscillation patterns: A Synthesis of methods for spatial-temporal decomposition of random fields. *Journal of the American Statistical Association* 91(436):1485–1496.

Kuhn, M., W. Bosch, and R. Kaniuth. 2005. Low-frequency variations of the North Atlantic sea level measured by TOPEX/Poseidon altimetry. *Marine Geodesy* 28:19–37.

Kusche, J. 2007. Approximate decorrelation and non-isotropic smoothing of time-variable GRACE-type gravity field models. *Journal of Geodesy* 81(11):733–749.

Kusche, J. and E. J. O. Schrama. 2005. Surface mass redistribution inversion from global GPS deformation and Gravity Recovery and Climate Experiment (GRACE) gravity data. *Journal of Geophysical Research* 110:B09409.

Lambert, A., T. S. James, J. O. Liard, and N. Courtier. 1995. The role and capability of absolute gravity measurements in determining the temporal variations in the Earth's gravity field. In *Global gravity and its temporal variations*, eds. R. H. Rapp, A. Cazenave, and R. S. Nerem, vol. 116, 20 – 29. International Association of Geodesy Symposia, Berlin: Springer.

Lemoine, F., S. Kenyon, J. Factor, R. Trimmer, N. Pavlis, D. Chinn, C. Cox, S. Klosko, S. Luthcke, M. Torrence, Y. Wang, R. Williamson, E. Pavlis, R. Rapp, and T. Olson. 1998. The development of the joint NASA GSFC and the National Imagery and Mapping Agency (NIMA) geopotential model EGM96. Tech. Rep. NASAITP-1998-206861, Goddard Space Flight Centre, Greenbelt.

Leuliette, E. W., R. S. Nerem, and G. L. Russell. 2002. Detecting time variations in gravity associated with climate change. *Journal of Geophysical Research* 107:2112.

Lorenz, E. N. 1956. Empirical Orthogonal Functions and Statistical Weather Prediction. Tech. Rep. 1, Dept. of Meteorology, MIT.

Luthcke, S. B., D. D. Rowlands, F. G. Lemoine, S. M. Klosko, D. Chinn, and J. J. McCarthy. 2006. Monthly spherical harmonic gravity field solutions determined from GRACE inter-satellite range-rate data alone. *Geophysical Research Letters* 33:L02402.

Manly, B. F. J. 1986. *Multivariate statistical method : A primer*. New York: Chapman and Hall.

Mikhailov, V., S. Tikhotsky, M. Diament, I. Panet, and V. Ballu. 2004. Can tectonic processes be recovered from new gravity satellite data? *Earth and Planetary Science Letters* 228:281–297.

Morison, J., J. Wahr, R. Kwok, and C. Peralta-Ferriz. 2004. Recent trends in Artic Ocean mass distribution revealed by GRACE. *Earth and Planetary Science Letters* 228:281–297.

Nerem, R. S., C. Jekeli, and W. M. Kaula. 1995. Gravity field determination and characteristics: Retrospective and prospective. *Journal of Geophysical Research* 100(B8):15,053–15,074.

Nerem, R. S., J. Wahr, and E. W. Leuliette. 2003. Measuring the distribution of ocean mass using GRACE. *Space Science Review* 108(1-2):331–344.

Obukhov, A. M. 1947. Statistically homogeneous fields on a sphere. *Uspheti Mathematicheskikh Nauk* 2:288–291.

Ogawa, R. and K. Heki. 2007. Slow post seismic recovery of geoid depression formed by the 2004 Sumatra-Andaman earthquake by mantle water diffusion. *Geophysical Research Letters* 34:L06313.

Preisendorfer, R. W. 1988. *Principal component analysis in Meteorology and Oceanography*. New York: Elsevier.

Ramillien, G., A. Cazenave, and O. Brunau. 2004. Global time variations of hydrologycal signals from GRACE satellite gravimetry. *Geophysical Journal International* 158:813–826.

Rangelova, E. and M. G. Sideris. 2007. Combination of GRACE, gravity and GPS data for determination of long-term geoid changes in North America. In *Proceedings of the 1st International Symposium of the International Gravity Field Service*,

ed. Kiliçoğlu, A. and Forsberg, R., vol. 18, 437–442. Ankara: Harita Genel Komutanliği.

Rangelova, E., W. van der Wal, A. Braun, M. G. Sideris, and P. Wu. 2007. Analysis of Gravity Recovery and Climate Experiment time-variable mass redistribution signals over North America by means of principal component analysis. *Journal of Geophysical Research* 112:F03002. DOI 10.1029/2006JF000615.

Rapp, R. H. 1994. Global geoid determination. In *Geoid and its geophysical interpretations*, eds. P. Vanicek and N. Christou, 57–76. Boca Raton: CRC Press.

Reigber, C., G. Balmino, P. Schwintzer, R. Biancale, A. Bode, J. Lemoine, R. König, S. Loyer, K. H. Neumayer, J. C. Marty, F. Barthelmes, F. Perosanz, and S. Y. Zhu. 2003. Global gravity field recovery using solely GPS tracking and accelerometer data from CHAMP. In *Earth gravity field from space - From sensors to Earth sciences*, eds. G. Beutler, R. Rummel, M. R. Drinkwater, and R. v. Steiger. Dordrecht: Kluwer Academic Publisher.

Reigber, C., H. Lühr, P. Schwintzer, and J. Wickert, eds. 2005a. *Earth observation with CHAMP: Results from three years in orbit*. Berlin: Springer.

Reigber, C., R. Schmidt, F. Flechtner, R. König, U. Meyer, K.-H. Neumayer, P. Schwintzer, and S. Y. Zhu. 2005b. An Earth gravity field model complete to degree and order 150 from GRACE: EIGEN-GRACE02S. *Journal of Geodynamics* 39(1):1–10.

Rodell, M. and J. S. Famiglietti. 1999. Detectability of variations in continental water storage from satellite observations of the time dependent gravity field. *Water Resources Research* 35(9):2705–2723.

Rodell, M., J. S. Famiglietti, J. Chen, S. I. Seneviratne, P. Viterbo, S. Holl, and C. R. Wilson. 2004. Basin scale estimates of evapotranspiration using GRACE and other observations. *Geophysical Research Letters* 31:L20504.

Rowlands, D. D., S. B. Luthcke, S. M. Klosko, F. G. R. Lemoine, D. S. Chinn, J. J. McCarthy, C. M. Cox, and O. B. Anderson. 2005. Resolving mass flux at high spatial and temporal resolution using GRACE inter satellite measurements. *Geophysical Research Letters* 32:L04310.

Rummel, R. 2003. How to climb the gravity wall. In *Earth gravity field from space - from sensors to Earth sciences*, eds. G. Beutler, R. Rummel, M. R. Drinkwater, and R. v. Steiger, 1–14. Dordrecht: Kluwer Academic Publishers.

———. 2005. Geoid and gravity in Earth sciences - An overview. *Earth, Moon, and Planets* 94(1-2):3–11.

Rummel, R., G. Balmino, J. Johannessen, P. Visser, and P. L. Woodworth. 2002. Dedicated gravity field missions - principles and aims. *Journal of Geodynamics* 33(1-2):2–30.

Sabadini, R., G. Dalla Via, and M. Hoogland. 2005. A splash in Earth gravity from the 2004 Sumatra earthquake. *EOS Transaction, AGU* 86(15):149–146.

Sabadini, R., R. E. M. Riva, and G. Dalla Via. 2007. Coseismic rotation changes from the 2004 Sumatra earthquake: the effects of Earth's compressibility versus earthquake induced topography. *Geophysical Journal International* 171:231–243.

Schmidt, R., P. Schwintzer, F. Flechtner, C. Reigber, A. Güntner, P. Döll, G. Ramillien, A. Cazenave, S. Petrovic, H. Jochmann, and J. Wünsch. 2006. GRACE observations of changes in continental water storage. *Global and Planetary Change* 50:112–126.

Schrama, E. J. O., B. Wouters, and D. A. Lavallée. 2007. Signal and noise in Gravity Recovery and Climate Experiment (GRACE) observed surface mass variations. *Journal of Geophysical Research* 112:B08407. DOI 10.1029/2006JB004882.

Seeber, G. 1993. *Satellite Geodesy : Foundations, methods and applications*. Berlin: Walter de Gruyter.

Seo, K.-W. and C. R. Wilson. 2005. Simulated estimation of hydrological loads from GRACE. *Journal of Geodesy* 78:442–456.

Seo, K.-W., C. R. Wilson, F. J. S., J. L. Chen, and M. Rodell. 2006. Terrestrial water mass load changes from Gravity Recovery and Climate Experiment (GRACE). *Water Resources Research* 42:W05417.

Shum, C. K., S.-C. Han, C. Kuo, K. Seo, and C. Wilson. 2004. Assessment of GRACE time-variable gravity observables: a new filtering technique to enhance signal spatial resolutions. San Francisco, USA.

Sun, W. and S. Okubo. 2004. Coseismic deformation detectable by satellite gravity mission: A case study of Alaska (1964, 2002) and Hokkaido (2003) earthquakes in the spectral domain. *Journal of Geophysical Research* 109:B04405. DOI 10.1029/2003JB002554.

Swenson, S. and J. Wahr. 2002. Methods for inferring regional surface-mass anomalies from gravity recovery and climate experiment (GRACE) measurements of time-variable gravity. *Journal of Geophysical Research* 107(B9):ETG3–1 – ETG3–13.

———. 2006. Post-processing removal of correlated errors in GRACE data. *Geophysical Research Letters* 33:L08402.

Swenson, S., J. Wahr, and P. Milly. 2003. Estimated accuracies of regional water storage variations inferred from the gravity recovery and climate experiment (GRACE). *Water Resources Research* 39(8):1223.

Tamisiea, M., E. Leuliette, J. Davis, and J. Mitrovica. 2005. Constraining hydrological and cryospheric mass flux in southeastern Alaska using space-based gravity measurements. *Geophysical Research Letters* 32:L20501.

Tapley, B., J. Ries, S. Bettadpur, D. Chambers, M. Cheng, F. Condi, B. Gunter, Z. Kang, P. Nagel, R. Pastor, T. Pekker, S. Poole, and F. Wang. 2005. GGM02 - An improved Earth gravity field model from GRACE. *Journal of Geodesy* 79(8):467–478.

Tapley, B. D., S. Bettadpur, J. C. Ries, P. F. Thompson, and M. M. Watkins. 2004a. GRACE measurements of mass variability in the Earth system. *Science* 305:503–505.

Tapley, B. D., S. Bettadpur, M. Watkins, and C. Reigber. 2004b. The gravity recovery and climate experiment: Mission overview and early results. *Geophysical Research Letters* 31:L09607.

Thompson, P. F., S. Bettadpur, and B. D. Tapley. 2004. Impact of short period, nontidal, temporal mass variability on GRACE gravity estimates. *Geophysical Research Letters* 31:L06619.

Torge, W. 1989. *Gravimetry*. Berlin: Walter de Gruyter.

———. 2001. *Geodesy*. 3rd ed. Berlin: Walter de Gruyter.

Trenberth, K. E. 1975. A quasi-biennial standing wave in the southern hemisphere and interrelation with sea surface temperature. *Quarterly Journal of the Royal Meteorological Society* 101:55–74.

UTCSR. 2008. Gravity recovery and climate experiment homepage. http://www.csr.utexas.edu/grace/ (accessed January,2008).

Vaníček, P. and E. J. Krakiwsky. 1986. *Geodesy : the Concepts*. 2nd ed. Amsterdam: Elsevier.

Velicogna, I. and J. Wahr. 2002. Postglacial rebound and Earth's viscosity structure from GRACE. *Journal of Geophysical Research* 107(B12):2376.

———. 2005. Greenland mass balance from GRACE. *Journal of Geophysical Research Letters* 32:L18505.

Velicogna, I., J. Wahr, E. Hanna, and P. Huybrechts. 2005. Short term mass variability in Greenland, from GRACE. *Journal of Geophysical Research Letters* 32:L05501.

Viron, O. d., I. Panet, and M. Diament. 2006. Extracting low frequency climate signal from GRACE data. *eEarth* 1:9–14.

Visser, P. 1999. Gravity field determination with GOCE and GRACE. *Advance Space Research* 23(4):771–776.

Visser, P., K. Wakker, and B. Ambrosius. 1994. Global gravity field recovery from the ARISTOTELES satellite mission. *Journal of Geophysical Research* 99(B2):2841–2851.

Wagner, C., D. McAdoo, J. Klokočník, and Kostelecký. 2006. Degradation of geopotential recovery from short repeat-cycle orbits: application to GRACE monthly fields. *Journal of Geodesy* 80:94–103.

Wahr, J., M. Molenaar, and F. Bryan. 1998. Time-variability of the Earth's gravity field: Hydrological and oceanic effects and their possible detection using GRACE. *Journal of Geophysical Research* 103:30,205 –30,230.

Wahr, J., S. Swenson, V. Zlotnicki, and I. Velicogna. 2004. Time-variable gravity from GRACE: First result. *Geophysical Research Letters* 31:L11501.

Wahr, J. and I. Velicogna. 2003. What might GRACE contribute to studies of post glacial rebound? *Space Science Reviews* 108:319–330.

Wang, H. 2001. Principal component analysis on temporal-spatial variations of sea level anomalies from T/P satellite altimeter data over the Northwest Pacific. In *Gravity, Geoid and Geodynamics 2000*, ed. M. G. Sideris, 165–170. International Association of Geodesy Symposia, Berlin: Springer.

White, D., L. Hinzman, L. Alessa, J. Cassano, M. Chambers, K. Falkner, J. Francis, J. Gutowski, M. Holland, R. M. Holmes, H. Hutington, D. Kane, A. Kliskey, C. Lee, J. McClelland, B. Peterson, T. S. Rupp, F. Straneo, M. Steele, R. Woodgate, D. Yang, K. Yoshikawa, and T. Zhang. 2007. The arctic freshwater system: Changes and impacts. *Journal of Geophysical Research* 112:G04S54.

Wikle, C. K. 2002. Spatio-temporal methods in Climatology. *Encyclopedia of Life Support Systems* (in-press).

Woodworth, P. L. and J. M. Gregory. 2003. Benefits of GRACE and GOCE to sea level studies. *Space Science Reviews* 108:319–330.

APPENDIX A: ANNUAL VARIABILITY OF GRACE GRAVITY FIELD

This appendix provides the annual plots of GRACE gravity field both as EWT and potential value. The annual value is obtained by calculating the mean value of EWT and potential within one year period (June to May, inclusive).

Equivalent Water Thickness

June 2002 - May 2003

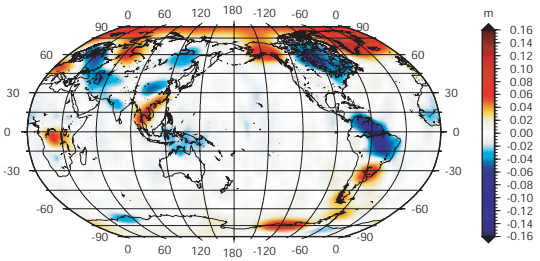

June 2003 - May 2004

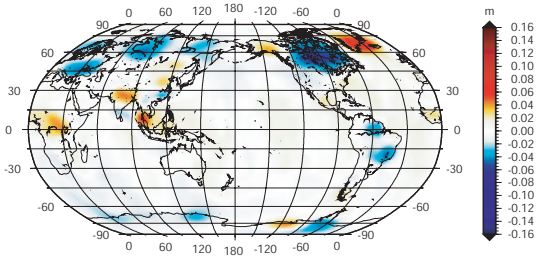

June 2004 - May 2005

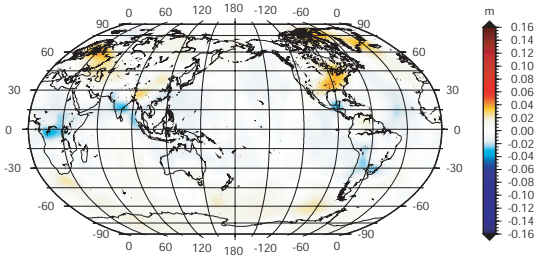

June 2005 - May 2006

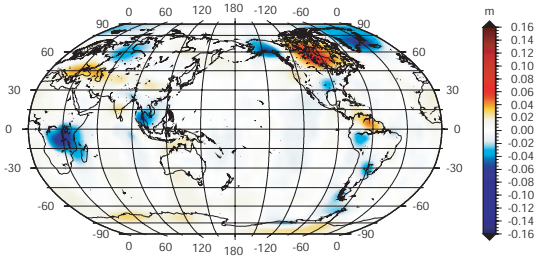

June 2006 - May 2007

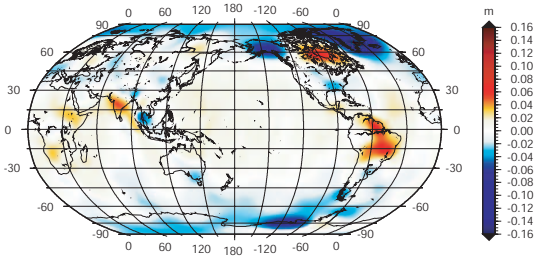

Potential

June 2002 - May 2003

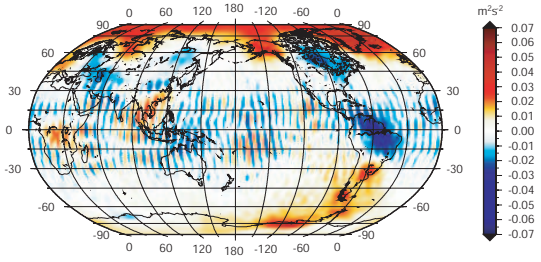

June 2003 - May 2004

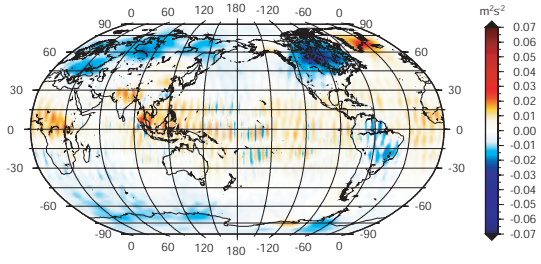

June 2004 - May 2005

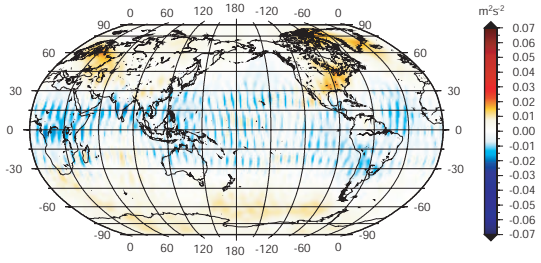

June 2005 - May 2006

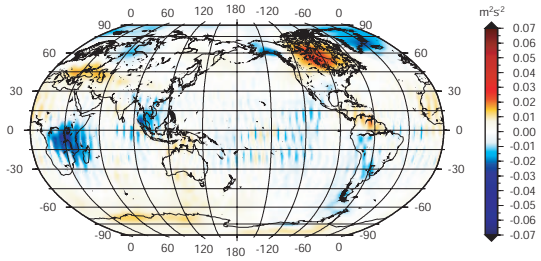

June 2006 - May 2007

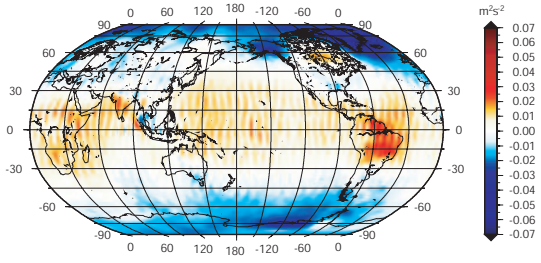

APPENDIX B: SEASONAL VARIABILITY OF GRACE GRAVITY FIELD

This appendix provides the seasonal plots of GRACE gravity field both as EWT and potential value. Seasonal values are derived by averaging three monthly data. In this study seasonal term is use with respect to the northern hemisphere; Spring is take place during March and May, Summer during June and August, Autumn during September and November, and Winter during December and February.

2003

Equivalent Water Thickness

Spring

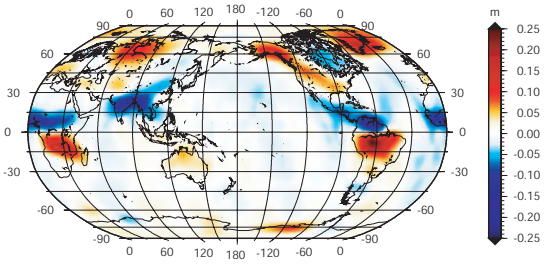

Summer

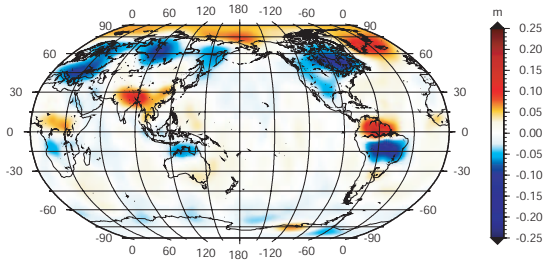

Autumn

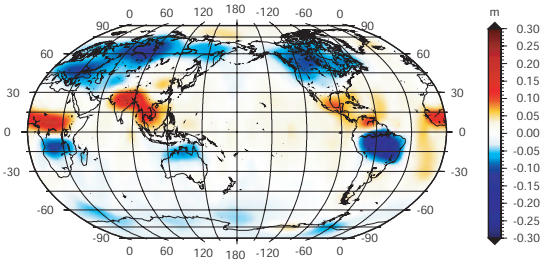

Winter

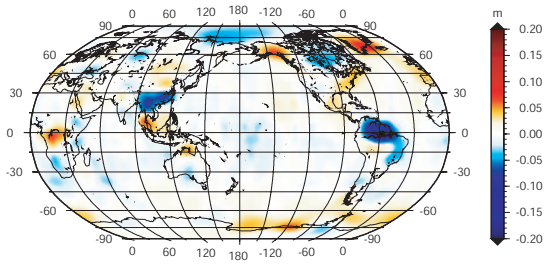

Potential

Spring

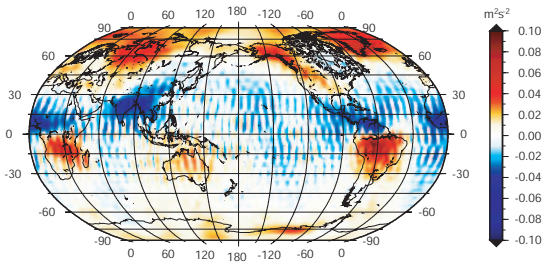

Summer

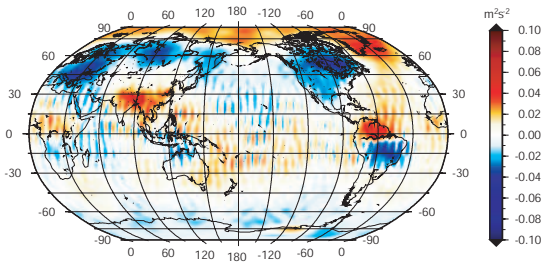

Autumn

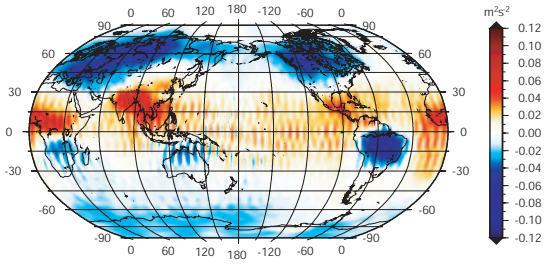

Winter

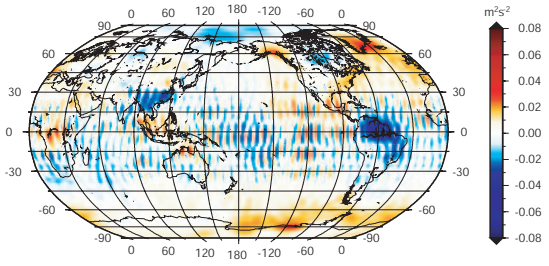

2004

Equivalent Water Thickness

Spring

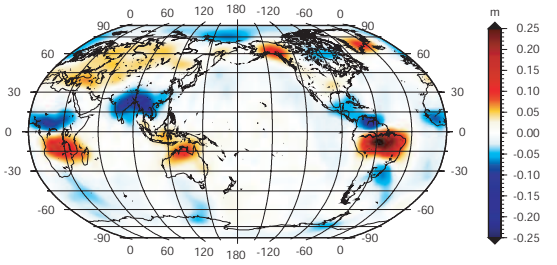

Summer

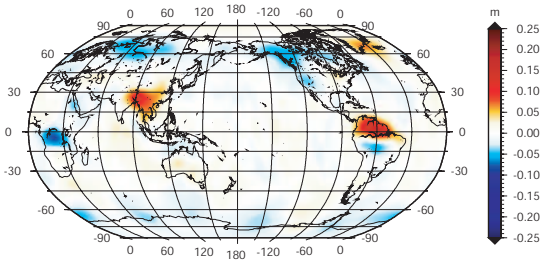

Autumn

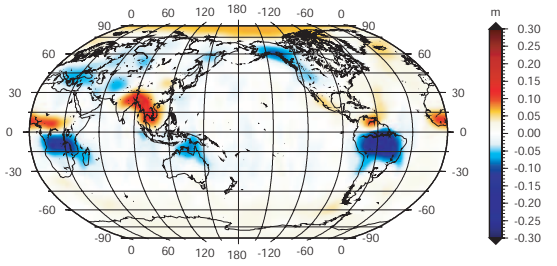

Winter

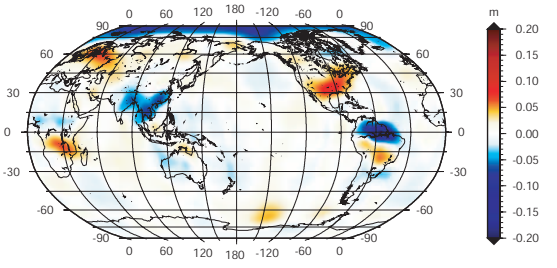

Potential

Spring

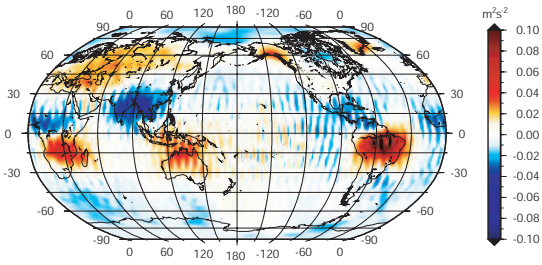

Summer

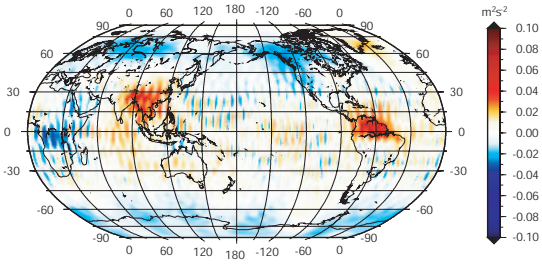

Autumn

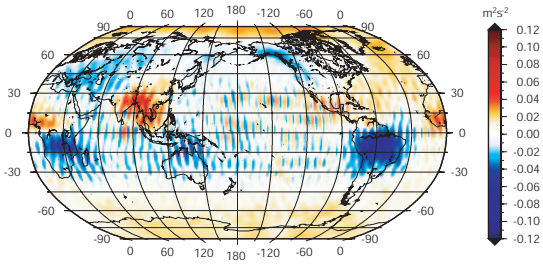

Winter

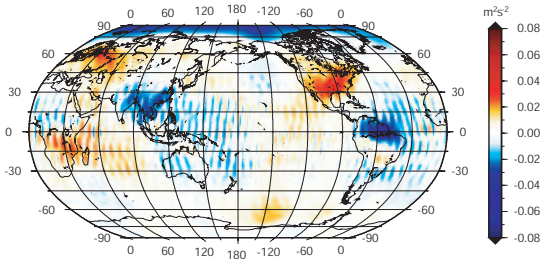

2005

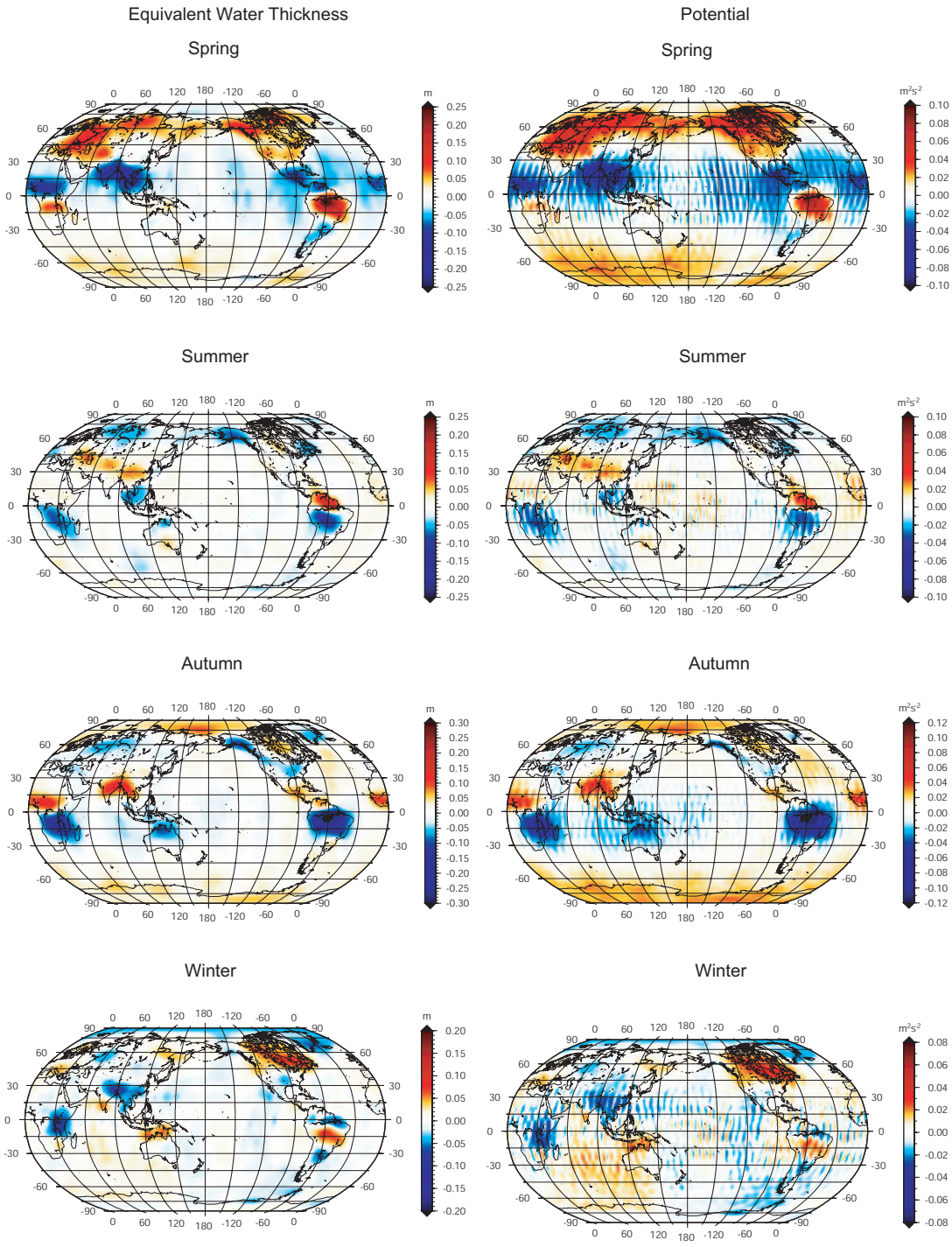
Equivalent Water Thickness
Potential
Spring
Spring
Summer
Summer
Autumn
Autumn
Winter
Winter
m
m²s⁻²

2006

Equivalent Water Thickness

Spring

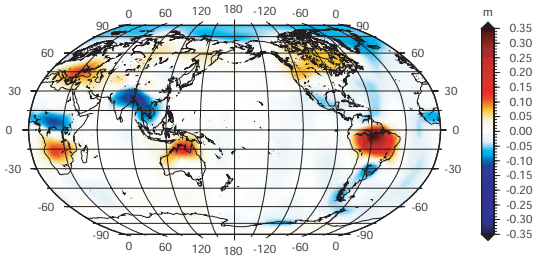

Summer

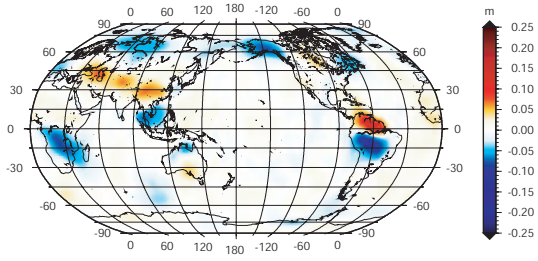

Autumn

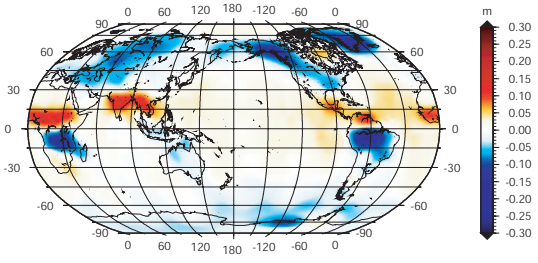

Winter

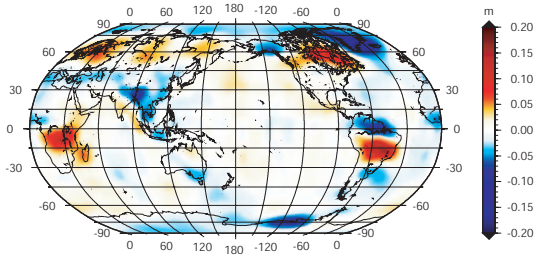

Potential

Spring

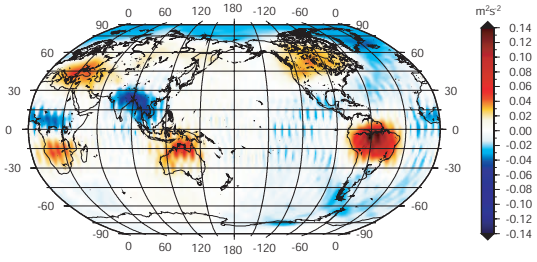

Summer

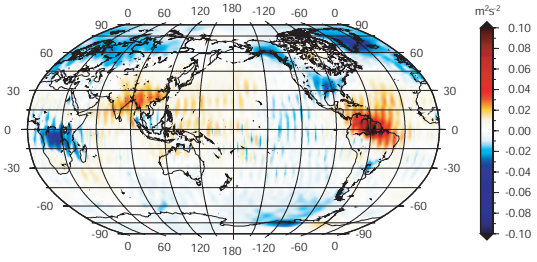

Autumn

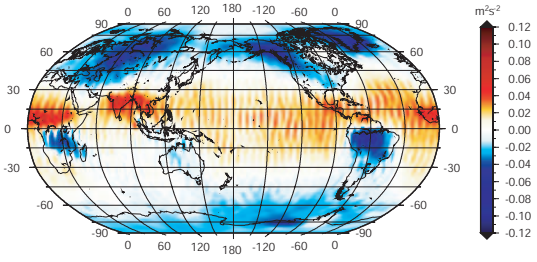

Winter

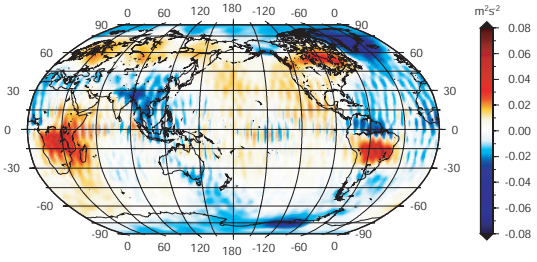

APPENDIX C: PCA RESULTS

This appendix provides the PCA results from global and local analyses as follow:

1. PCA for Global coverage
2. PCA for Sumatra-Andaman region
3. PCA for Australia region
4. PCA for Africa region
5. PCA for Antarctic region
6. PCA for South America region
7. PCA for Arctic region
8. PCA for Greenland region
9. PCA for South Asia region
10. PCA for North America region
11. PCA for Central Europe region

The PCA results are only presented up to the first five modes, as the remaining modes (for all analyses) only capture small part of the overall variability. Moreover, the higher modes of the PCA tend to be difficult to interpret.

PCA results : Global

a) Data reduced by mean

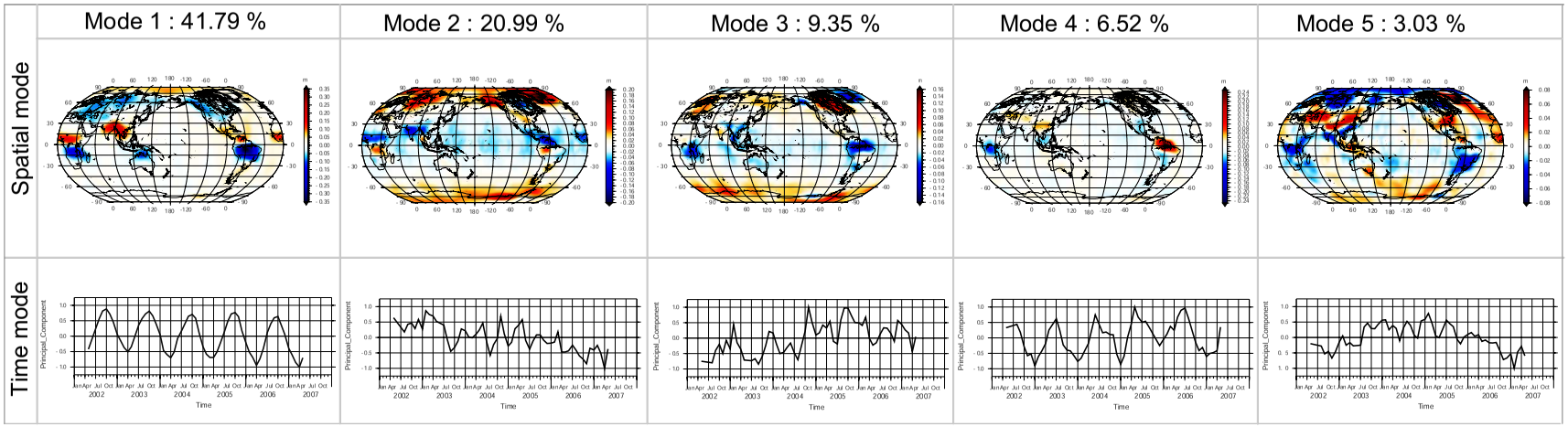

b) Data reduced by mean, trend and annual signal

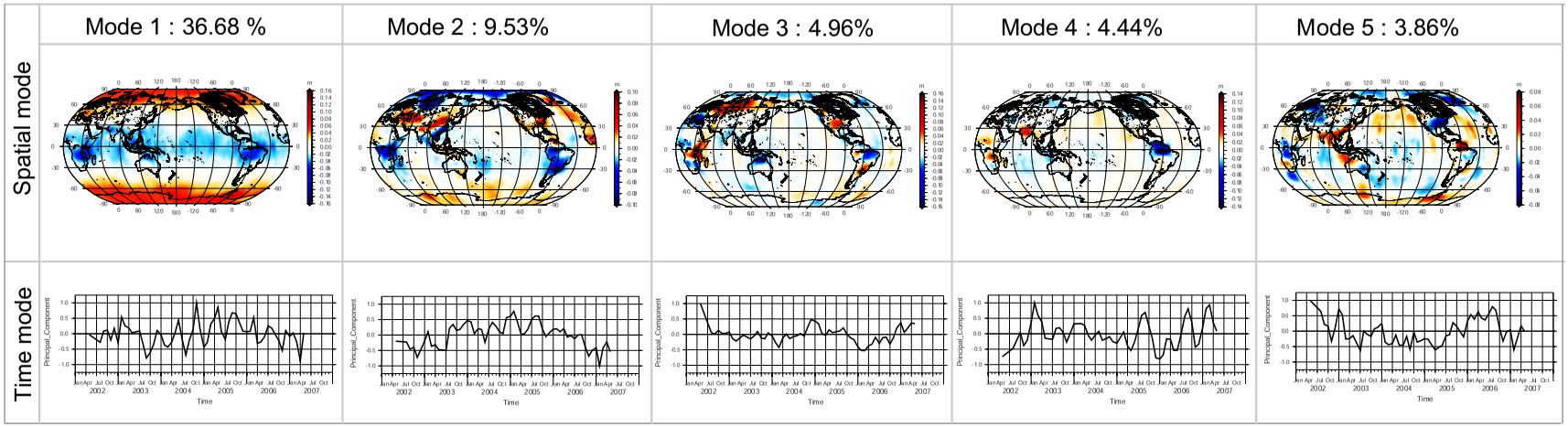

PCA results : Sumatra-Andaman

a) Data reduced by mean

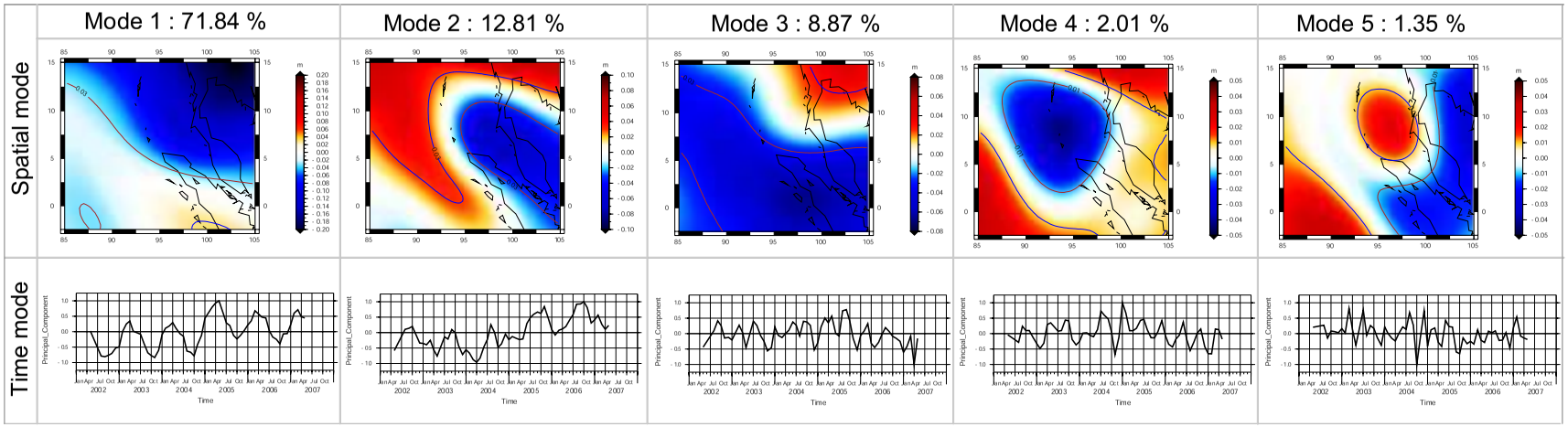

b) Data reduced by mean, trend and annual signal

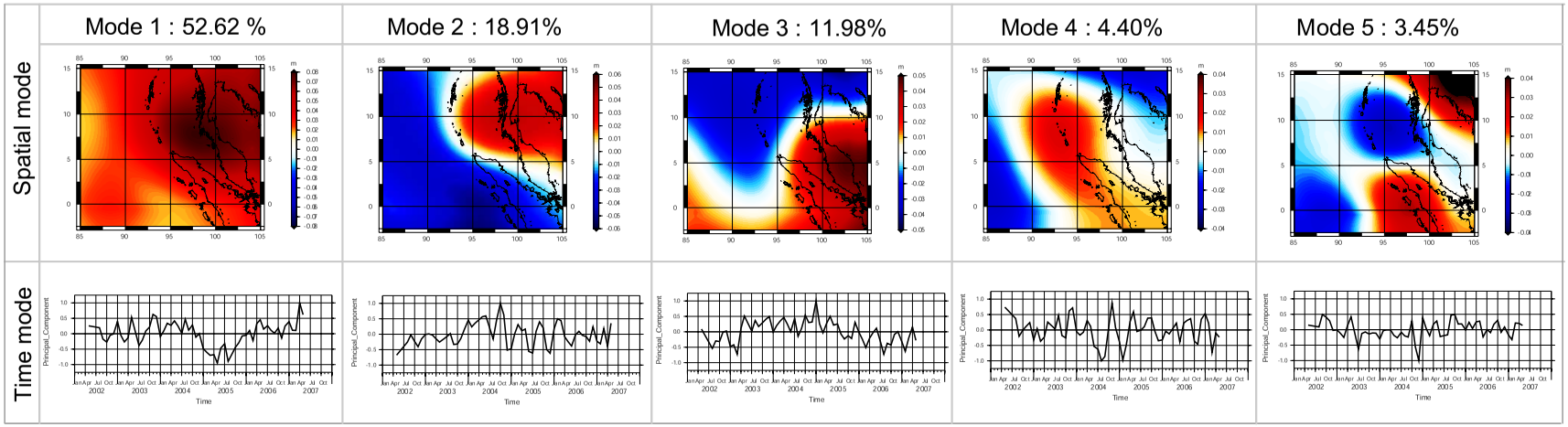

PCA results : Australia

a) Data reduced by mean

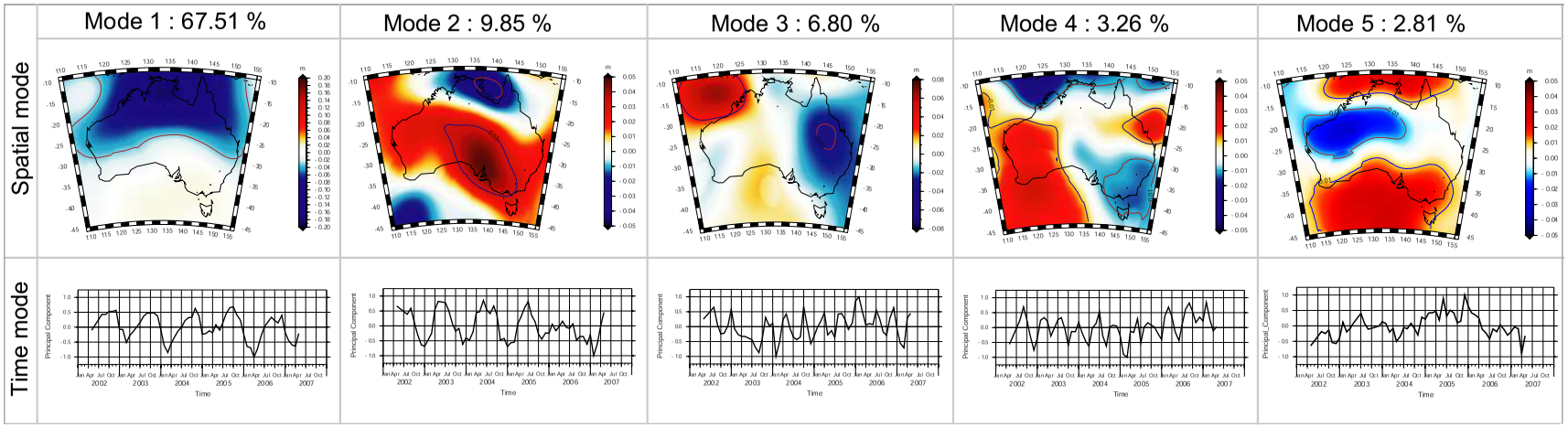

b) Data reduced by mean, trend and annual signal

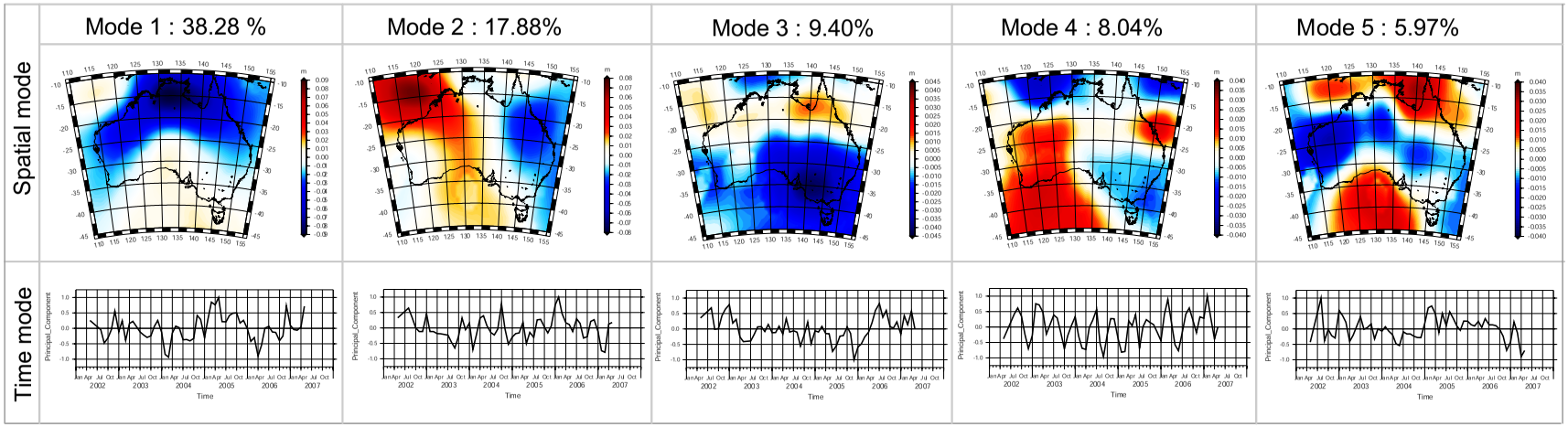

PCA results : Africa

a) Data reduced by mean

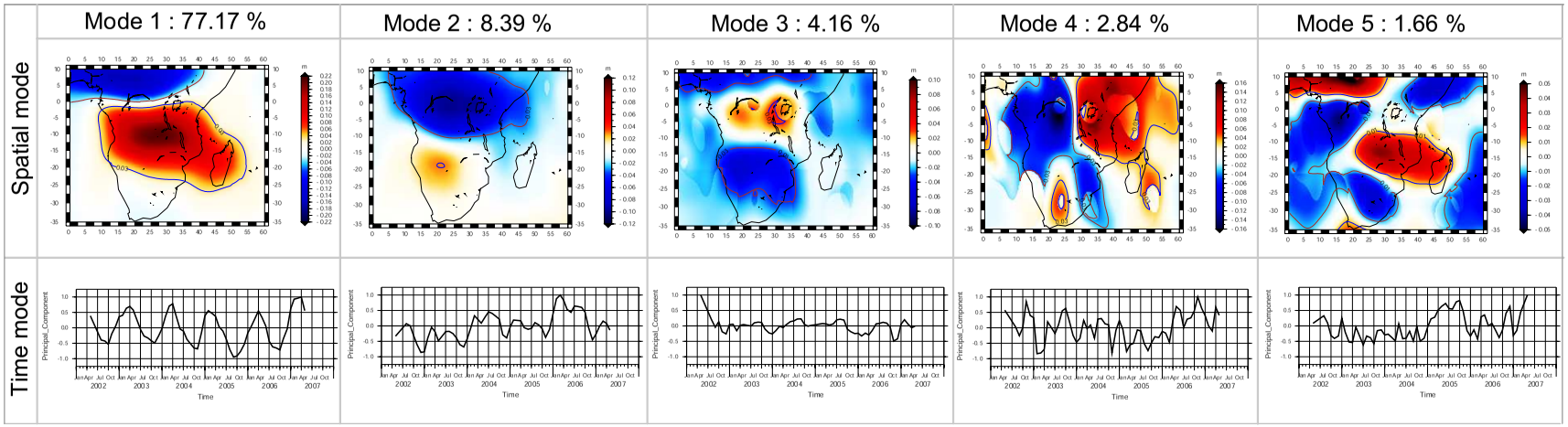

b) Data reduced by mean, trend and annual signal

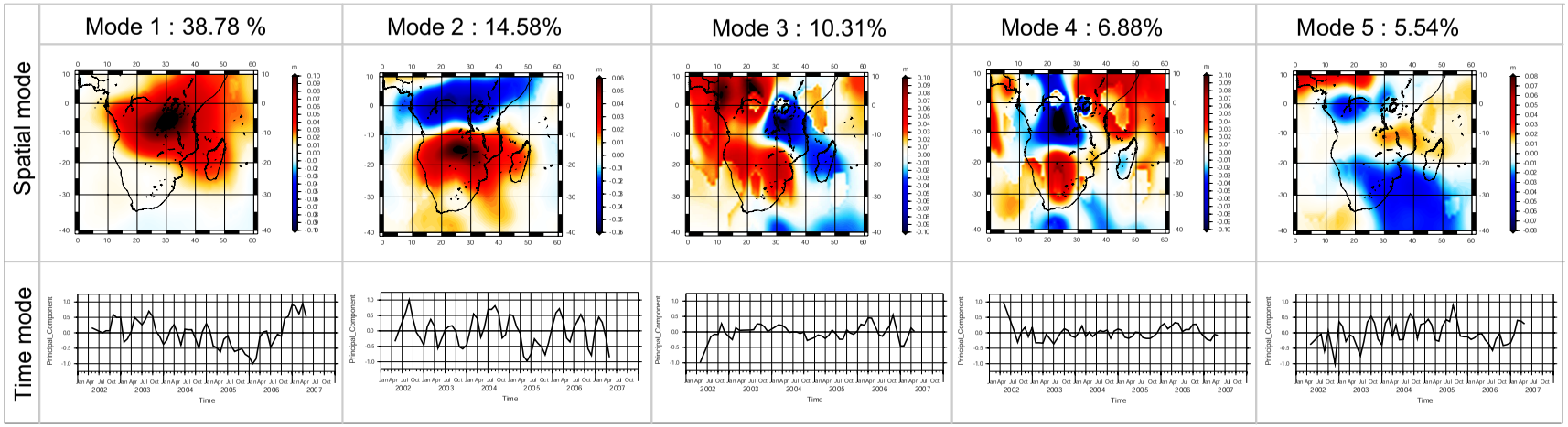

PCA results : Antarctic

a) Data reduced by mean

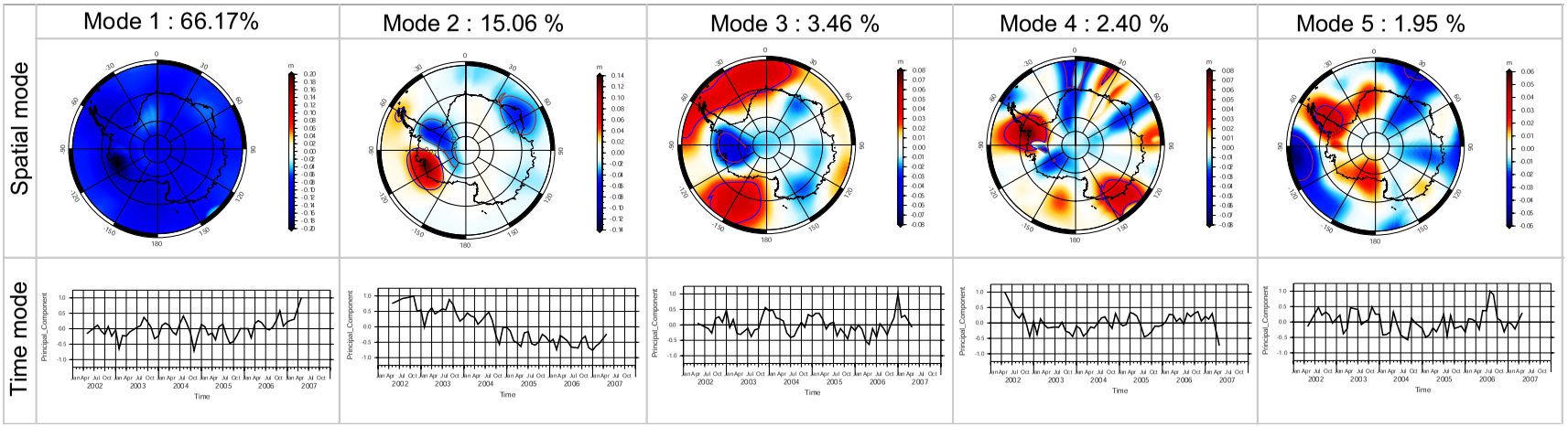

b) Data reduced by mean, trend and annual signal

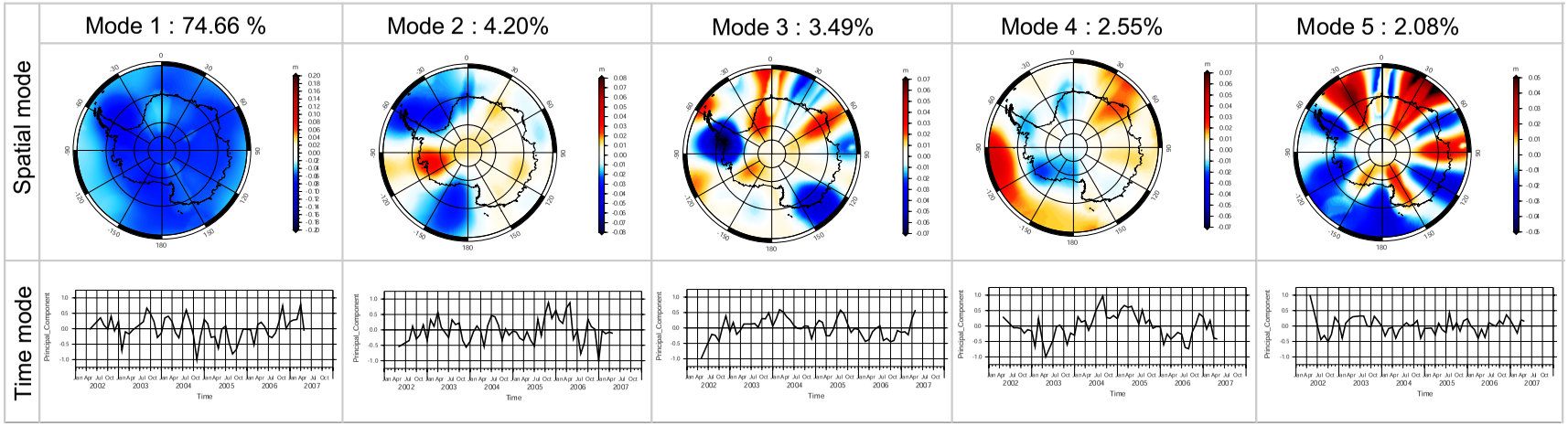

PCA results : South America

a) Data reduced by mean

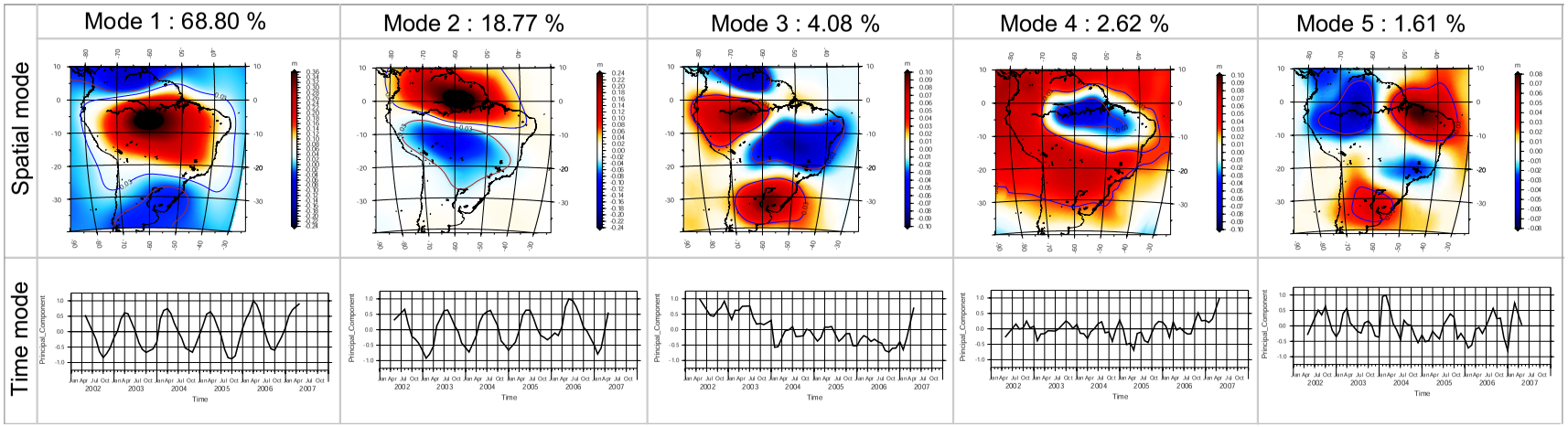

b) Data reduced by mean, trend and annual signal

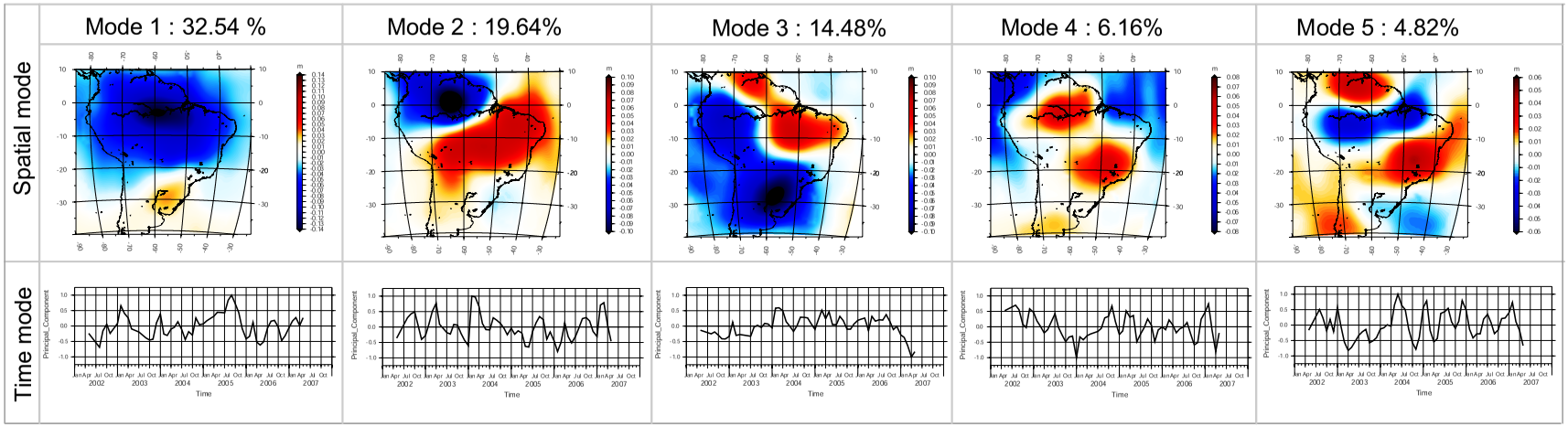

PCA results : Arctic

a) Data reduced by mean

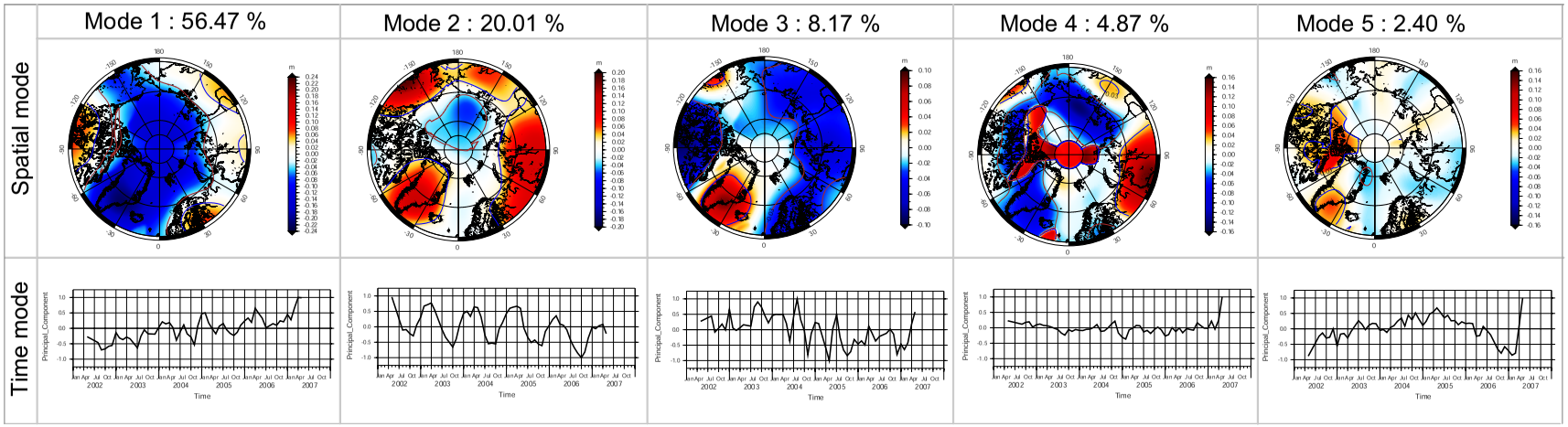

b) Data reduced by mean, trend and annual signal

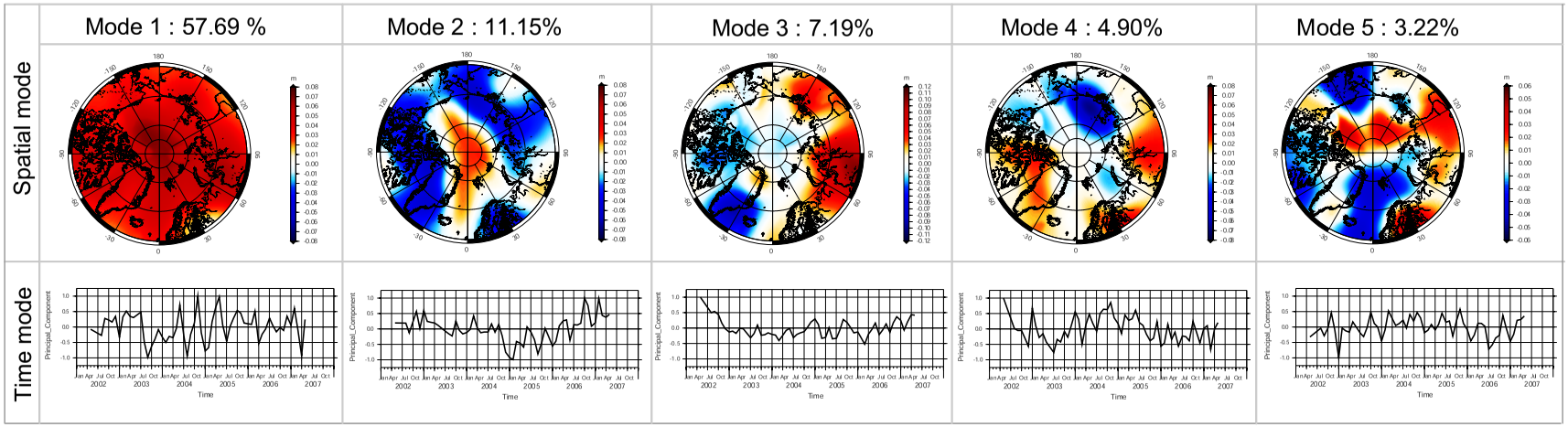

PCA results : Greenland

a) Data reduced by mean

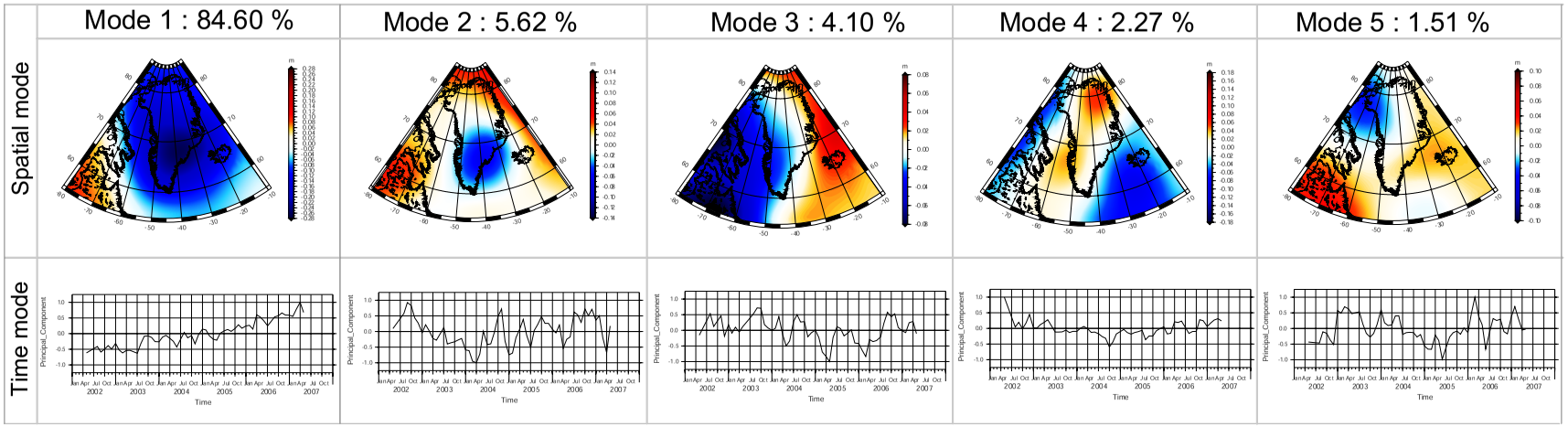

b) Data reduced by mean, trend and annual signal

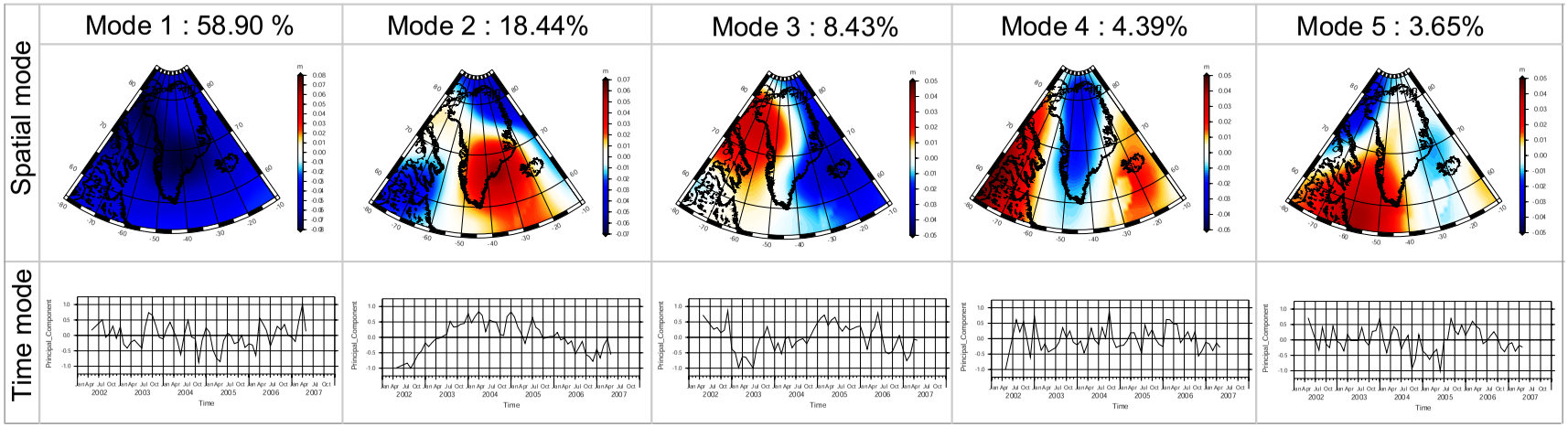

PCA results : South Asia

a) Data reduced by mean

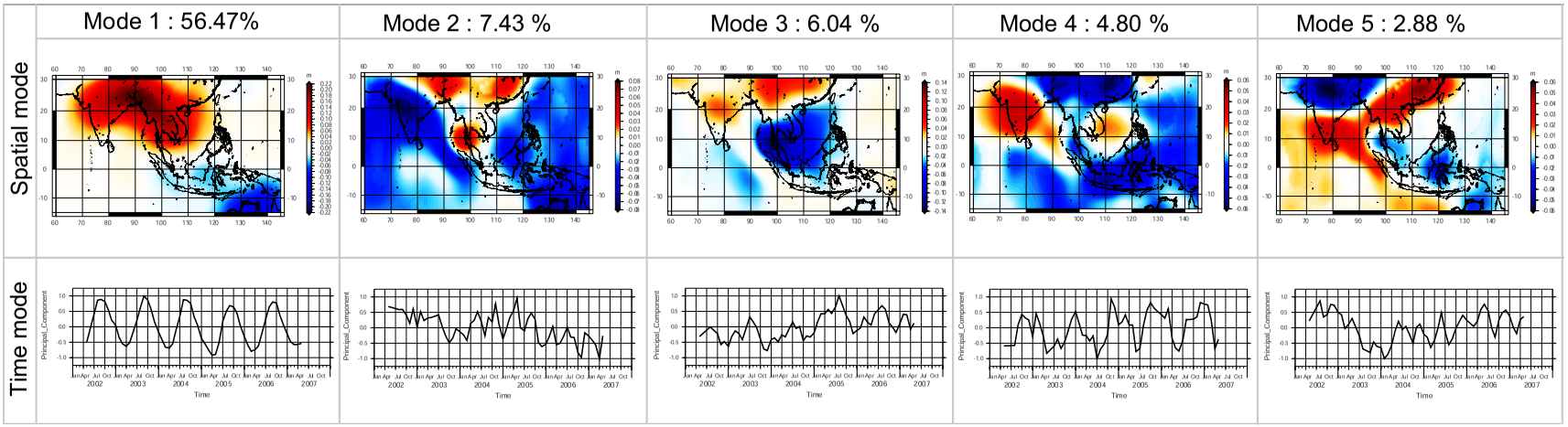

b) Data reduced by mean, trend and annual signal

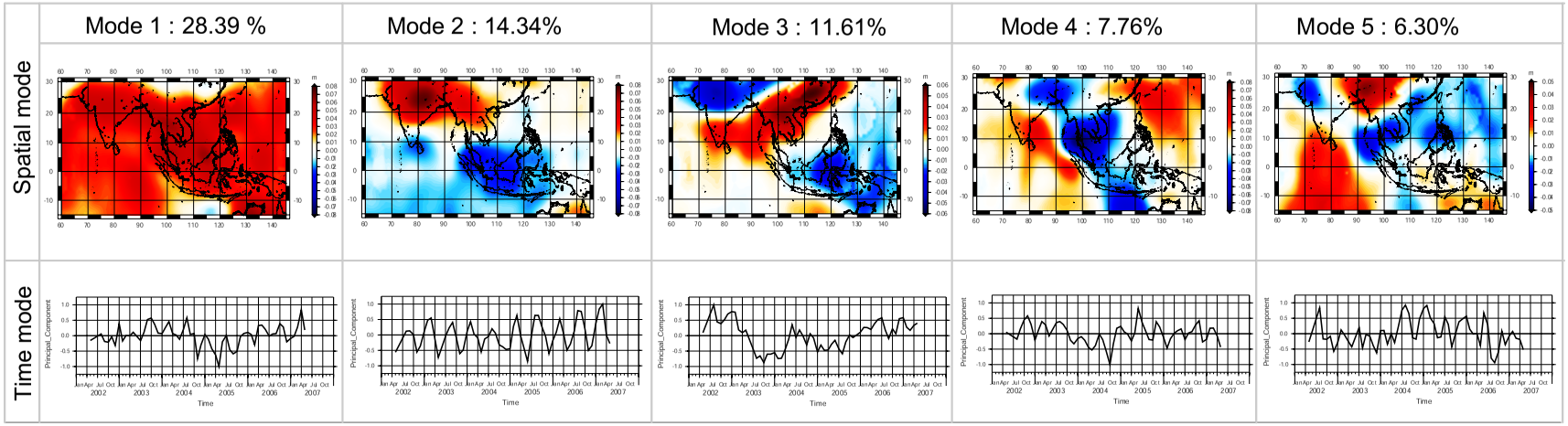

PCA results : North America

a) Data reduced by mean

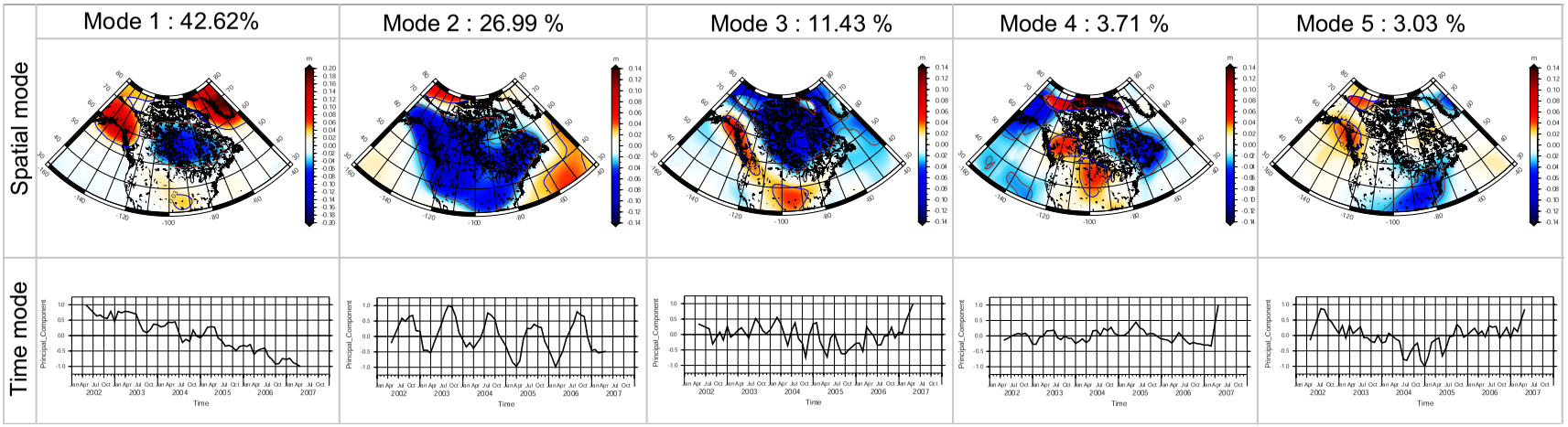

b) Data reduced by mean, trend and annual signal

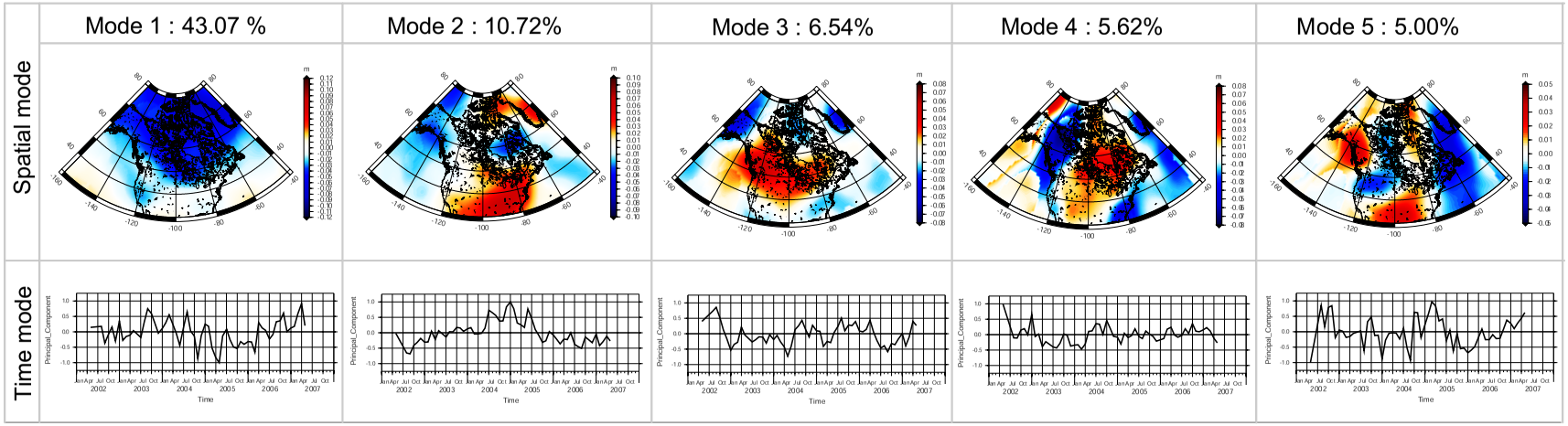

PCA results : Central Europe

a) Data reduced by mean

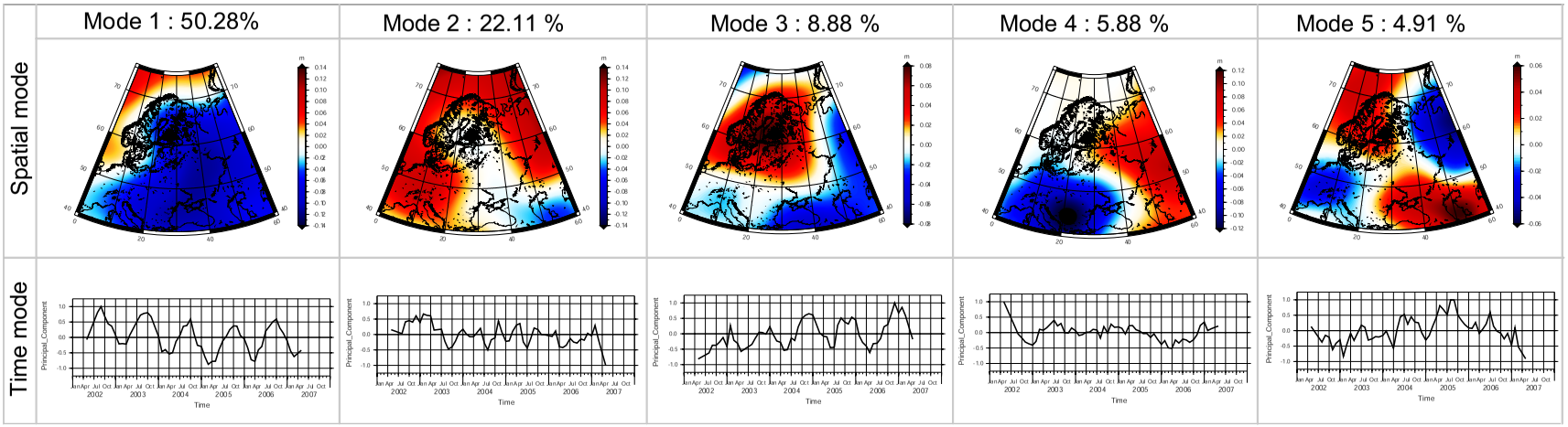

b) Data reduced by mean, trend and annual signal